Professur für Hydrologie
der Albert-Ludwigs-Universität Freiburg i. Br.

Jasper Opdenhoff

Estimating Rainfall from an Open Radio Network

Masterarbeit unter Leitung von apl. Prof. Dr. Jens Lange

Freiburg i. Br., Oktober 2019

Professur für Hydrologie
der Albert-Ludwigs-Universität Freiburg i. Br.

Jasper Opdenhoff

Estimating Rainfall from an Open Radio Network

Referent: apl. Prof. Dr. Jens Lange

Korreferent: Prof. Dr.-Ing. Erwin Zehe

Masterarbeit unter Leitung von apl. Prof. Dr. Jens Lange

Freiburg i. Br., Oktober 2019

Contents

Figures

Tables

Appendix: Figures

Abstract

In the light of the globally decreasing number of rain gauges on the one hand and increasing hydrometeorological risks on the other hand new means of measurement for the localization and calibration of rain fall events located by precipitation radars would prove themselves valuable. One rather new approach involves deriving rainfall intensities from the attenuation of microwave radio transmission which are used for the communication between cellphone towers. In regard to the upcoming age of Internet of Things, new radio networks of various scales and frequencies are expected to evolve and spread globally. The goal of this thesis was to examine the transferability of the microwave link approach to two of such networks: LoRaWAN, operating at urban scale on frequency 868 MHz, and common Wi-Fi, operating at the scale of local networks on frequencies 2.4 and 5 GHz. First, the frequencies were examined in plot-scale experiments using sprinkling systems to assess the general impact of precipitation on radio transmissions at the respective frequency. A reference and sprinkling setup and different time periods were compared using ANOVA and the effect size Cohen's d. Additionally, LoRaWAN was investigated at urban scale in a network of 24 nodes and 24 receiving gateways for a duration of six month. After determining the most influential environmental parameters and decoupling them from the analysis, linear regression between precipitation and the signal strength was used to assess the impact of precipitation.

It was found that precipitation does not impact LoRaWAN-transmissions and that it cannot be exploited for precipitation measurements. While there was no direct attenuation of 2.4 GHz and 5 GHz transmissions, the connectivity of the network was significantly altered during sprinkling at extreme rates, especially for 5 GHz. This is attributed to the formation of puddles on the ground which acted as reflective planes and altered the transmission paths of the network.

Keywords: rain attenuation, rain fade, precipitation measurement, wireless networks, LoRaWAN, 868 MHz, 2.4 GHz, 5 GHz, microwave link, reliability, Internet of Things

Zusammenfassung

In Anbetracht der weltweit schrumpfenden Zahl der Wetterstationen einerseits und der Zunahme der hydrometeorologischen Risiken andererseits würden sich neue Messmethoden für die Lokalisierung und Kalibrierung der durch Niederschlagsradar gemessenen Regenereignisse als wertvoll erweisen. Ein relativ neuer Ansatz ist das Ableiten von Niederschlagsintensitäten aus der Dämpfung von Mikrowellen-Übertragungen zwischen Mobilfunkmasten. Das Ziel der Masterarbeit war es, die Übertragbarkeit des Mirowellenansatzes auf zwei weitere weit verbreitete Netzwerke zu untersuchen: LoRaWAN, das auf 868 MHz sendet und für den urbanen Maßstab konzipiert ist, und das weit verbreitete Wi-Fi, das auf 2,4 und 5 GHz sendet und in lokalen Netzwerken angewandt wird. Zunächst wurden alle drei Frequenzen in Experimenten auf Plotgröße unter der Zuhilfenahme einer Beregnungsanlage untersucht, um die allgemeinen Auswirkungen von Niederschlag auf Funkübertragungen in diesen Frequenzen zu analysieren. Hier wurden jeweils ein Referenz- und ein Beregnungssetup sowie verschiedene zeitliche Perioden mittels ANOVA und der Effektstärke Cohen's d verglichen. Zusätzlich wurde LoRaWAN in einem sechsmonatigen Experiment in einem Netzwerk in urbaner Größe bestehend aus 24 Sendern und 24 Gateways (Empfängern) untersucht. Hier wurden zunächst die einflussreichsten Umweltfaktoren festgestellt und entkoppelt. Anschließend wurden lineare Regressionen zwischen Niederschlag und Signalstärke durchgeführt um den Einfluss des Niederschlages untersucht. Es wurde festgestellt, dass Niederschlag LoRaWAN-Übertragungen nicht beeinflusst und diese Netzwerke daher nicht für die Niederschlagsmessung verwendet werden können. Zwar wurden auch 2.4 GHz- und 5 GHz-Übertragungen nicht durch Niederschlag abgeschwächt, allerdings wurde die Stabilität des gesamten Netzwerkes während der Beregnung mit sehr hohen Intensitäten maßgeblich beeinflusst, insbesondere bei 5GHz. Ursache hierfür waren möglicherweise Pfützen auf dem Untergrund, die als reflektierenden Oberflächen die Übertragungswege des Netzwerkes signifikant veränderten.

Stichworte: Regendämpfung, Niederschlagsmessung, drahtlose Netzwerke, LoRaWAN, 868 MHz, 2,4 GHz, 5 GHz, Mikrowellen-Link, Zuverlässigkeit, Internet der Dinge

1 Introduction

The accurate measurement of precipitation is one of the basic requirements for meaningful hydrologic analysis and modelling. Traditionally, point precipitation measurements are conducted through rain gauges. In wide areas of the world, this system has been complemented by precipitation radars which can localize precipitation events for large areas. However, since they measure precipitation in high elevations above ground (Fencl *et al.*, 2017), they have to be adjusted to ground truth data. This data provided by rain gauges is declining in many parts of the world (Overeem, Leijnse and Uijlenhoet, 2011) while on the other hand the hydrometeorological risks are increasing (Doumounia *et al.*, 2014). Even dense rain gauge networks and precipitation radars do not provide reliable and adequate input data: rain gauges might fail during heavy rainfall events and the resolution of radar data - which often comes in grids of 1 km^2 cell size and a maximum temporal resolution of 5 minutes – is not high enough for today's urban hydrological applications (Fencl *et al.*, 2017). During the last two decades, a new concept has come up to support the means of precipitation measurements under what is commonly known as estimation of rainfall from microwave links. This method exploits the existing radio communication of cellphone towers by measuring the attenuation of the radio waves by precipitation. Cellphone towers are widely available in the more densely populated parts of the world and can thereby form a dense network of precipitation measurements with high temporal resolution (approx. 1 s interval). Instead of point measurements like rain gauges, they provide data for the connecting line between two towers. Hence, the precipitation deduced from the attenuation therefore has to be considered a path-averaged precipitation. Precipitation maps can be created by combining the attenuation information of multiple links. Overeem, Leijnse and Uijlenhoet (2016) have presented precipitation maps for the Netherlands which show high accordance with the traditional methods of measurement. Microwave links therefore represent a good way of complementing precipitation radar for the localization of

precipitation especially in regard to the decreasing number of rain gauges and the worldwide spread presence of cellphone towers (estimated at 4 million (Uijlenhoet, Overeem and Leijnse, 2018)).

The transmission frequency of microwave links normally ranges between 10 to 50 GHz (Schleiss and Berne, 2010), but the method has also been implemented for frequencies as low as 7 GHz (Doumounia *et al.*, 2014). Since the concept has shown such high potential it is worth considering if it can be transferred to other networks operating under different frequencies. There are other widespread networks around the world however, they are typically designed for local applications and operate at much lower ranges and typically lower frequency. Two of such networks are LoRaWAN-networks operating at 868 MHz and Wi-Fi-networks operating at 2.4 and 5 GHz. While in theory only minimal attenuation has to be expected at local scale for such low frequencies, reports from scientists provide an inconclusive picture of the impact of precipitation. The goal of this thesis is therefore to investigate the applicability of the method of precipitation measurements through microwave links on the aforementioned networks.

First, the theoretical background of rain attenuation of radio waves is presented alongside with a selection of other environmental factors which also have the potential to impede radio transmissions and therefore must be considered during the evaluation. Scientific reports concerning the respective parameters are presented along with the theoretical foundation. Afterwards the conclusions for the two networks in question are drawn on the basis of the theoretical background and the hypotheses required to test them are presented. Three experiments were conducted throughout this thesis to this end, two at plot-scale and one at urban-scale. Their outcome was statistically assessed using ANOVA and effect size. The methods and results are presented in the subsequent section. Afterwards, their relevance for the hypotheses especially with the background of other impacting factors is discussed before the final conclusions are drawn in the last section.

2 Theoretical Background

2.1 Radio Waves and Path Loss

2.1.1 Propagation of Radio Waves

Radio waves are man-made electromagnetic waves. Although there are radio waves originating from astronomical phenomena, the most common purpose is to wirelessly transmit human-relevant information between two locations in a point-to-point link. These locations might be far apart, such as rovers roaming the surface of Mars and an institute of NASA, or close, such as the fridge and the router in a residential building in the age of the internet of things.

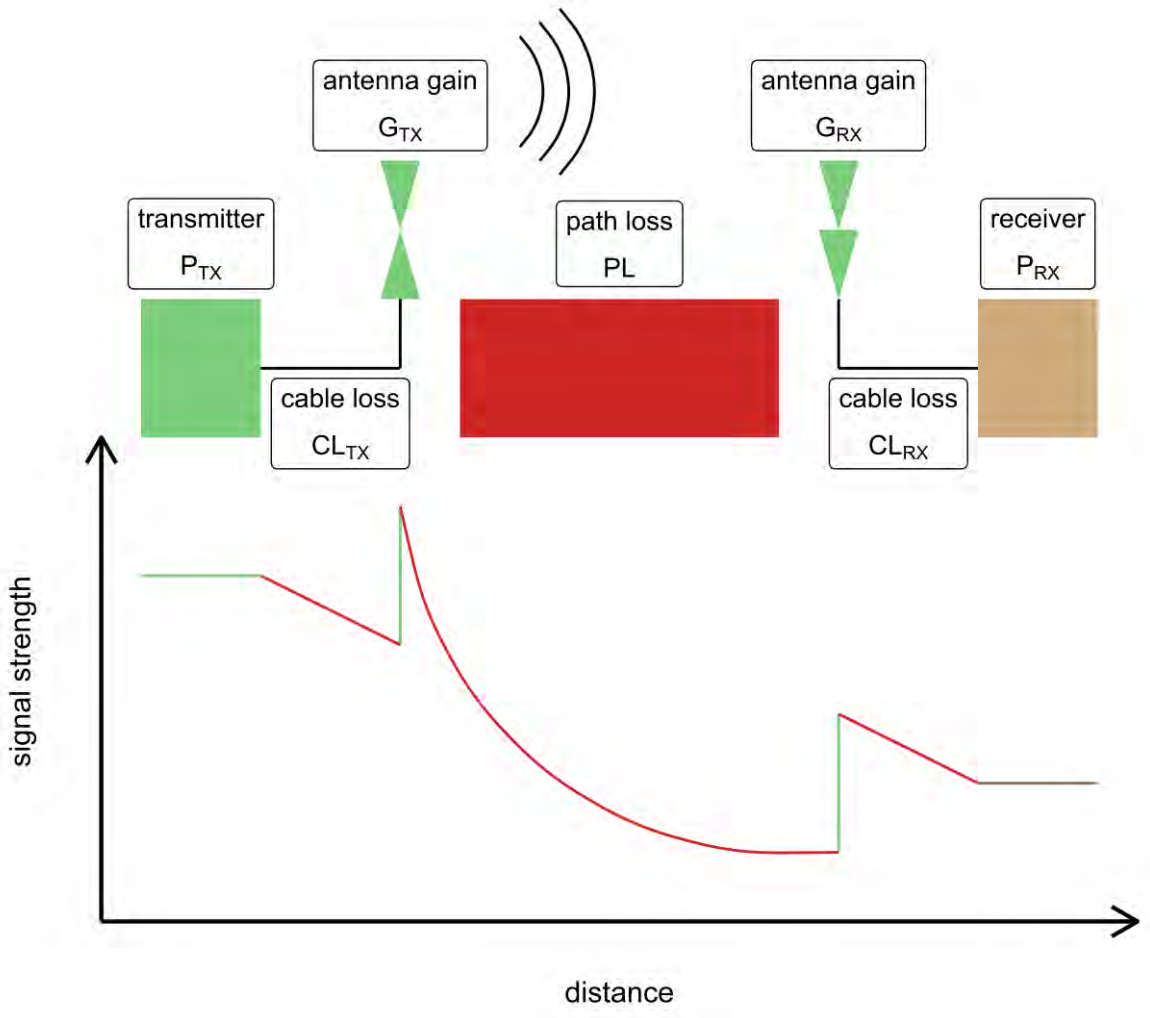

Figure 2.1: Gain and loss factors of signal strength (not to scale).

Two characteristics of radio waves are relevant to this thesis: frequency and signal strength. As illustrated in the lower part of Figure 2.1, the strength of an electromagnetic wave of a certain frequency is altered before it reaches a receiver (RX). A transmitter (TX) sends the wave with a certain transmission power P_{TX}. Due to the resistance of the circuits and cables, the strength of the signal is reduced by every electronic component it has to pass (cable loss, CL_{TX}). The antennas of transmitter and receiver on the other hand increase the signal strength, an effect commonly known as antenna gain (G_{TX}). In the gap between the two antennas where the wave travels through open space, the signal is exposed to various exterior effects and subject to so-called path loss (PL). On the other end, the signal may again be strengthened by an antenna (G_{RX}) or degraded by cable losses (CL_{RX}) before it reaches the receivers demodulator with a final signal strength (P_{RX}).

The individual stages can be balanced with:

$$P_{RX} = P_{TX} - CL_{TX} + G_{TX} - PL + G_{RX} - CL_{RX} \quad (1)$$

If P_{TX} and the electronic components are kept constant, the received signal strength depends only on the path loss which is a function of the current exterior conditions. Multiple mechanisms influence path loss. Engineers and researchers have tried to capture the effect in models. Free space path loss (PL_{FS} [dB]) – path loss in a perfect vacuum only as a function of frequency (f[MHz]) and distance (d[km]) - is one of the basic criteria, thus it is common to calculate it as an initial reference assessment (ITU, 2019):

$$PL_{FS} = 32.4 + 20 * \log_{10} f + 20 * \log_{10} d \quad (2)$$

However, this formula is not suitable for obstructed environments such as cities. Adjustments are often implemented through empirical regression, since the environment is just too complex for analytical models (Jorke *et al.*, 2017, p. 5). Aside from static obstructions by buildings and vegetation, environmental conditions, random effects like

people walking through the path or objects or cars obstructing the line of sight contribute to path loss. This results in a location-specific distribution of deviation values around a mean path loss. The mean path losses for three cities (Oulu in Finland (Petajajarvi *et al.*, 2015 - 2015), Dortmund (Jorke *et al.*, 2017) and Freiburg in Germany (result of this thesis)), along with the theoretical free space path loss are depicted in Figure 2.2. Not only is there a notable range among the cities, but – illustrated by the gap between mean path loss and free space path loss - there is also a significant amount of path loss caused by exterior influences, especially at lower distances.

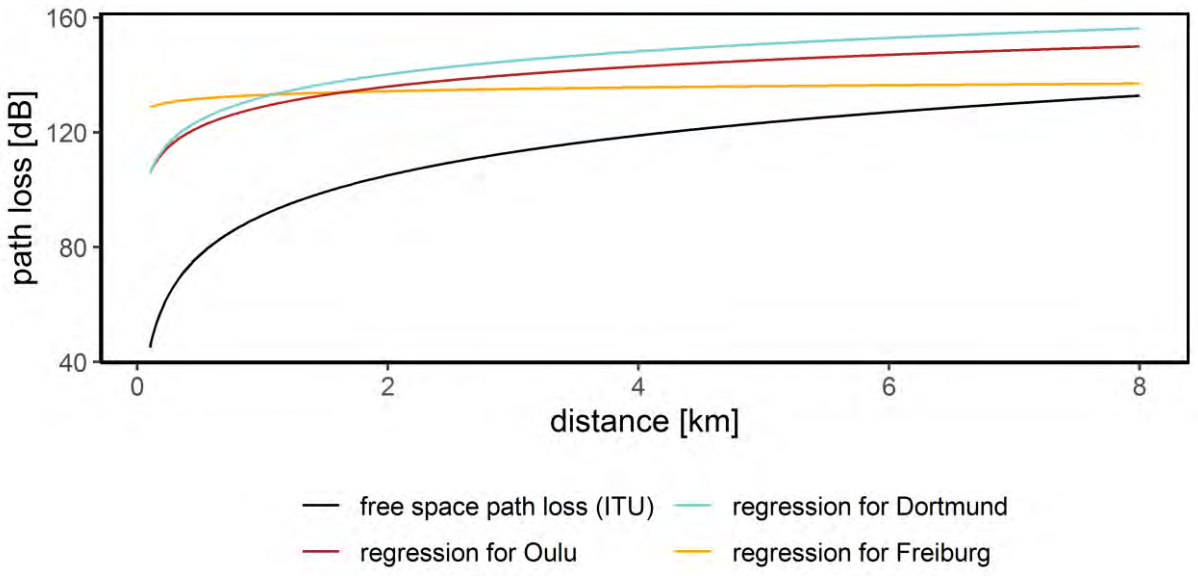

Figure 2.2: Mean path loss calculated for three cities along with free space path loss according to ITU-R for 868 MHz.

These influencing factors are complex and cannot be captured and assessed entirely with today's methods. Some research groups have found that it is possible to deduce the state of the environmental conditions from path loss; specifically, they managed to infer precipitation rates from path loss of microwave links from the communication network of cellphone towers (Messer, Zinevich and Alpert (2006), Leijnse, Uijlenhoet and Stricker (2007), Zinevich, Messer and Alpert (2009), Chwala *et al.* (2012), Doumounia *et al.* (2014), Overeem, Leijnse and Uijlenhoet (2016), Uijlenhoet, Overeem and

Leijnse (2018)). However, also other influences play a significant part and must be taken into account for a full understanding of the mechanism. Hence, the theory of the most notable of those circumstances will be outlined in the following. Additionally, assessments of researchers regarding the impact of the environmental parameters on experimental and real-world deployments of wireless sensor networks (WSN) will be presented.

2.1.2 Causes of Path Loss

2.1.2.1 Obstruction

The most influential property of a transmitter receiver link is the degree of obstruction of the space between them. There are two main effects of obstruction: first, parts of the radio wave might be reflected or diffracted by objects on their way and shifted in phase relative to the original wave (López-Vicario *et al.*, 2014). A phase-shifted signal might be canceled out by a signal in phase (a phenomenon called multipath-fading (Michalek *et al.*, 2015)) or even constructively enhance the power of the original signal if both signal parts arrive in phase (Aref and Sikora, 2014, p. 20).

The second effect is absorption by matter. Both effects are commonly referred to by the degree of clearance of the Fresnel zones (Crane, 2003). As illustrated in Figure 2.3, the space between the two link terminals is specified as Fresnel zones. These are imagined elliptical areas around the link with foci on the locations of transmitter and receiver. The greater the distance between the two endpoints, the longer the radius of the Fresnel zone needs to be, thereby requiring more space. The Fresnel zone is divided into parts according to their influence on the signal transmission. The first Fresnel zone, the innermost region, is crucial for a successful link since most of the transmission energy travels within this zone. The second and third Fresnel zones surround the first Fresnel zone but exclude the space of the respective previous zone and therefore contribute less to the path loss. Thus, especially objects inside the first Fresnel zone reduce the signal strength. Hence, it is common to place the link endpoints in high elevation

to keep the space of the first Fresnel zone as free as possible (Anastasi *et al.*, 2004). If the first Fresnel zone is free, the link is commonly classified as line-of-sight connection, in contrast, when it is obstructed it is classified as non-line-of-sight connection (López-Vicario *et al.*, 2014).

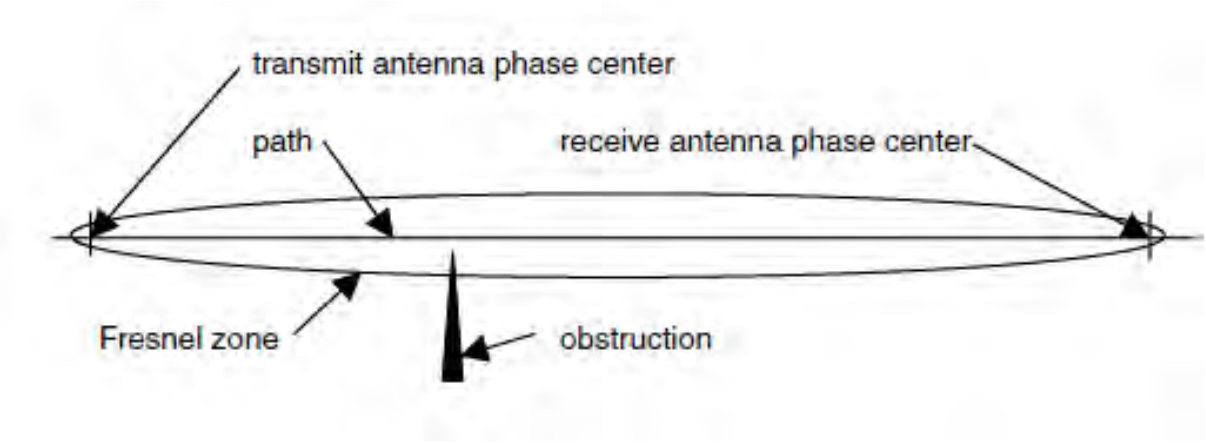

Figure 2.3: Concept of Fresnel zones (Crane, 2003).

For real-world networks, obstruction of the Fresnel zones is unavoidable due to the deployment of the transmitters in an urban environment. Each signal will travel through buildings, trees and even through people. While some of these obstructions are permanent, e.g. buildings, others might evolve dynamically during the time of the experiment. Examples are construction sites, the canopy growth of a tree in the spring season or even daily patterns like opening and closing blinds of a window (Crane, 2003). Since it is impossible to quantify all obstructions in the analysis of the data, it can be difficult to filter the effect of dynamic obstructions while investigating environmental impacts. Wennerstrom *et al.* (2013) stated that there are diurnal and slower moving seasonal cycles in the overall performance of outdoor WSN. For instance, in their small range network, the packet reception ratio (PRR), i.e. the ratio of successful transmission, was higher in the nighttime than during the daytime. They suspect "meteorological conditions" which will be discussed in the following sections.

First, the origin and potential impact of "rain fade" will be presented in section 2.1.2.2. The effect of humidity, less influential but still noticeable, will be discussed in section

2.1.2.3. Temperature which does not directly contribute to path loss but rather on the electronical parts has been identified as a major contributor as will be shown in section 2.1.2.4. Finally, the potential and implications of the change of vegetal canopy will be presented in section 2.1.2.5.

2.1.2.2 Rain Fade

2.1.2.2.1 Physical Background

When an electromagnetic signal is travelling through rain, it may lose power due to two mechanisms: absorption and scattering. On the one hand, a part of the energy is absorbed by the raindrops and transformed into heat. If the wavelength is above 1 mm, the polar nature of the water molecules – hence, an interaction between molecules - is more important, if it is below 1 mm, resonance absorptions within the water molecules are more pronounced (Oguchi, 1983).

On the other hand, when an incident planar wave hits a drop, it induces a transmitted and a scattered field. This can be mathematically described as Rayleigh- and as Mie-scattering (Okamura and Oguchi, 2010). Since scattering can happen in all directions the wave's energy is reduced when it reaches the receiver. Scattering depends on drop radius, drop shape, permittivity (a function of temperature) and frequency (Cermak *et al.*, 2004). Each drop on the path of a radio wave attenuates the radio beam, resulting in a total path attenuation as the sum of the attenuation caused by all raindrops (Medhurst, 1965).

Further, not only the different loss mechanisms need to be considered but also the type of precipitation: raindrops attenuate radio waves at a much higher rate compared to fog or clouds with the equivalent water content (Crane, 2003). Crane (2003) sets the minimum frequency where the rain attenuation effect becomes significant at 6 GHz, while Medhurst (1965) goes as low as 2 GHz. Summarizing the different attenuation factors, attenuation increases with frequency and number and size of raindrops

(Overeem, Leijnse and Uijlenhoet, 2011) as depicted in Figure 2.4: Typically, attenuation is measured at 1 dB increments. Even for a heavy precipitation event of 25.4 mm/h, attenuation for 1 km links is probably only detectable for frequencies of approx. 12 GHz and higher. Uijlenhoet, Overeem and Leijnse (2018, p. 3) summarize the relation:

"1. the harder it rains, the stronger the specific attenuation at a given frequency;

2. the higher the frequency, the stronger the specific attenuation at a given rain rate."

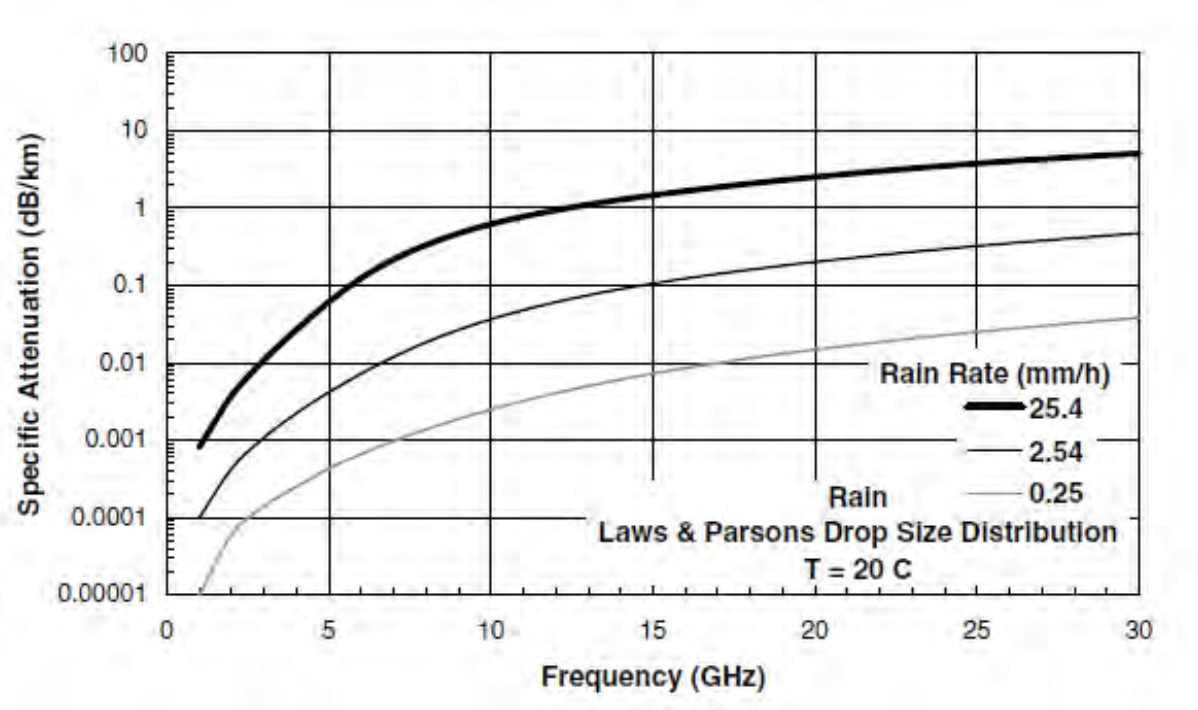

Figure 2.4: Specific attenuation caused by rainfall (Crane, 2003). Given a attenuation measuring resolution of 1 dB, attenuation caused by heavy precipitation events of 25.4 mm/h can only be detected for 1 km links of frequencies 12 GHz and higher.

2.1.2.2.2 Calculation of Rain Attenuation

The method for the estimation of rainfall rates from radio attenuation generally follows three steps: First, the existence of significant attenuation at the respective frequency needs to be confirmed. Then, since there are other effects which contribute to path loss, a procedure has to be chosen to reliably identify the portion of the attenuation that is caused by rain. Finally, the rain rate is calculated from the attenuation.

For the second step, many different methods have been developed in the field of microwave links. Most of them include the determination of a baseline of path loss from the dry periods. If a link or better multiple links in the same area experience path loss higher than the baseline, this period is identified as wet period. This deviation from the baseline can be based on correlation (Overeem, Leijnse and Uijlenhoet, 2011) or based on standard deviation (Schleiss and Berne, 2010)or by recognizing specific patterns of attenuation in sub-frequencies (Chwala *et al.*, 2012). Another approach makes use of dual polarized links which transmit radio waves simultaneously in two polarizations. The differential signal can be used to identify rainfall events: The deviation of the signal strength of the vertical and horizontal polarizations can only be caused by the diameter of the traversed body of water which is different due to the falling motion of the raindrops (Chwala *et al.*, 2012).

After the wet periods have been identified, the rain rates can be calculated from the attenuation. This is done using an empirical power law for a uniform rainfall event on a given point (Olsen, Rogers and Hodge, 1978). Here, the specific attenuation k [dB/km] depends on the rainfall intensity R [mm/h] and the factor and exponent c and d, which are functions of frequency and rain properties:

$$k = c * R^d \tag{3}$$

Since a wave travels along a path and experiences multiple attenuations, the integral of the point attenuations along the path x from 0 to L must be formed for the total attenuation A [dB]:

$$A = \int_0^L k(x)dx \tag{4}$$

Substituting equation (3) here gives

$$A = c * \int_0^L R(x)^d dx \tag{5}$$

For a given total attenuation A, equation (5) can now be inverted to yield the path-averaged precipitation but this is not easily feasible due the presence of exponent d. In Uijlenhoet, Overeem and Leijnse (2018) it is stated that for frequencies around 30 GHz d is nearly 1, therefore equation (5) is:

$$A = c * \left[\int_0^L R(x)\, dx\right]^d \tag{6}$$

After dividing both sides by L and inverting the formula the path-averaged rain rate $\bar{R}$ [mm/h] can be calculated from the path-averaged specific attenuation $\bar{k}$ [dB/km] with the two factors $a = 1/c)^{1/d}$ and $b = 1/d$ (Uijlenhoet, Overeem and Leijnse, 2018):

$$\bar{R} = a * \bar{k}^b \tag{7}$$

Any spatial nonuniformity along the path cannot be distinguished from one link only. Instead, the path-averaged attenuation of multiple links has to be evaluated together (Olsen, Rogers and Hodge, 1978, p. 318).

While this derivation is common and valid for microwave links, it does not hold for lower frequencies where $d \neq 1$. Hence, Doumounia *et al.* (2014) suggest to use a similar approach but recommend to adjust c and d using an empirical method for frequencies where d $\neq 1$. C and d can be calculated from empirically developed formulas or found in lookup tables. They are available for many different frequencies starting at 1 GHz (ITU, 2005).

A second approach to the calculation of the rain rate is the analytical method which considers the interactions between hydrometeors and radio signal. Detailed information about drop size, shape, orientation and temperature would theoretically allow to calculate the attenuation of each drop and sum it up for all drops along the signal path (Medhurst, 1965), but such information usually is not available. Hence, a number of statistical models are employed for the design of attenuation resistant radio links (Crane, 2003). Raindrop distributions play an important role in these models and are discussed widely in the respective scientific community (Crane, 1996). The level of

detail can be increased infinitely, if the influence of direction and strength of wind gusts on the spatial variability and size of raindrops is considered (Medhurst, 1965).

The specific attenuation of radio waves calculated with equation (3) for 1 GHz, 2.5 GHz and 5 GHz are depicted in Figure 2.5. These frequencies are the ones closest to those used in this thesis (868 MHz, 2.4 GHz, 5 GHz) where literature values for c and d were available. As already shown in Figure 2.4, the attenuation according to the ITU equation of the frequencies of concern is minimal other than for extremely high rainfall intensities which will unlikely to occur naturally for longer periods.

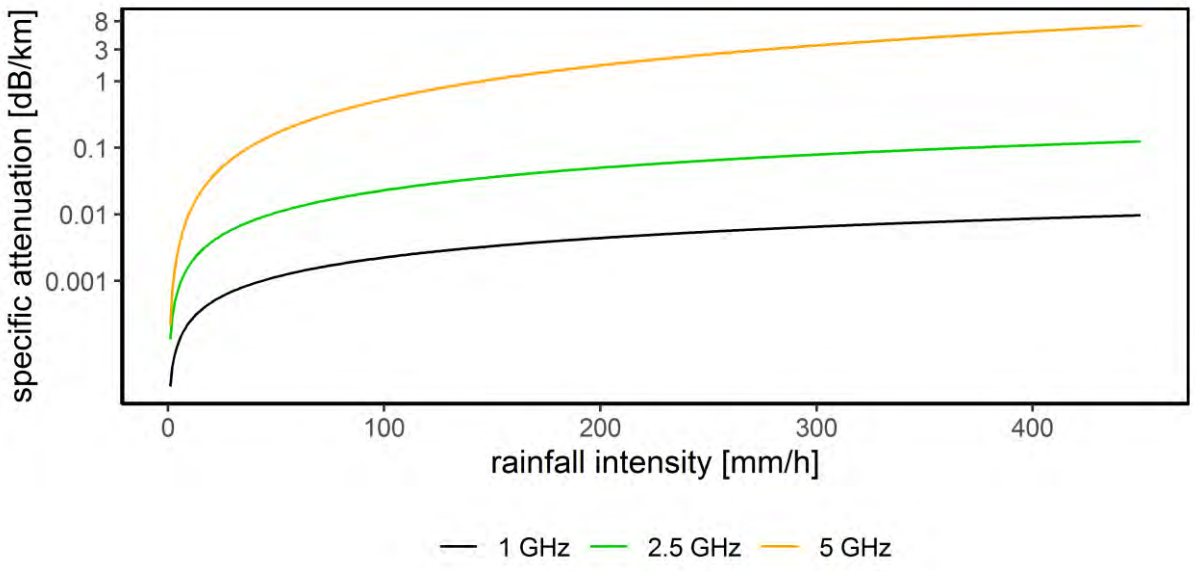

Figure 2.5: Specific attenuation of three low frequencies according to ITU. Heavy rainfall of 25 mm/h cause modelled specific attenuations of 0.0006, 0.005 and 0.05 dB/km for 1, 2.5 and 5 GHz respectively.

2.1.2.2.3 Reports of Rain Attenuation in WSN

Most microwave links operate at 10 to 50 GHz. When it comes to experimental WSN which operate at frequencies typically much lower than those, the science community did not reach consensus about the impact of precipitation. The following reports have used the frequencies which are within the range of those used in this thesis.

Anastasi *et al.* (2004) (2.4 GHz) observed severe degradations of the radio signal: the signal range dropped from 55 m to 10 m during foggy or rainy conditions. Capsuto and

Frolik (2006) (2.4 GHz) also experienced a decrease of signal strength during precipitation events, so did Tatsis *et al.* (2018) (2 GHz), although their experiment was based on very few observations. They used a high accuracy system to detect minimal attenuation values and found an exponential relationship between rainfall and attenuation. Christofilakis *et al.* (2018) were using the same system and claimed to be able to detect precipitation rates as low as 0.2 mm/h. Fang and Yang (2016) tested the vulnerability of mobile communication networks to weather conditions by analyzing the signal strength of connections from common cell phones to telephone towers and found that monsoon events severely degrade the signal strength. Rankine, Sanchez-Azofeifa and MacGregor (2014) (2.4 GHz) have also observed a signal degradation following storm events, but did not actually quantify the effect. Alonso *et al.* (2017) (5.2 GHz) and Bri *et al.* (2012) (2.4 GHz) also reported light impacts by rainfall but found the effect negligible. The only researchers in the range of LoRa-frequencies (868 MHz) who noticed a decrease in link quality after rainfall events are Wark *et al.* (2008) (915 MHz). On the other hand, Thelen, Goense and Langendoen (2005) (433 MHz) saw an improvement of signal strength which they contributed to the increased humidity coming along with rain. Boano and Brown *et al.* (2010) (2.4 GHz) reported only a light impact of rainfall, but speculated that the effect might increase with higher intensities and might even endanger weak links at the border of their communication range. Wennerstrom *et al.* (2013) (2.4 GHz) criticized most of the aforementioned studies for imperfect methodologies and concluded that there was no observable effect of rain on signal strength at all. Instead, they contributed most of the observed signal degradations to temperature effects which will be discussed in chapter 2.1.2.4.

2.1.2.2.4 Wet Antenna Attenuation and Wet Surfaces

Next to the direct attenuation by rainfall there is also a secondary effect which often comes along with precipitation events. Markham, Trigoni and Ellwood (2010) (2.4 GHz) observed a significant negative correlation between signal strength and rainfall

and also included the presence of wet surfaces subsequent to a precipitation event into their evaluation. While Michalek *et al.* (2015) (2.1 GHz) rejected a significant cause of rainfall for signal degradation, they explained that a secondary effect, the creation of wet surfaces (roofs, foliage, puddels,…) might act as reflective planes consequently increasing scattering and a reduction of signal strength.

This wet surfaces effect might play an important role for signal degradation which is less dependent on frequency: liquid water has a high relative static permittivity of ~80 at 20 °C. If water pools between transmitter and receiver (such as on the transmitter housing), it creates a reflective plane (Michalek *et al.*, 2015). Further, it might act as a capacitive loading for the antenna and therefore improve or decrease the signal strength (Markham, Trigoni and Ellwood, 2010). The path loss introduced by snow covered ground can also be significant (Cheffena and Mohamed, 2017), however it will not be considered in this thesis.

Additionally, depending on design, the antenna of either side might become wet during rainfall and might stay like that for a certain period. This could cause unpredictable changes in the antennas radiation pattern and the signal strength (Luomala and Hakala, 2015) and has been reported to cause systematic overestimations of rainfall in the field of microwave links (Fencl *et al.*, 2017). This phenomenon - called wet antenna attenuation - can be considered by incorporating constants into the models describing the relation between rainfall intensity (Overeem, Leijnse and Uijlenhoet, 2011).

2.1.2.3 Humidity

Atmospheric gases such as water vapor and oxygen can cause significant attenuation of radio waves at higher frequencies. There are attenuation peaks at 22.3, 50, 70 and 183 GHz (Figure 2.6); the regions between these are called atmospheric windows and

are exploited by common transmission schemes such as earth to satellite communication and remote sensing. On the paper waves at lower frequencies benefit from very low to nil attenuation (Crane, 2003).

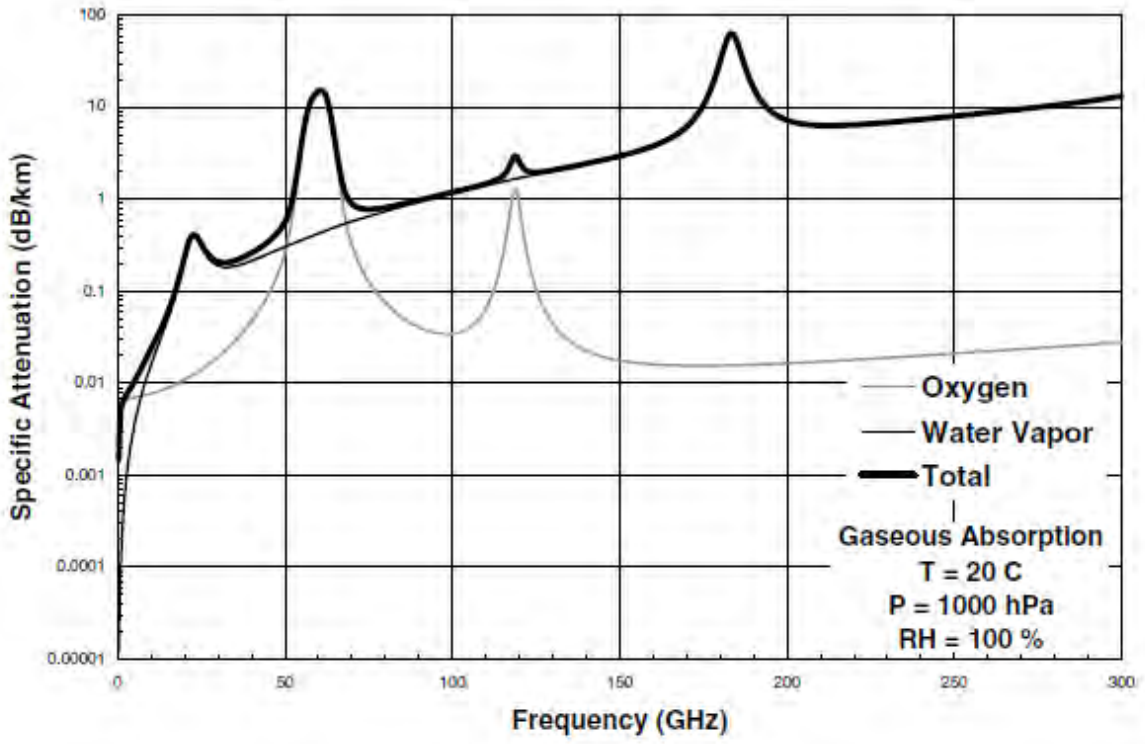

Figure 2.6: Specific attenuation caused by atmospheric gases (Crane, 2003).

The practical experiences made by research teams are more ambiguous: while some found a negative correlation between signal strength and humidity (Wennerstrom *et al.* (2013) and Bri *et al.* (2015), both 2.4 GHz), others found a positive correlation (Thelen, Goense and Langendoen (2005), 433 MHz). Luomala and Hakala (2015) (2.4 GHz) even reported a conditional correlation (positive correlation above 0 °C and negative correlation below 0 °C) and Anastasi *et al.* (2004) and Rankine, Sanchez-Azofeifa and MacGregor (2014) (2.4 GHz) no correlation at all.

Because of the close relation between temperature and humidity, relative humidity is regarded as skewed and should not be considered (Wennerstrom *et al.*, 2013). Luomala

and Hakala (2015) state that even absolute humidity and should only be taken into account under high humidity conditions.

Absolute humidity (AH[g/m³]) can be calculated as a function of temperature (T[°C]) and relative humidity (RH[%]) (Luomala and Hakala, 2015):

$$AH = 216.7 * \left[\frac{\frac{RH}{100\ \%} * 6.112\ hPa * e^{\left(\frac{17.62 * T}{243.12\ °C + T}\right)}}{273.15 + T} \right] \quad (8)$$

Condensed water vapor in terms of fog and clouds can also cause significant attenuation at higher frequencies but not for frequencies below 10 GHz (see Figure 2.7) (Crane, 2003).

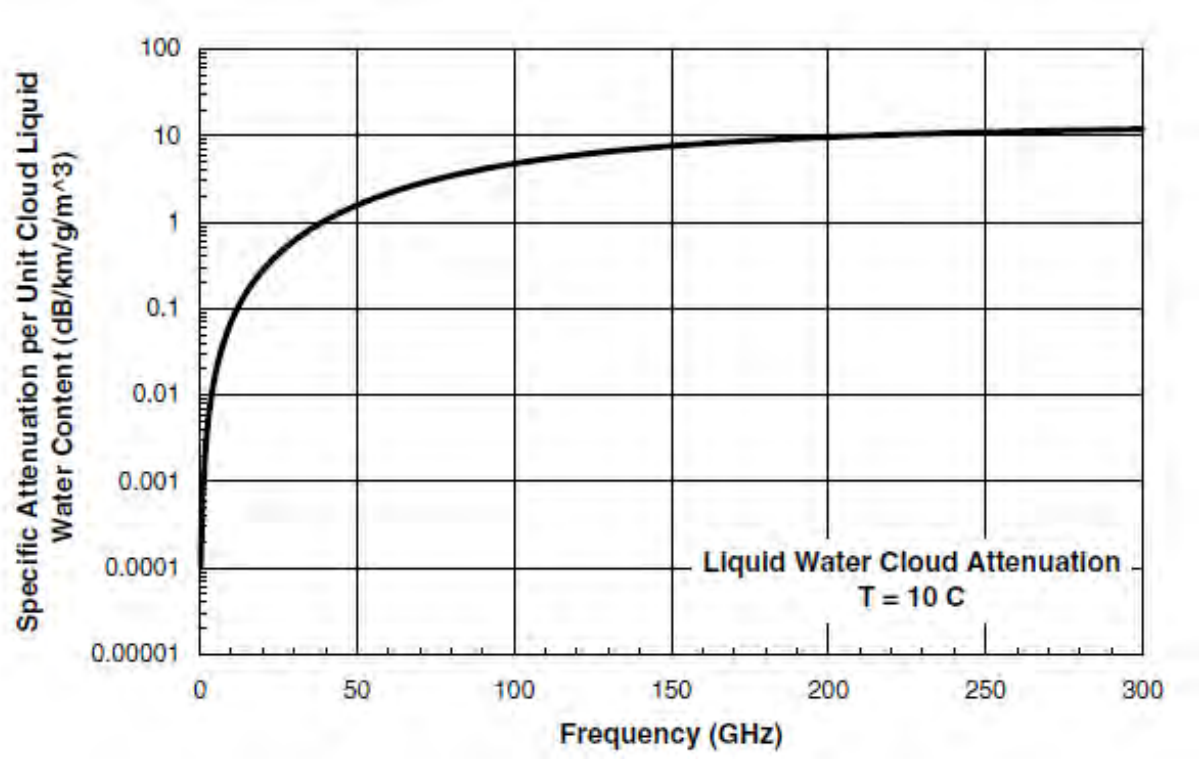

Figure 2.7: Specific attenuation caused by cloud and fog (Crane, 2003).

Nonetheless, Anastasi *et al.* (2004) (433 MHz) report a severe performance degradation during foggy weather. In contrast, Boano and Brown *et al.* (2010) did not observe a significant impact of thin or thick fog on their 2.4 GHz sensor network.

2.1.2.4 Temperature

Although temperature does not directly affect the propagation of radio waves, it can contribute to the cable losses. Thereby, the received signal strength is reduced.

Higher temperatures increase the resistance of the electronic conductors and cause current leakages in semiconductors. Thereby, current and power of the signal on its way through the electronical components of receiver and transmitter are reduced (Boano *et al.*, 2013). At the extreme, the signal strength is decreased so much that the radio cannot successfully distinguish between signal and environmental noise (Bannister, Giorgetti, and Gupta, 2008).

This phenomenon has been described for the HopeRF RFM95 LoRa radio (equivalent to the chip used in this thesis) by Cattani, Boano and Römer (2017) where they measured a reduction of 6 dB for the temperature range of 0 – 60 °C. Since the decrease has also been reported for many other devices and frequencies (2.4 GHz: Boano *et al.* (2013), Wennerstrom *et al.* (2013), Bannister, Giorgetti, and Gupta (2008); 433 MHz: Thelen, Goense and Langendoen (2005)), it appears to be a cross-platform effect. The temperature impact on LoRa-devices is also confirmed by Iova *et al.* (2017) who measured a drop in communication range from 550 m to 270 m due to a change of temperature from 20 °C to 36 °C.

This effect is most hazardous for links which are on the edge of connectivity (Wennerstrom *et al.*, 2013).

Packets might either not be received at all or their content might be corrupted (Cattani, Boano and Römer, 2017). It is unclear if the impact is more severe if the transmitter or the receiver has an increased temperature: While the receiver was heated, Boano *et al.* (2013) observed a slightly stronger decrease of signal strength than for a heated transmitter. However, if the receiver is heated, not only the signal of the transmission is decreased but also the signal of the environmental noise. Therefore the ability of the receiver to distinguish between transmission and noise is not affected. Hence, while a heated receiver will measure lower signal strengths, the stability of the link is

not necessarily affected. The most severe reduction has been found if both receiver and transmitter are heated (Boano *et al.*, 2013).

The only study which did not concur this relationship is the 15 years old paper by Anastasi *et al.* (2004) who operated at 433 MHz. This might also be based on the fact that their setup was subject moderate ambient temperatures.

Boano *et al.* (2013) report daily and seasonal differences caused by temperature which concurs with the diurnal patterns observed by Wennerstrom *et al.* (2013) mentioned in the introduction of this section. Their experiment took place in Sweden where the measured temperature ranged from -22.2. °C to 61.3 °C. They even suggest to use dynamic transmission powers to respond to low temperatures in order to save energy (Boano and Tsiftes *et al.*, 2010).

2.1.2.5 Vegetation

Path loss induced by vegetation depends on six conditions: the number of vegetal obstacles along the path, the species, season, amount of water in and on the leaves (for higher frequencies) and the height and orientation of the propagation path (Crane, 2003).

Rankine, Sanchez-Azofeifa and MacGregor (2014) (2.4 GHz) state that for lower frequencies, the signal mainly does not get absorbed by the plant matter but reflected or scattered by the leaves and branches of vegetation since the wavelength does not coincide with the plants material. Thiagarajah *et al.* (2013) (2.3 GHz) emphasized the negative impact of vegetation especially after rainfall events, since wet foliage attenuates radio signals even stronger.

Thelen, Goense and Langendoen (2005) (433 MHz) observed a reduction of the communication range from 23 m to 10 m while a potato field was flowering. They also did not directly link the attenuation to the tissue of the plants. Instead, they referred a change of the reflection coefficient to the canopy layer - which also came along with

higher humidity which they suspected to facilitate transmission greatly.

Iova *et al.* (2017) (and also Ahmad *et al.* (2018)) (868 MHz) found a substantial drop in link range by an order of magnitude: from 450 – 550 m to 50 -90 m maximum range when the network was moved into the forest. However, once the network was deployed in the forest, they noticed a constant packet delivery ratio which indicates that the vegetation might be considered a static parameter when considered in a limited temporal frame. This is supported by Yim *et al.* (2018) (915 MHz), who reported short connectivity ranges in a tree plantation but no impact from other environmental factors. Marfievici *et al.* (2013), who compared node deployments in open and forest environments, also observed a signal strength degradation caused by vegetation (also depending on tree species).

2.1.3 Summary of the Discussion of the Environmental Impact Factors

Concluding the theory and experiences of the environmental factors impacting the signal strength of radio waves, it becomes clear that the severity of the effects depends mainly on frequency and distance. In theory - except for the heat effect - the total attenuation always relates to the amount of medium the radio wave has to pass. The lower the frequency, the lower the specific attenuation caused by obstruction, vegetation, humidity and rainfall that has to be expected.

Nonetheless, reports from practical applications using WSN are unequivocal. Especially concerning humidity and precipitation, the conclusions cover a wide spectrum: degradations of signal strength, an increase of signal strength and no effect at all have all been reported.

2.2 Radio Networks

Radio networks consist of two or more devices communicating by radio waves. They differ in frequency, protocol and network topology and are more or less ubiquitous in

the more densely populated parts of the world. Basically any network is a candidate for precipitation measurements. However, only those two which are utilized in this thesis – LoRaWAN and Wi-Fi - will be described in the following section.

2.2.1 LoRa and LoRaWAN

LoRa is a proprietary radio modulation technology owned by the company Semtech. Chirp spread spectrum modulation – the physical layer - is its key component. In the upcoming age of Internet of Things LoRa is becoming increasingly popular and widespread across the globe. One reason for its success is the availability of low-power, long-range, low-cost and low-throughput end devices which can be deployed in high numbers. Their range can reach up to several km in urban areas and up to hundreds of km under line-of-sight conditions. Network designers have the choice between either high range and low throughput or lower range and higher throughput: multiple transmission properties can be adjusted which all trade range (i.e. sensitivity) for transmission interval (Boano, Cattani and Römer, 2018).

LoRaWAN on the other side is the MAC layer of the framework. It is an open standard set by the LoRa-Alliance and organizes the network topology (Augustin *et al.*, 2016). Due to the high range of the links, LoRaWAN follows a simple star network topology (IMST GmbH, 2018). This reduces the organizational load and the requirements for the nodes since the packets do not have to be forwarded through a multihop mesh scheme (Ismail, Rahman and Saifullah, 2018). The nodes can therefore be countless low-power end devices which communicate asymmetrically with one or multiple gateways placed at strategic positions (Boano, Cattani and Römer, 2018). The gateways serve as backhauls connected to the servers via Ethernet or 3G which allows for much higher data rates than the LoRa transmission (Augustin *et al.*, 2016). Hence, the end devices can remain cheap and powerless, while the load of computation and transmission is shifted to the powerful gateways (Cattani, Boano and Römer, 2017). It is also

possible and desired to deploy multiple gateways in a "star-of-stars-fashion" to increase redundancy. One message can be received by multiple gateways and forwarded to the servers where it is deduplicated and decoded. On request, the server can also schedule downlink messages to the nodes (Augustin *et al.*, 2016).

The chirp spread spectrum modulation which is employed for LoRa allows the signal to travel over long distances. In a transmission sent with this modulation, the signal spreads over a range of frequencies over time, forming an "upchirp" or a "downchirp" (Boano, Cattani and Römer, 2018). The direction of the chirp and intermissions in between represent a "symbol", i.e. a pattern that conveys the information. Due to the characteristic shape of chirps, this modulation can be successfully demodulated, even if the signal is weak, i.e. for a signal power of up to 20 dB below the environmental noise floor (Cattani, Boano and Römer, 2017). The result of one of these conversions is given in Figure 2.8. The bottom right graph clearly shows the characteristic chirps, with the preamble consisting of ten up-chirps (the last up-chirps beginning seems to be missing) followed by two down-chirps. The frequencies used are the free industrial, scientific and medical (ISM) bands. In Europe, those are 433 and 868 MHz and while there are others in other regions of the world, they are all sub-1-GHz frequencies (Boano, Cattani and Römer, 2018). These bands are regulated regarding maximum transmission power and duty cycle. Duty cycle denotes the amount of transmission airtime a single device is allowed to use. If the duty cycle of a device is 1%, it has to wait 100 times the duration of its last transmission before it can transmit again on the same channel (Augustin *et al.*, 2016).

The transmission power is capped by the band regulations and can be adjusted between -4 and +20 dB (Boano, Cattani and Römer, 2018). A higher transmission power reduces the signal-to-noise-ratio but consumes more energy (Cattani, Boano and Römer, 2017). The three most characteristically parameters of a LoRa transmission are bandwidth, spreading factor and coding rate. The bandwidth is the range of frequencies, across which the chirps vary. A smaller bandwidth - so to say, a finer resolution - increases

the visibility of a signal. A wider bandwidth means less airtime but also less sensitivity (Boano, Cattani and Römer, 2018).

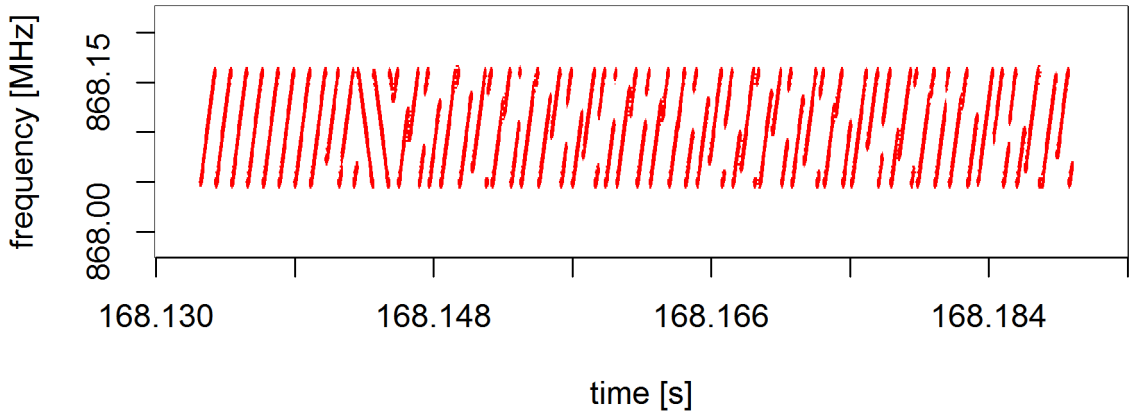

Figure 2.8: Example of a LoRa-packet. The antenna excitations have been transferred using fast Fourier transformation with a Hamming window. The characteristic first ten upchirps (increasing frequency), followed by two downchirps represent the preamble, identifying the signal as a LoRa-transmission.

The spreading factor (SF) can range between 7 and 12 and represents the resolution of the data modulation into symbols. A symbol is a unique combination of frequency sweeps and jumps that represents an interpretable value after demodulation. Each symbol is divided into 2^{SF} chips. The higher the spreading factor, the more chips and the higher is the resolution that a symbol is presented in. With a high SF, a lower receiver sensitivity is required, just like somebody listening to somebody else speaking quickly (low spreading factor) versus somebody speaking slowly (high spreading factor). A high spreading factor increases the signal-to-noise-ratio, but also leads to more airtime (Boano, Cattani and Römer, 2018). LoRa uses a forward error correction algorithm which is supposed to reduce decoding errors and to increase its resilience to packet corruption. This is set in the coding rate. It is advised to use a higher coding rate in radio traffic congested areas (Boano, Cattani and Römer, 2018) but this comes along with longer transmissions (more airtime) and higher energy consumption (Cattani, Boano and Römer, 2017). Iova *et al.* (2017) have found that setting these three

parameters is key for successful transmissions, unlike previous WSN where network engineers generally simply increase the transmission power. The LoRaWAN protocol even has an implementation for an automatic dynamic adaption of these parameters to the environmental conditions and retransmission of failed packets (Augustin *et al.*, 2016), which would also represent the most energy efficient mode of operation (Cattani, Boano and Römer, 2017).

2.2.2 Wi-Fi

Nowadays, Wi-Fi-networks which operate at 2.4 and 5 GHz can be found in many public and private buildings. However, due to the low range transmitter and receiver communicate in most applications within the same building. Its potential for environmental monitoring is therefore not obvious unless in situations where high power public Wi-Fi-gateways provide long range networks. E. g. a nationwide 5 GHz-network used as Monsoon alarm system (Labuguen *et al.*, 2015). Nonetheless, since Wi-Fi capable devices are so commonly available an investigation towards applicability might beuseful.

5 GHz trades higher data rates (due to the increased frequency) for range. While 2.4 GHz has ranges of up to 100 m outdoors, the 5 GHz is ranked only at one third of this distance. The higher the frequency and therefore the shorter the wavelength, the more attenuation by obstacles such as walls and people is expected (Crane, 2003).

3 Knowledge Gap and Research Question

Given the need for new means of precipitation measurements and considering the success of research projects in the field of microwave links (Overeem, Leijnse and Uijlenhoet, 2016), the question arises whether this principle could be transferred to other widely spread radio networks. Among such networks could be the in urban areas omnipresent Wi-Fi-networks and - in the upcoming age of internet of things - LoRaWAN-networks. LoRaWAN-networks stand out through their long range which provides them with the same coverage as Wi-Fi, at least in cities where there are already LoRaWAN-communities. Especially in countries where rainfall monitoring networks are sparse or even shrinking, a transfer of the method would have the potential to facilitate and improve the work of meteorologists, hydrologists and in general the field of environmental monitoring. Precipitation is the most important input-variable for hydrologic research (Fohrer *et al.*, 2016). Hence, the investigation of any precipitation related process would benefit from a higher accuracy of the rainfall measurements. Even while the deduction of actual rain rates from radio wave attenuation might be not 100 % accurate, it can still help to localize the portion of radar-detected precipitation that actually reaches the ground.
Furthermore, if precipitation was measurable through radio waves on close distances, this method could replace gauges on e.g. experimental sprinkling plots where they inevitably cover a part of the ground and distort the very parameter they were meant to measure.

The technological feasibility remains unclear. While the theory regarding rain attenuation states that no significant rain attenuation is expected for frequencies below approx. 10 GHz, researchers operating WSN at the frequencies in question paint an inconclusive picture of the impact of precipitation. The first objective of this thesis is therefore directed at the question:

1. Do electromagnetic waves with frequencies 868 MHz, 2.4 GHz and 5 GHz in transmission ranges common in widespread radio networks get directly attenuated by liquid precipitation?

With a more precise null hypothesis subject to falsification:

H1: The attenuation caused by rainfall droplets for electromagnetic waves at frequencies 868 MHz, 2.4 GHz and 5 GHz can be identified through the signal strength of the received signal at transmission ranges of up to 10 km for the 868 MHz and ranges of up to 20 m for 2.4 GHz and 5 GHz.

This question focuses solely on the physical effect of radio waves interacting with rainfall droplets and the relevance of this effect for the signal strength measured by a receiver. As it became clear from the theory of radio waves and also from the empirical evidence of experiments conducted with WSN there are many other influences on signal strength, mainly obstruction, distance, temperature (mostly on electronical components of the devices), humidity and the formation of liquid surfaces especially on housings or antennas in the aftermath of precipitation events. Therefore, it is uncertain if, for one, whether rain attenuation can be identified through those exterior effects or, secondly, if radio networks experience an alteration of stability during precipitation events which might not necessarily relate to direct attenuation effects but to a change of other environmental parameters accompanying precipitation events. Therefore, the second research question of this thesis is:

2. Do widely used radio networks suffer a recognizable alteration of connectivity related to rainfall events?

With null hypothesis:

H2: The signal strength of radio networks with frequencies 868 MHz, 2.4 GHz and 5 GHz is significantly different during rainfall events compared to dry weather conditions.

4 Materials and Methods

4.1 Approach

In total, three different experiments were conducted throughout the data gathering of this thesis. Two were experiments under "controlled" conditions at plot-scale while the third experiment can be described as a real-world large-scale deployment.

1. plot-scale experiment, 868 MHz
2. large-scale deployment, 868 MHz
3. plot-scale experiment, 2.4 GHz and 5 GHz

While the plot-scale experiments aimed primarily on research question 1 for their respective frequencies the real-world deployment is an attempt to test research question 2 and an assessment of the hypothesis of research question 1 under real-world conditions.

Since the target parameter, the signal strength, is affected by circumstances a two-pronged comparative strategy for the two laboratory experiments by contrasting in total four states was chosen: a reference setup versus an influenced/altered experimental setup and a reference period versus an experimental period.

The strength of this approach is that the importance of the exterior influencing factors such as temperature or obstacles does not have to be investigated in detail because they would be present in both experimental and reference setup and could therefore be identified and put aside. If the measured values from the experimental setup/period differed significantly from the measurements from the reference setup/period rain attenuation would be rated as existent or non-existent.

In the real-world deployment the urban area of Freiburg was covered as widely as possible under the given circumstances in order to model a real LoRaWAN-network which may be built by the communities in any other city of the world. Here, a black

box approach was pursued, focusing mostly on precipitation and signal strength. Despite environmental temperature (T_{env}), relative humidity (RH), atmospheric pressure (p_{atmos}) and receiver CPU-temperature (T_{CPU}) also being metered, a lot of outside effects where not known or not recorded. Information about changes of vegetation, human and animal interaction with the transmitters were not available and beyond the scope of this thesis.

4.2 Experiment 1, Möhringen: Plot-Scale, 868 MHz

4.2.1 Setup

The experimental site was situated in a forested area close to the settlement Möhringen on a hillslope. The site was equipped with sophisticated metrology devices including lateral flow measurements from three different trenches, in-situ isotope analysis and not less than seven rain gauges measuring throughfall and stemflow. The site was divided in a reference plot and a sprinkling site, where six sprinklers mounted 2 m above ground delivered a spray with an approximate intensity of 15-20 mm/h for 10.5 h. The total duration of the experiment was 29 h.

The setup of the nodes and gateway are depicted in Figure 4.1. The gateway was placed in one of the corners (top left) of the sprinkling plot to maximize the propagation path of the radio waves which should give the attenuation the best chance to become visible in the signal strength.

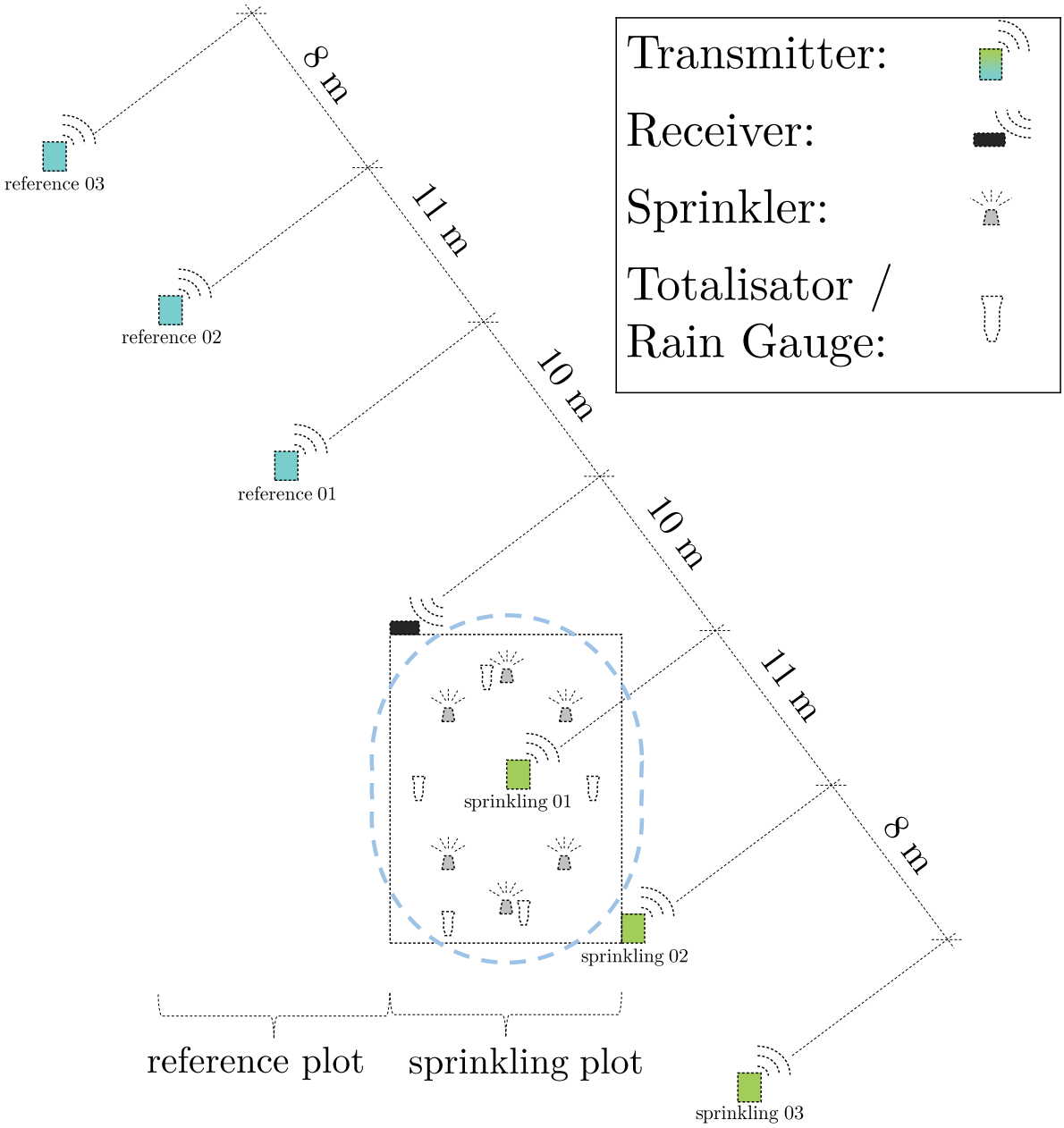

Figure 4.1: Experiment 1, Möhringen: layout of the setup. There was one receiver in the middle of the layout, three reference nodes on a straight line pointing to the top left and three sprinkling nodes on line crossing the sprinkling plot towards the bottom right corner. The sprinkled parameter is depicted by the blue dotted ellipse.

4.2.2 Nodes

In total, 6 Arduino Pro Mini-nodes (for details about devices used in the experiment see appendix B) mounted on poles about 50 cm above the ground were deployed on the site. Three of them were located on the line of sight running through the sprinkling

plot, the other three were located point symmetrically on the extension of the line starting from the gateway and leading away from the sprinkling plot. Thereby, they formed a system of three same-distance-to-the-gateway-pairs of which the data packets of one of them was passing through the sprinkling system while the signal from the other one was passing through unaffected air space and served as reference.

Four of the nodes measured the covariates temperature, relative humidity and atmospheric pressure. These were the two pairs which were at the shortest (10 m, sprinkling and reference 01) and the longest distance (29 m, sprinkling and reference 03) from the gateway as illustrated in Figure 4.1. The last two nodes – the middle pair at 21 m distance to the gateway, sprinkling and reference 02 – did not measure anything but sent a data packet of the same structure as the other nodes but with dummy values which stayed the same throughout the experiment. The LoRaWAN packets are structured in a preamble identifying the packet as LoRaWAN-encoded, a header containing the transmitter identification, packets completeness checking values (CRC) and the actual data values (LoRa Alliance Technical Committee, 2017). In this setup, the header size was 13 bytes while the data (the payload) had 7 bytes. Therefore, the packets sent by these two dummy-nodes where identical throughout the experiment and almost identical between the two nodes. The purpose of these dummy-nodes was to analyze the impact of precipitation on the data-packets before the LoRaWAN-decoding compensates or corrects any signal weaknesses and converts them into actual numbers and letters. Since the LoRa-modulation traverses a range of frequencies, the impact of precipitation might be visible in only a part of this range or the waves might be shifted towards shorter or longer wavelengths, a phenomenon commonly known as red- or blueshift. The raw antenna excitations captured by a software defined radio (SDR) had to be first matched to the packets received by the gateway before they could be associated with a specific node.

The procedure involved the identification of a packet reception event and setting an initial frame around a high percentile of antenna excitations of this event then shrinking

the frame by adjusting the percentile within the initial frame until the frame was equivalent to the expected packet airtime (0.06 seconds).

The lines-of-sight of the nodes to the receiver were all more or less unobstructed except for some leaves dangling from cut tree branches or tree saplings or equipment, e.g. the sprinkler poles. Once per hour, people where crossing the links during readouts of the totalizators.

4.2.3 Gateway

The receiver – the gateway – was placed on the top left corner of the sprinkling plot. Its antenna was mounted on a pole while the gateway itself was stored in its waterproof box in a big plastic bag. The gateway was controlled (i.e. checked for correct functionality) periodically via remote control of its desktop over Wi-Fi. Therefore, the Wi-Fi-card of the gateway was switched on and a router providing the local network was located right beside it in the plastic bag. The router operated at 2.4 GHz. Other than capturing the LoRaWAN-packets, the gateway was also recording its CPU-temperature in 30 s-intervals.

4.2.4 Software Defined Radio (SDR)

The SDR-dongle was plugged in a laptop placed in the plastic bag next to the gateway. Because of RAM- and hard drive-limitations it was not possible to record the antenna excitation during the whole period of the experiment. Instead, apporaximatly every hour, the recording was manually started for 20 minutes. For this, the plastic bag had to be lifted briefly.

4.2.5 Sprinklers and Precipitation Measurements

The sprinkler system consisted of six sprinklers mounted on poles at two meters height. During the experiment, 50 m^3 of water were fed by elevation energy from a big storage

bag located a few hundred meters uphill. The sprinkling intensity was measured by three Hellmann rain gauges on the sprinkling site complemented by two calibrated homemade totalizators. At first the totalizators where read out every hour, later on every two hours.

4.2.6 Computation

Before the actual data analysis the packets received by the gateway and stored on its hard drive had to be decrypted first, using an LoRa-decoder available on the internet (Kirby, 2019). The "precipitation time series", i.e. the mix of natural rainfall and the sprinklers output was converted into a categorical variable of the sprinkler systems state: turned on or off. The timestamp of every data record had to be rounded to the next full minute and the values aggregated so that the measured covariates and the signal strength which came with each data packet, the CPU-temperature and the precipitation would fall together.

The signal strength was then related to the covariates through Spearman-correlation. Spearman's rank correlation is better suited for non-normal distributions, since it converts the absolute values in ranks (Bri *et al.*, 2015). Also, it accounts better for non-linear change rates as it is expected due to the rain attenuation model (Wennerstrom *et al.*, 2013).
Afterwards, histograms of the signal strength of each node and period were created. The analysis was then completed by ANOVA and effect size calculations for each node and period.

The SDR stored the recorded data as i/q-data, which indicates amplitude and phase of a wave in a polar coordinate system (Heuberger and Gamm, 2017). It had to be converted from the time domain to the frequency domain using a Fast-Fourier-Transformation (FFT). "Windowing", the process of aligning the beginning and end of a wave period, is an important mechanism here. The window of shape and size which

gave the best visual results for the identification of a LoRaWAN packet was chosen. The result was a continuous time series for range of the 250 KHz width around the main channel of 868.1 MHz with a resolution of 2 KHz steps. This data did not contain any readable information about the origin of the excitation. Therefore, the antenna excitations had to be matched with the packets recorded by the gateway. Afterwards, all antenna excitations in each sub frequency for each node were extracted, sorted into the sprinkling and reference period and their distributions compared.

4.3 Experiment 2, Vauban: Large-Scale, 868 MHz

4.3.1 Setup

In this "real world" deployment of LoRaWAN, the existing *The Things Network* of Freiburg, Germany was used and extended. The Things Network is a community-based implementation of LoRaWAN that aims to establish a wireless network in as many locations throughout the globe as possible.

In Freiburg, there is a quickly growing *The Things Network* community with currently 24 deployed gateways providing a good coverage. They are mostly operated by private community members and a few tech companies. In addition to these existing gateways a study-gateway was deployed at a strategic position.

24 nodes were placed into this network of receivers. According to the nature of the non-directional transmissions of *The Things Network* each of these nodes broadcasted its data packets into the air regardless if and which gateway would receive it. So – in theory – there would 24 times 24 links between transmitter and receiver, providing a good coverage of the entire city (see Map 4.1).

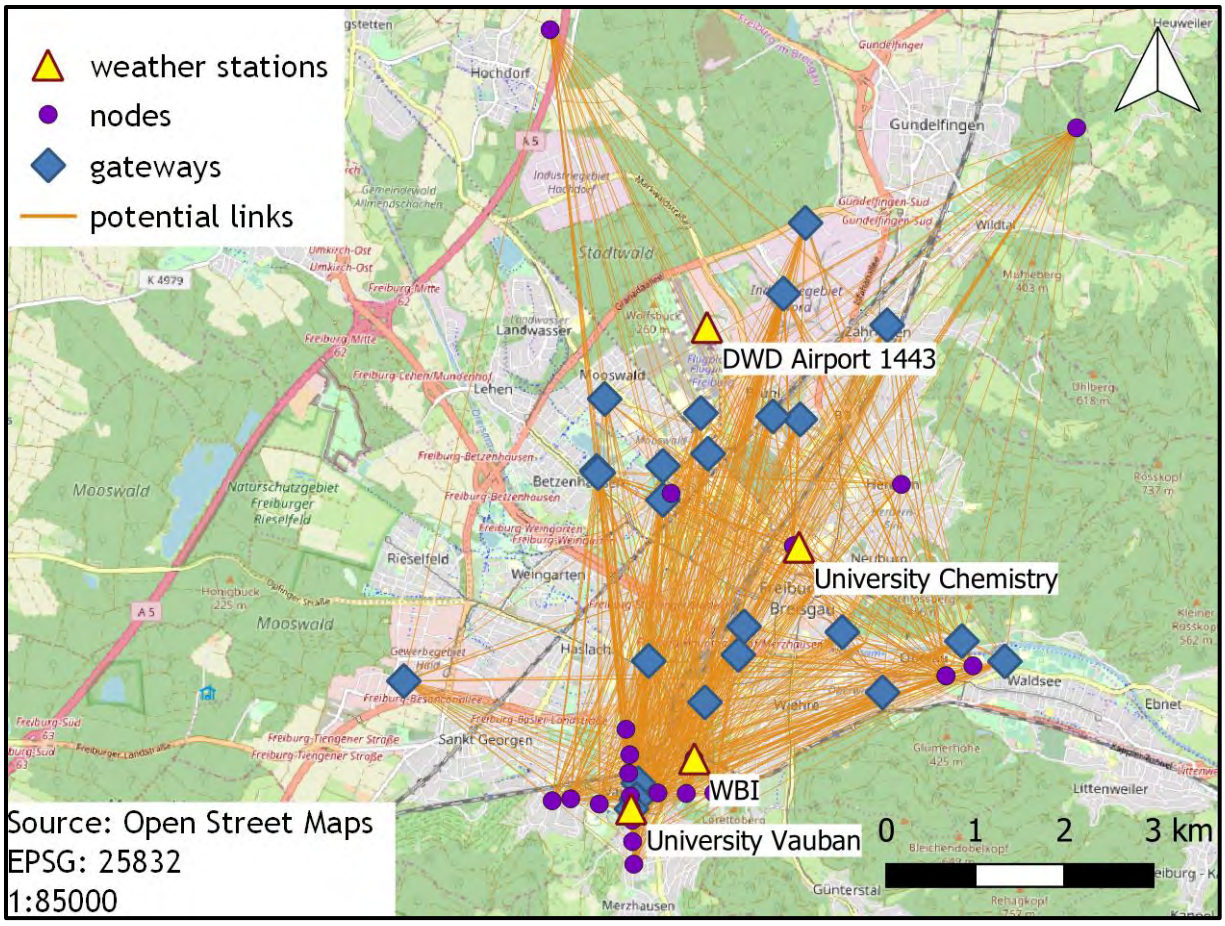

Map 4.1: Experiment 2, Vauban: Potential links assuming perfect connectivity between nodes and gateways for experiment 02.

The deployment lasted 6 months from the beginning of February 2019 till the end of July 2019. Given a transmission interval of three minutes and a perfect connectivity as claimed in the LoRaWAN specifications one would estimate 50 million transmissions. While the transmitted package would be the same for each receiver the connection characteristics would be different.

However, not all nodes were deployed at the same time, some were down due to maintenance and the connectivity was lower than expected.

4.3.2 Nodes

19 of the deployed nodes were Arduino Pro Minis and five were The Things Unos. 15 of the Arduino Pro Minis were placed in a cross shaped geometry in one suburb of the city, Vauban. At the center of the cross was the study-gateway. The nodes were placed

at defined distance intervals which made the categorizing into distance-bins easier and more structured. These intervals were 0 – 250m, 250 – 500 m, 500 – 750 m and 750 – 1000 m. They were positioned in such a way that there would always be three to four nodes in one range interval in regard to study-gateway and a second third-party gateway.

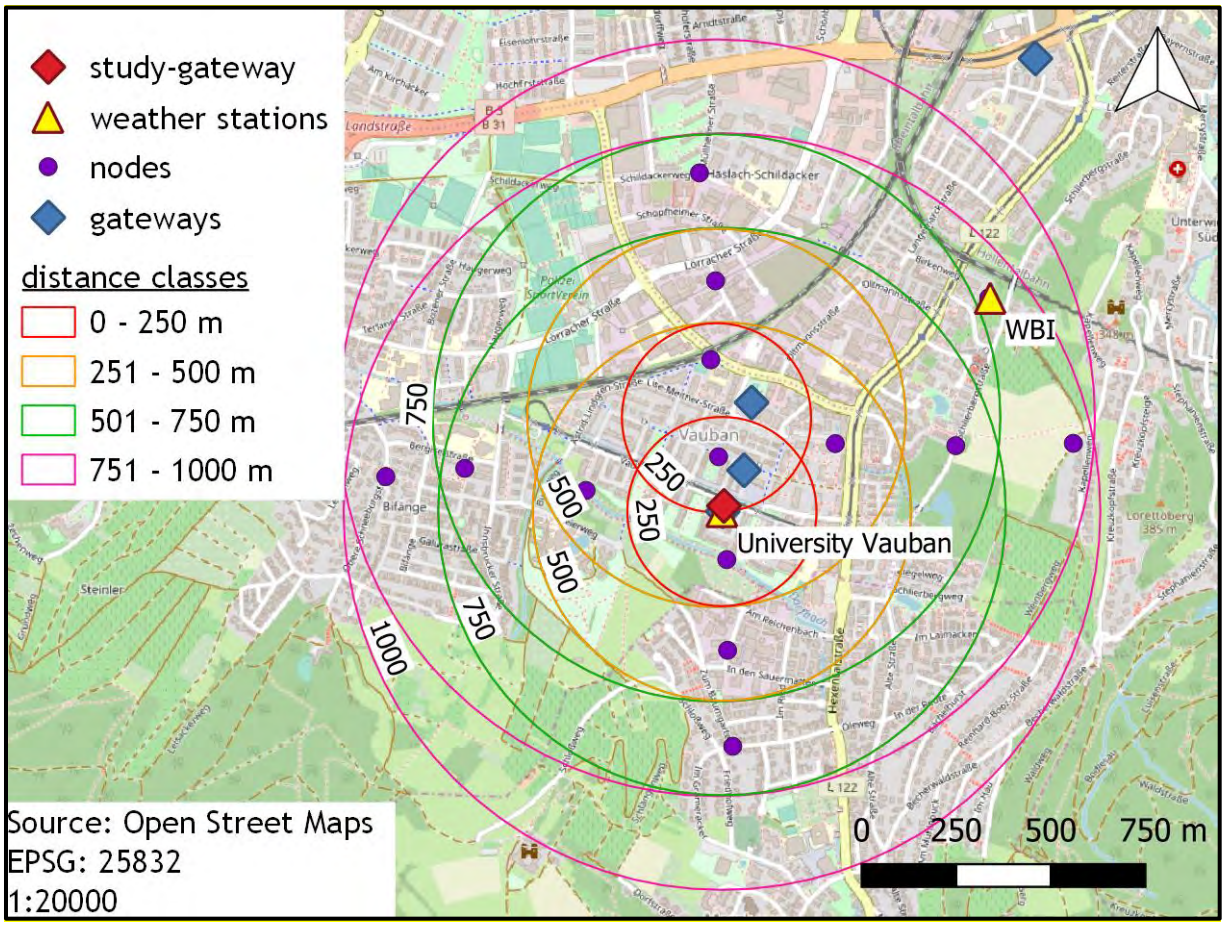

Map 4.2: Experiment 2, Vauban: Placement of nodes and gateways in the suburb Vauban. Nodes are placed according to preset distance classes.

4.3.3 Attenuation along a Line

Aside from the cross deployment two more long range Arduino Pro Minis were deployed. They operated at spreading factor 9, giving them a much higher range but lower transmission interval. Each one of them was placed on the highest point of elevation on a straight 10 km line connecting multiple gateways and weather stations. Their purpose was to investigate the attenuation of a single transmission while it passes

multiple receivers in a row one after the other. Local precipitation clusters on the way (revealed by the weather stations on the line) would attenuate the signal, consequently resulting in a drop of signal strength along the rainy parts of the line.

In addition to the to patterned configurations, five The Things Unos were more or less evenly distributed depending on where households were willing to host them and two more Arduino Pro Minis were deployed on the poles of the weather stations.

4.3.4 Gateways

The receivers used in this experiment were the gateways available in Freiburg plus the study-gateway. Information about the third-party gateways is not complete: all technical specifications were taken from the information given on The Things Network website or found in the metadata of the data transmissions. The most valuable information is the location of the gateway. It is normally given on the website in a list of all gateways available in The Things Network. This list for gateways was filtered for a confined area around Freiburg (Longitude: 7.742214° to 7.914807° and Latitude: 47.945248° to 48.056477°). This list was then matched with all gateways mentioned in the collection of successful transmissions, which also carried information about the location of the gateway.

There are many different models among the third-party gateways. Some were self-made, others were fully assembled professional devices. Information about microcontroller, antenna, concentrator board and placement (indoor or outdoor) was not available or to diverse hence it is not listed here. An assumption is therefore made that the gateways configuration partwise and location wise did not change at large and the reception characteristics of each gateway did not differ significantly throughout the experiment.

The study-gateway was placed on the pole of the weather station of the University of Freiburg in Vauban. The antenna was fixed in around two meters height and the

waterproof box containing the electronic parts placed close to the roof of the building where it was shaded by adjacent solar collectors for most of the day.

4.3.5 Weather Stations

Four different weather stations provided the precipitation data. The weather station of the *DWD*, the German Weather Service, is located next to the airport (48.0233°, 7.8344°), 236 m.a.s.l. (DWD CDC, 2019a). It conforms completely with the requirements for meteorological stations of the *DWD* (DWD Abteilung Messnetze und Daten, 2017). Its data is available at 1-minute intervals.

The two university weather stations, one located on the roof of the high-rise of a building of the chemistry department (48.0004°, 7.5055°) at 283.8 m.a.s.l. (University of Freiburg, Chair of Environmental Meteorology, 2019) and one located on the roof of an apartment building (47.974523, 7.824104) in the suburb Vauban at approx. 265 m.a.s.l. (University of Freiburg, Chair of Hydrology, 2019) did not comply with the *DWD*-requirements since they are placed on building roofs. The measurement interval of *University Chemistry* station is 1 minute; the interval of *University Vauban* is 10 minutes.

The fourth station is operated by the *Weinbauinstitut* (*WBI*, institute of viniculture) in one of their experimental vineyards (47.97967, 7.8335) at 275 m.a.s.l. (Weinbauinstitut Freiburg, 2019). The conformity with the *DWD* requirements is unclear, however, the surroundings (buildings, vines) are somewhat obstructing the natural precipitation. Its measurement interval is also 10 minutes.

In addition to the weather station point data, raster data from the DWD Radolan program was used. This data originates from radar data captured by a radar station on the Feldberg, the highest peak of the Black Forest. Its measurements are adjusted to match the ground truth from weather stations. During the year of measurement, the

temporal resolution is one hour; in the year afterwards (not within the time frame of this thesis), post processing allows for 5-minute intervals (DWD CDC, 2019b).

4.3.6 Computation

Any data packet received by at least one of the third-party gateways was forwarded to the The Things network server, decoded and then saved in a MongoDB database. The packets captured by the study-gateway were stored in the gateways hard drive, transferred at the end of the experiment and decrypted locally. Due to the "brute-force"-technique of the LoRa-decoder (Kirby, 2019), this process was very time consuming. The result was combined with data stored in the MongoDB-database and cleansed: any irrelevant or implausible data was filtered, e.g. for random far distance links to gateways at the French border or atmospheric pressure values below 900 hPa. The CPU-temperature data from the study-gateway was added by assigning a CPU-temperature-value to each data packet received by the study-gateway which fell in the time step of a record.

Next, the data was merged with the precipitation measurements. As stated in the previous chapter, the precipitation data was available in two formats: point measurements from weather stations and raster data from the Radolan precipitation radar system. The aim was to obtain a single path-averaged precipitation value for each data packet sent. The crucial factor here was the minimum time interval of each format, as this was decisive regarding which precipitation value a data packet was assigned to. For the weather station data, the maximum time interval was 10 minutes from the *WBI* and *University Vauban* weather stations. This means that all data packets received were assigned to the next available 10-minute precipitation value. For each timestamp, the weather station was interpolated with inverse distance weighting to a 10 m by 10 m cell size grid. Then, a line was drawn for each link between node and gateway. Cells from the precipitation raster lying on this line were then extracted and

the mean calculated which yielded a path averaged precipitation. The same procedure was followed for the Radolan rasters, except that there was no interpolation.

Afterwards, the precipitation extracted from the weather station data was compared to the Radolan rasters in two ways in order to validate the procedure:

For each weather station, the raster cell values at the location of the weather station for all available Radolan-raster files were extracted. The cumulative sums of the extracted values were then compared to the cumulative sum of the precipitation measured by the weather station to determine the total volume error.

In the second approach the cumulative sum of path-averaged-precipitation of each node-to-gateway-link from the interpolated data was compared to the cumulative sum of path-averaged-precipitation from the extracted data.

After the gathering of all data sources the sizes of the effects of each covariate on signal strength for each link were calculated. The three most prevalent covariates were selected for decoupling and transformed into a categorical variable for the sorting into bins. Finally, within each bin-combination, linear regression between precipitation and standardized signal strength using the rain attenuation model (equation (3)) was conducted.

Values (X) can be standardized (Z) with the mean (μ) and standard deviation (σ):

$$Z = \frac{X - \mu}{\sigma} \tag{9}$$

4.4 Experiment 3, Rektorat: Plot-Scale, 2.4 GHz and 5 GHz

4.4.1 Setup

The two-day-experiment was conducted on the lawn in front of one of the buildings of the University of Freiburg. Two receivers were placed in varying distances with a transmitter halfway in between them. It was attempted to keep the line of sight between transmitter and receiver as unobstructed by equipment as possible. Between the transmitter and one of the receivers, the sprinkler system was installed. The setups of

the two experiment sessions differed slightly. They are depicted in Figure 4.2 and Figure 4.3.

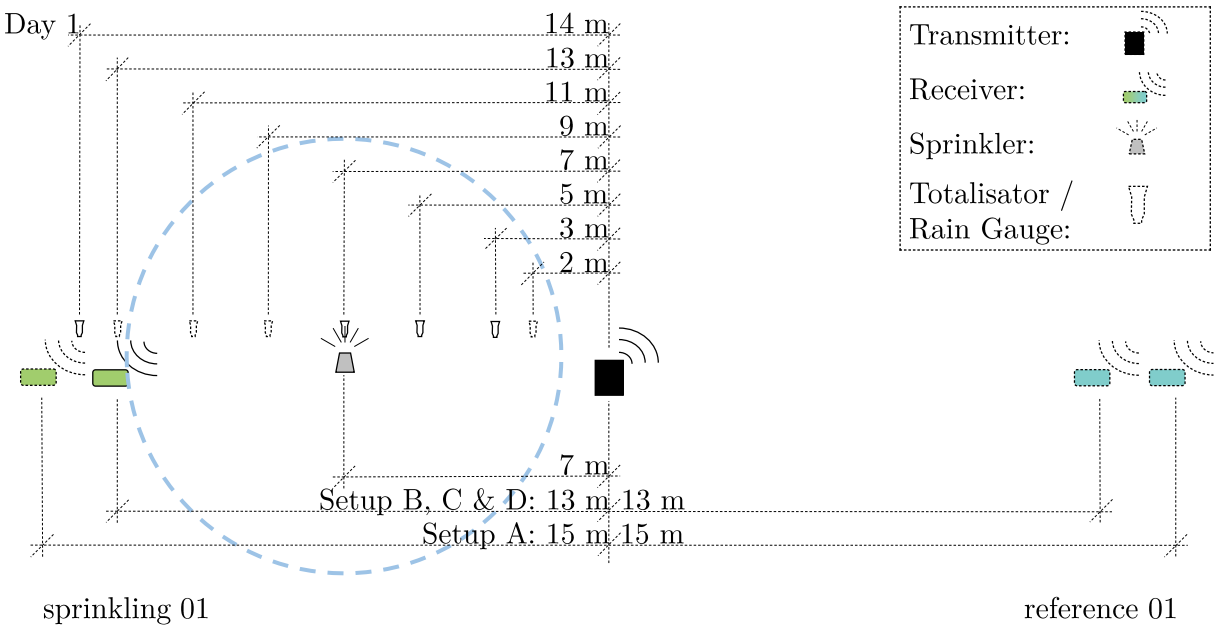

Figure 4.2: Experiment 3, Rektorat: Layout of the setup of first day. The transmissions from the transmitter in the middle of the setup was received by two receivers at varying distances. For the sprinkling node, the transmissions had to pass the sprinkled perimeter marked by the blue dotted line. The line-of-sight of the reference node on the right side was unobstructed.

On day 1, only one sprinkler was used. The experiment was repeated four times, each setup consisting of a sprinkling period and a prior reference period. Setup B had an additional subsequent reference period to monitor the recovery of the signal strength after the sprinkling system had been turned off. In setup A, the nodes were placed at a distance of 15 m from the transmitter, in setup B, C and D at 13 m. Setup A and B used 5 GHz Wi-Fi, setup C and D 2.4 GHz. In setup D, the sprinkling system was not used. Instead, following the remarks of Markham, Trigoni and Ellwood (2010), water was manually poured on the plastic bag covering the transmitter in order to evaluate if droplets on the bag or a wet surface between transmitter and receiver in general played a role in signal attenuation.

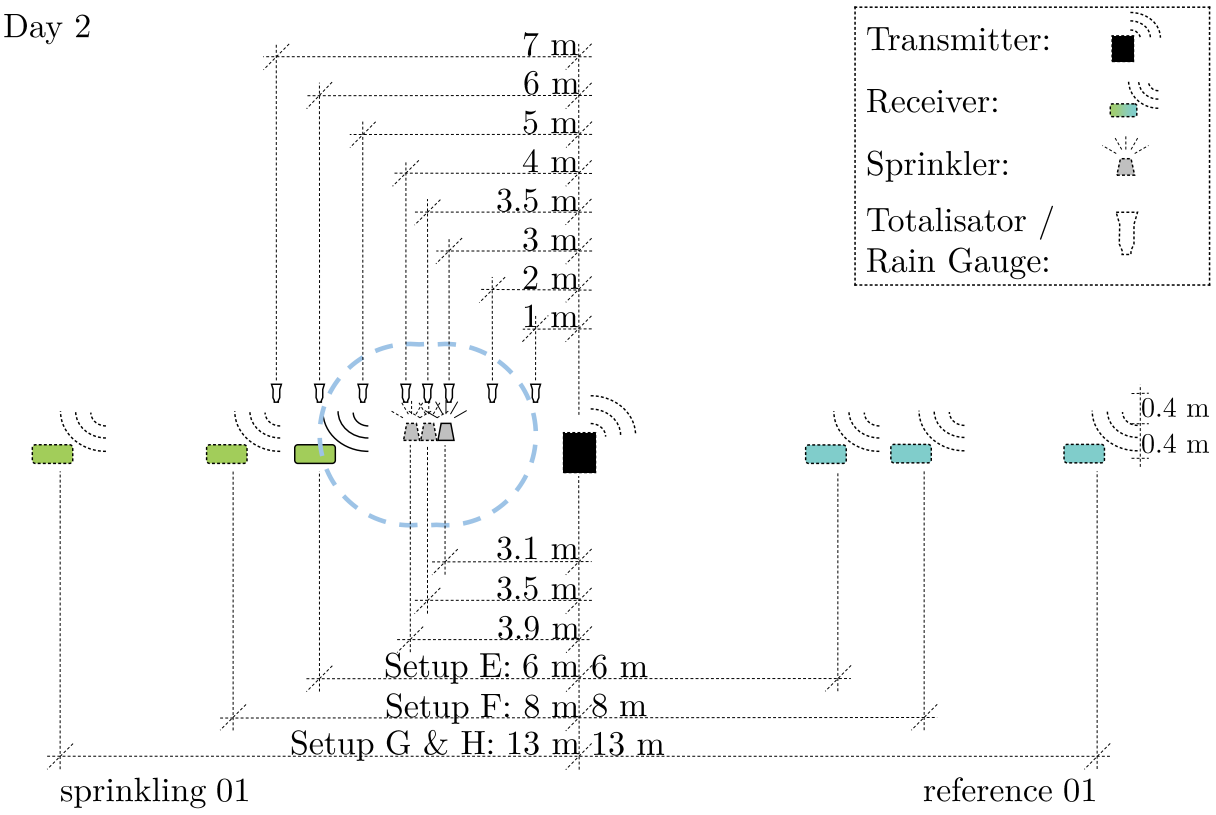

Figure 4.3: Experiment 3, Rektorat: Layout of the setup of the second day. The transmissions from the transmitter in the middle of the setup was received by two receivers at varying distances. For the sprinkling node, the transmissions had to pass the sprinkled perimeter marked by the blue dotted line. The line-of-sight of the reference node on the right side was unobstructed.

The schedule on day 2 was similar to day 1. This time, three sprinklers were used, lined up in close proximity. They delivered significantly bigger drops and higher intensities; however the sprinkled perimeter was much smaller due to insufficient pipe pressure. Again, three setups (E, F & G) were carried out with the sprinkling system turned on and turned off, each setup having a prior reference period, then a sprinkling period and then a subsequent recovery period. In setup H, the same procedure as in setup D was followed. On day 2 all experiments were performed with the 5 GHz frequency.

4.4.2 Receivers

The receivers were two Raspberry Pi 3B+-microcontrollers. They established a Wi-Fi-connection with the transmitter and queried the signal strength every second. They were mounted on poles around 50 cm above ground. Alongside the signal strength they also measured temperature, relative humidity, atmospheric pressure and CPU-temperature every 5 seconds.

4.4.3 Transmitter

The transmitter in this experiment was an ordinary router capable of providing 2.4 GHz and 5 GHz Wi-Fi-networks. It was controlled via its browser interface through a laptop. The router was plugged into a cable reel and covered by a plastic bag. Inside the plastic bag was an additional Arduino Pro Mini node to record transmitter-side temperature, relative humidity and atmospheric pressure.

4.4.4 Sprinklers and Precipitation Measurements

Eight totalizators were placed inside the expected sprinkled perimeter. The distribution of spray is not uniform across the radius: using one sprinkler system one would expect high intensities close to the pole, then a plateau followed by a rapid decrease at the edge. Therefore to quantify the spray intensity accurately, the totalizators were placed along the suspected propagation path of the radio waves.During both days the totalizators were read out approximately every 10 minutes.

4.4.5 Computation

Except for the SDR-data, the procedure was the same as in experiment 1.

5 Results

5.1 Experiment 1, Möhringen

5.1.1 Overview

An overview of the execution of experiment 1 is given in Figure 5.1. The experiment lasted from 11:47 h of the first day until 17.10 h of the next day. During that time span, unexpected events occurred which made the separation into multiple sub-periods necessary. These periods are indicated by black lines in Figure 5.1. After the deployment on the morning of the first day the setup remained stable until the morning of the next day at 5:20 h. Then, an additional tarp was spanned between reference and sprinkling plot (to protect the reference soil from isotopic labelled sprinkling water during a parallel experiment) which blocked the line-of-sight of some nodes to the receiver. Hence, the receiver antenna had to be repositioned slightly.

This first period will be called “prior A” in the following. After this, period “prior B” starts, which lasted from 5:20 h until 6:00 h, when the receiver antenna fell and had to be re-erected at 7:05 h. During that downtime, the sprinkling system was started, hence the sprinkling period - called “sprinkling” - lasts from 7:05 h until 16:25 h, followed by the last reference period “subsequent”, lasting from 16:25 h until 17:10 h.

Six nodes where deployed, three of them on the sprinkling side of the antenna and three of them on the dry reference side. Node sprinkling 01 broke down soon after the start of the deployment and will not be considered further. It was replaced by node reference 03, which was then renamed to node sprinkling 04. In turn, this node then broke during the sprinkling period probably due to water shorting the circuits.

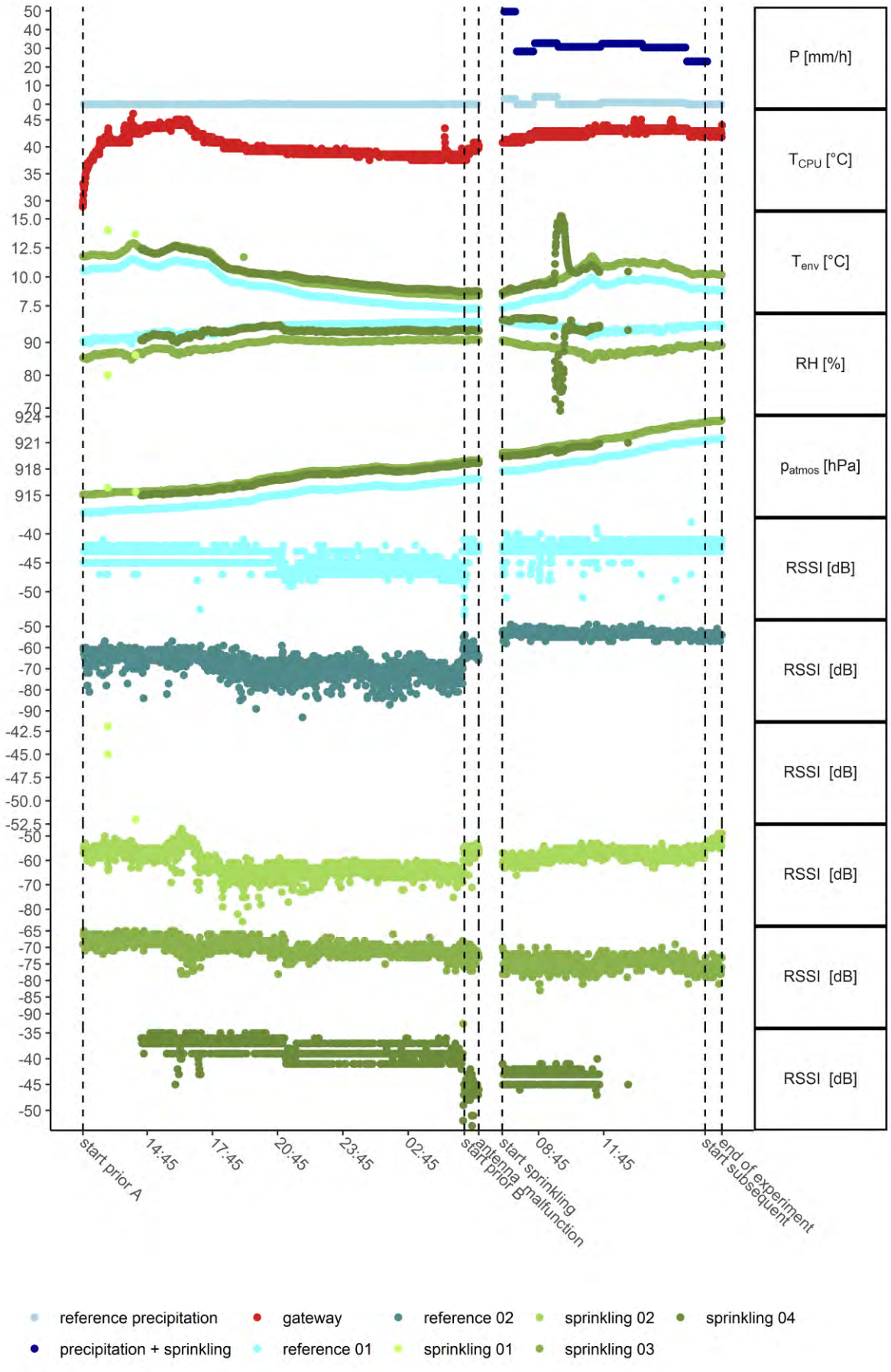

Figure 5.1: Experiment 1, Möhringen: Overview and timeseries of recorded parameters.

Table 5.1 provides an overview of the periods, nodes, PRR, mean and variance. These figures show that there are substantial differences for some of the nodes between prior A and the rest of the periods. All nodes except for reference 01 and sprinkling 03 exhibit a jump in mean signal strength after the start of prior B of approx. 5 to 8 dB. Reference 02 and sprinkling 01 experienced a large decrease of variance, plainly visible in their respective RSSI-scattering. Thus, period prior A is considered to be too different from the rest of the periods for the following comparison and is removed from the dataset.

Table 5.1: Experiment 1, Möhringen: Overview of periods and key values.
*low PRR likely due to erroneous decoding of the payload. PRR (packet reception ratio) in %, mean in dB and var in dB²

time	period		reference 01	reference 02	sprinkling 02	sprinkling 03	sprinkling 04
day 1, 11:45 h	prior A	PRR	91.10*	99.02	99.08	99.05	99.46
until day 2,		mean	-44.85	-68.97	-62.02	-70.04	-38.19
5:20 h		var	2.77	28.75	24.47	4.98	3.09
day 2,	prior B	PRR	100	100	100	100	100
5:20 h		mean	-43.15	-61.12	-56.94	-72.32	-46.04
until 6:00 h		var	5.23	6.19	9.28	2.99	4.04
day 2,	sprinkling	PRR	98.22	99.72	98.27	99.04	99.09
7:05 h		mean	-42.60	-53.50	-58.01	-74.78	-43.57
until 16:25 h		var	1.80	1.57	4.00	3.68	1.50
day 2,	subsequent	PRR	100	100	100	100	NA
16:25 h		mean	-42.42	-54.47	-52.74	-76.22	NA
until 17:10 h		var	0.63	0.97	2.27	3.52	NA

Environmental temperature, relative humidity and atmospheric pressure values recorded by the nodes are coherent and within the expected range, except for the sharp rise / drop of sprinkling 04 during the sprinkling period which again is probably caused by a short-circuit. The CPU-temperature recorded by the gateway stays within the safe operating range. The origin of the occasional spikes is unknown.

The correlations of RSSI (i.e. the signal strength) to the covariates has been correlated per node and per period in order to examine their relation to the network's connectivity. They are depicted in Figure 5.2. The maximum change of correlation throughout the experiment is 0.5. There is no pattern of correlation change (for example a uniform decrease during the sprinkling period followed by an increase during the subsequent period; contrasting the reference nodes behavior; …), that could be attributed to the node being on the reference or sprinkling side except for atmospheric pressure, where the correlation increases monotonically for the sprinkling nodes and decreases monotonically for the reference node. The absolute change of correlation for sprinkling 03, however, is only 0.31 and for reference 01 0.175.

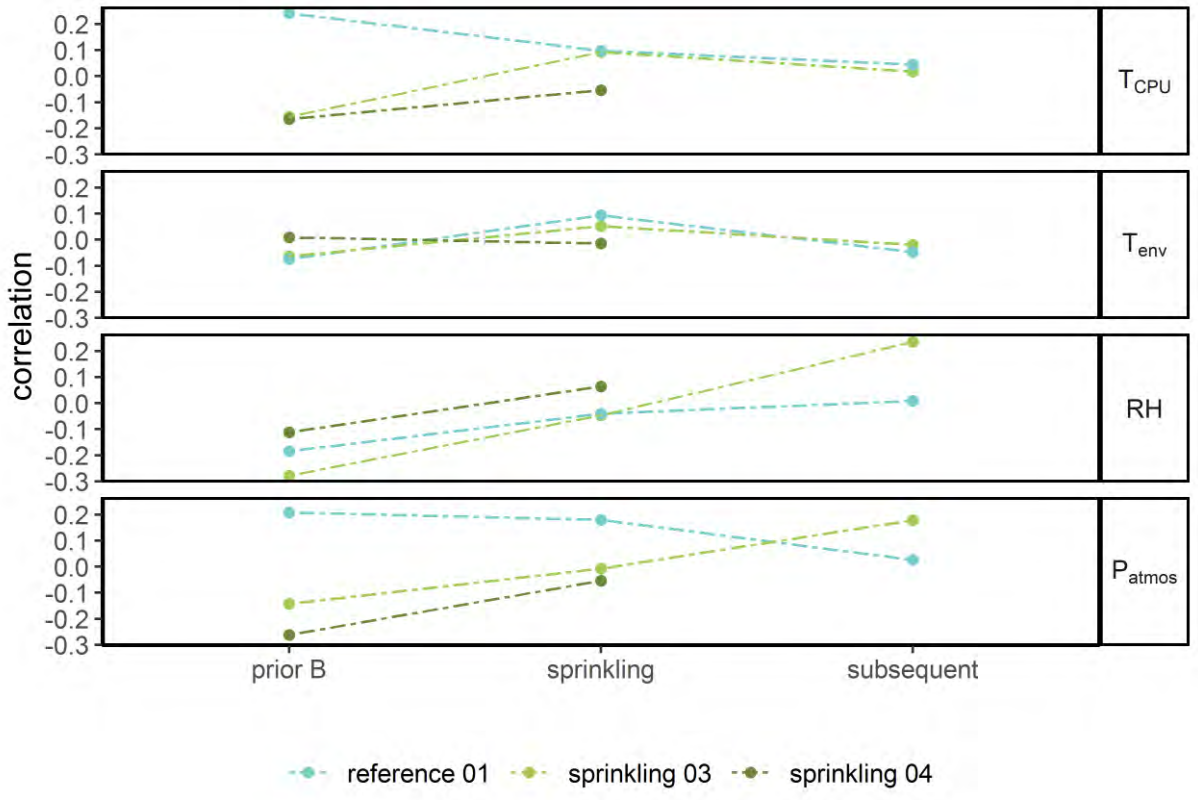

Figure 5.2: Experiment 1, Möhringen: Correlations of signal strength to covariates grouped by nodes and periods. No distinct pattern contrasting the sprinkling nodes from the reference node is revealed.

The reference precipitation data has been recorded by a tipping bucket rain gauge on the reference plot in 5-minute increments. The highest natural rainfall rate recorded during the experiment was 4 mm/h. "precipitation + sprinkling" combines natural

precipitation and sprinkled water and was measured by five gauges. The value indicated in Figure 5.1 is the maximum of these gauge-measurements for each time step and ranges between 23 and 49 mm/h.

5.1.2 Distributions

The influence of precipitation on the signal strength will be presented in the following chapters. First, the distributions of the periods will be compared to present an overview of the degree of discrepancy among them. A line fitted to the distribution of each node for each period is depicted in Figure 5.3. For each node, the distributions are more or less in the same shape during all periods. They appear to be normally distributed.

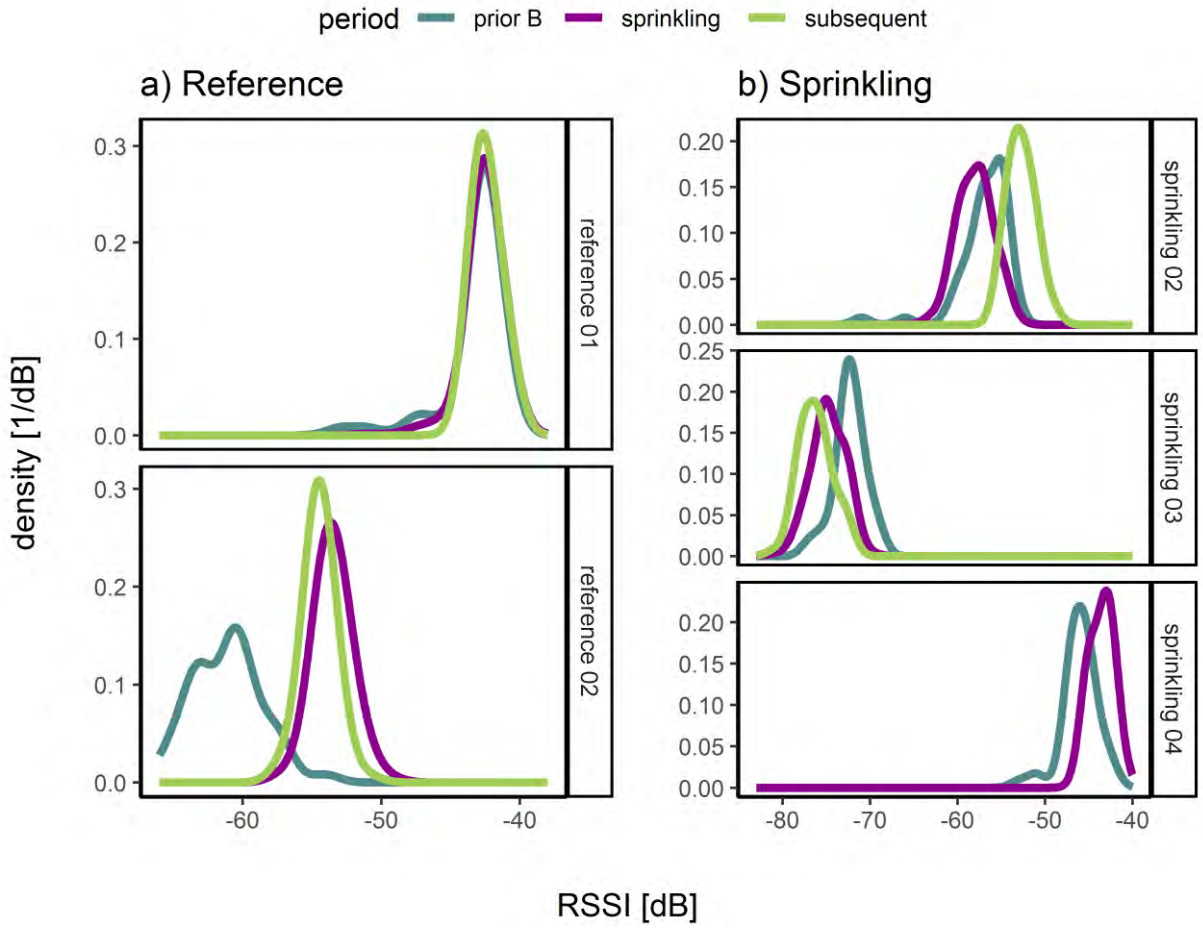

Figure 5.3: Experiment 1, Möhringen: Density estimates of the distributions of signal strength for different nodes and periods.

While the distributions mostly overlap for the reference nodes (except for prior B), they tend to be more offset from each other for the sprinkling nodes. If this is an effect of the sprinkling system turned on/off or an exterior effect is not obvious from the distributions alone. While the signal strength worsens from prior B to sprinkling for sprinkling 02 and sprinkling 03, it is improving for sprinkling 04, therefore there is no explicit sprinkling-side-wide attenuation. The subsequent period distributions are also equivocal: the improvement of the signal strength of sprinkling 02 after sprinkling could be interpreted as recovery of the system, on the other hand the signal of sprinkling 03 degrades further after the sprinkling.

5.1.3 Homoskedasticity

Levene's-test has been conducted for each node and for each period. The Levene's-test is a popular tool to assess the homoscedasticity (homogeneity of variance) between two groups, an essential requirement for the ANOVA. The results are given in Table 5.2 as significance levels. No significance means, that the null hypothesis holds and the variances of the two groups can be assumed to be equal. A high significance, i.e. different variances, is indicated by *** while low significance is indicated by *, no significance (homogenous variances) are indicated by an empty field.

Table 5.2: Experiment 1, Möhringen: Results of the Levene's test. *: p <= 0.05, **: p <= 0.01, ***: p <= 0.001, -: p > 0.05

	reference 01	reference 02	sprinkling 02	sprinkling 03	sprinkling 04
prior B to sprinkling	**	***	-	-	**
sprinkling to subsequent	-	*	*	-	NA

Homogeneity of variance is given for only half of the period-pairs. Homogeneity of variance is not given for the groups prior B -sprinkling for nodes reference 01, reference

02 and sprinkling 04 as well as sprinkling-subsequent for the nodes reference 02 and sprinkling 02.

5.1.4 ANOVA and Effect Size

The ANOVA confirmed for all node-period-groups – except for node reference 01 – significant inter-group differences. This result is given in Table 5.3 by the number of *, where *** means that assuming a significant difference between the groups is justified. Due to the prerequisite of homoscedasticity, only those pairs who passed the Levene's test are rated. In fact, all significant results, i.e. the period-pairs where the presence or absence of precipitation served as an explanatory variable for the differences between the pairs, are located on the sprinkling side. The only pair where precipitation was not explanatory was on the reference side, however this might also be an isolated result.

Table 5.3: Experiment 1, Möhringen: Results of the ANOVA. *: p <= 0.05, **: p <= 0.01, ***: p <= 0.001, -: p > 0.05

	reference 01	reference 02	sprinkling 02	sprinkling 03	sprinkling 04
prior B to sprinkling			***	***	
sprinkling to subsequent	-			***	

While the ANOVA might rate even small differences significant if the sample size is big enough (Sullivan and Feinn, 2012), the effect size gives a better impression of the actual impact of the grouping variable. The Kruskal-Wallis-test to overcome the requirement of homoscedasticity did not come into question here because the dataset consists of too many ties which poses problems for this test (Dormann, 2017).

The effect size, Cohen's d, is given in Table 5.4. While the grouping shows large to very large effects for the sprinkling nodes, small to medium effects are obtained for

reference 01, an extremely large effect for the prior B-sprinkling-period and an almost large effect for sprinkling-subsequent for reference 02.

The effect size can also be directly transferred to the amount of overlap of distributions (see Figure 5.3). The stronger the effect between two groups, the less do their distributions overlap. An extreme case is given by reference 02, where the distributions of prior B and sprinkling are fundamentally different not only in mean but also in shape. What exactly the reason for the unparalleled difference of the prior B dataset of reference 02 may be is unclear but it might be related to a significant exterior bias.

Overall, excluding this outlier, we see larger effect sizes for the sprinkling nodes, but still considerable effect sizes for the reference nodes.

Table 5.4: Experiment 1, Möhringen: Cohen's d. d >= 0.2: small, d >= 0.5: medium, d >= 0.8: large, d > 1.3: very large (Sullivan and Feinn, 2012)

	reference 01	reference 02	sprinkling 02	sprinkling 03	sprinkling 04
prior B to sprinkling	0.39	5.57	0.51	1.29	1.83
sprinkling to subsequent	0.14	0.79	2.68	0.75	NA

5.1.5 Software Defined Radio (SDR)

The results from the second analysis method involving the SDR will be presented in the following. First, the transmitted packets had to be matched with the antenna excitation recorded by the SDR. Then, the remaining antenna excitation time series were investigated period- and node-wise.

Out of the 2264 packets captured by the SDR, only 21 had to be excluded from further analysis (99.07 % success rate). Some examples of packet-failures are given in XX. Some reasons for these failures were packet collisions, too low signal strength and too small gaps between transmissions.

The conversion from the raw antenna i/q-data via fast-Fourier-transformation was

done using a Hamming-window with a resolution of 128 sub-frequencies.

After the transformation into the frequency-domain and the assignment to the nodes, the per-sub-frequency-signal-strength-data was again grouped into sprinkling and non-sprinkling periods to see if there was any partial attenuation of the frequency band and to compare the periods against each other. The result is illustrated in Figure 5.4 and Figure 5.5, for the two nodes reference 02 and sprinkling 02 which both sent only dummy-sensor data thus keeping the difference between individual packets minimal. For both nodes, there is nearly no difference between the boxplots in the upper part of the figures, except for some outliers. The means of the three periods are almost parallel, therefore there seems to be no influence in specific parts of the frequency range.

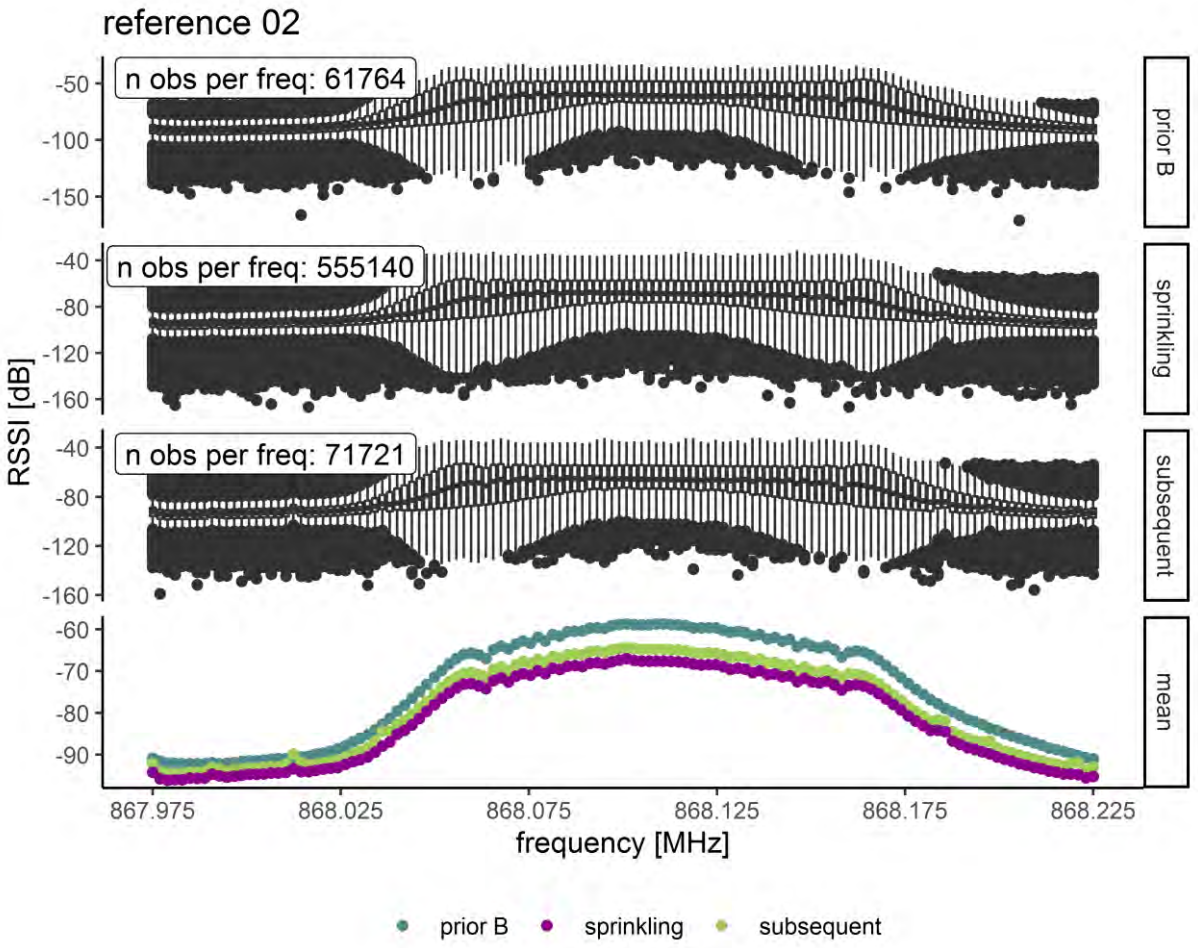

Figure 5.4: Experiment 1, Möhringen: Sub-frequency boxplots for all transmissions for node reference 02. Sorted into different periods. The boxplots do not reveal a distinct attenuation of a specific sub-frequency. The means of signal strength were lowest during the sprinkling period despite the node not being exposed to the sprinkling system.

The only difference between the nodes is the mean of the prior B period, the irregularity of which was already discussed in section 5.1.1. For reference 02, it is slightly more lifted while it stays in close formation with the other periods for sprinkling 02. Interestingly, the sequence of the medians does not coincide at all with the picture drawn by the distributions of the signal strengths from the gateway (Figure 5.3 and Table 5.1). With the SDR, comparatively better signal strengths were obtained during the prior B period and worse for the sprinkling period for node reference 02 – the reverse order of the gateway signal strengths. For sprinkling 02, prior B scored better than subsequent on the SDR in contrast to the gateway. This seems to hint that the receiver (different antenna plus circuits) plays a bigger role than the period-grouping.

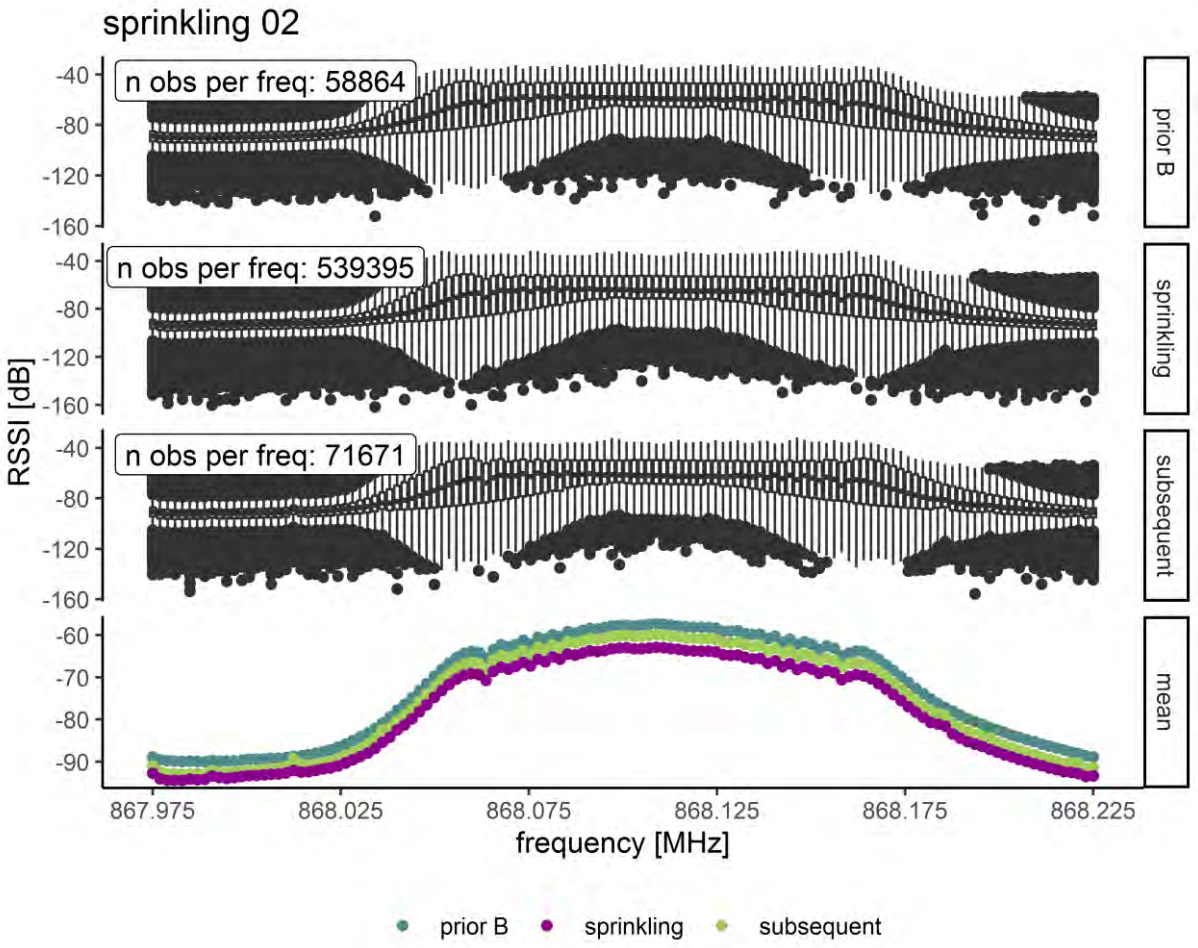

Figure 5.5: Experiment 1, Möhringen: Sub-frequency boxplots for all transmissions for node sprinkling 02. Sorted into different periods. The boxplots do not reveal a distinct attenuation of a specific sub-frequency. The means of signal strength were lowest during the sprinkling.

5.2 Experiment 2: Vauban

5.2.1 Overview

This experiment went on for six months from 2019/02/01 until 2019/07/31. 24 nodes were deployed which communicated with 24 gateways spread out in the vicinity of Freiburg. In total, they formed 167 links with over 1.5 successful data transmissions. The longest link distance was 9.79 km, topped by the overall maximum of 19.9 km to a neighboring town (not included in this analysis).

As depicted in Map 5.1, the link strengths differed strongly. While some links were very solid and constant (the strongest one with 165555 transmissions), others were merely lucky shots with one-time connections.

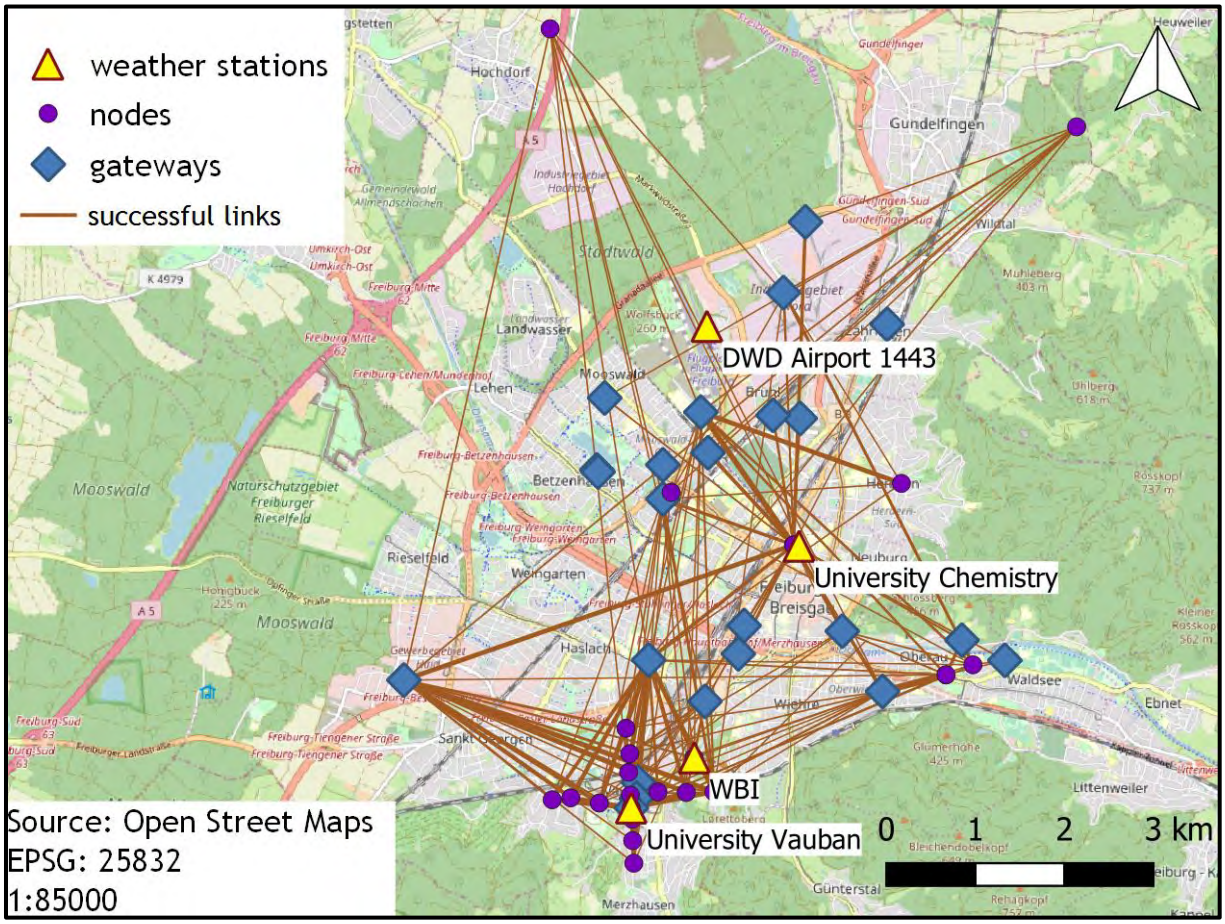

Map 5.1: Experiment 02, Vauban: Actual links established between nodes and gateways. The line thickness is relative to number of transmissions.

There was a good coverage in the southern part of the city, in the suburb Vauban where most of the nodes and the gateway were deployed strategically. A second focal

point was the node at the weather station *University Chemistry* which was located on a high rise with a node on its pole. Likely thanks to the high elevation it achieved a high number of line-of-sight connections and established the maximum of 21 links. The operating ranges during the experiment were -2.04 to 61.3 °C transmitter temperature, 33.2 to 79 C receiver temperature, 0.01 to 100 % relative humidity, 0 to 33.5 g/m³ absolute humidity and 961 to 1004 hPa atmospheric pressure

5.2.2 Propagation Model

Before the performance of the network could be assessed, the intercept and slope of the mean path loss had to be determined from the empirical relation referred to in section 2.1.1. However, information regarding antenna gain was limited to a few gateways, hence, assumptions had to be made for the calculation of the empirical path loss. The available antenna gain was averaged for those gateways without information. This resulted in antenna gains between 2 and 8 dB. The antenna gain of the nodes was assumed to be 5.16 dB (J. C. Logan and J. W. Rockway, 1997). The transmission power for all nodes was 14 dB.

After linear regression of the dry-day-path loss values, intercept and slope for the regression were determined as 130.164 [dB] and 0.363 [dB/km] for this experiment (not necessarily for Freiburg). The regression line along with the theoretical PL_{FS}-model and the dry weather signal strength ranges of all links depicted in Figure 5.6. Here it can be seen the establishment of a successful connection depends on distance as there are fewer links at higher than shorter distances. At the same time, once a link is established, the range of signal strength does not relate in general to distance because the differences among the signal strength ranges are quite high irrespective of distance. Therefore, the free space path loss model does not achieve a good alignment.

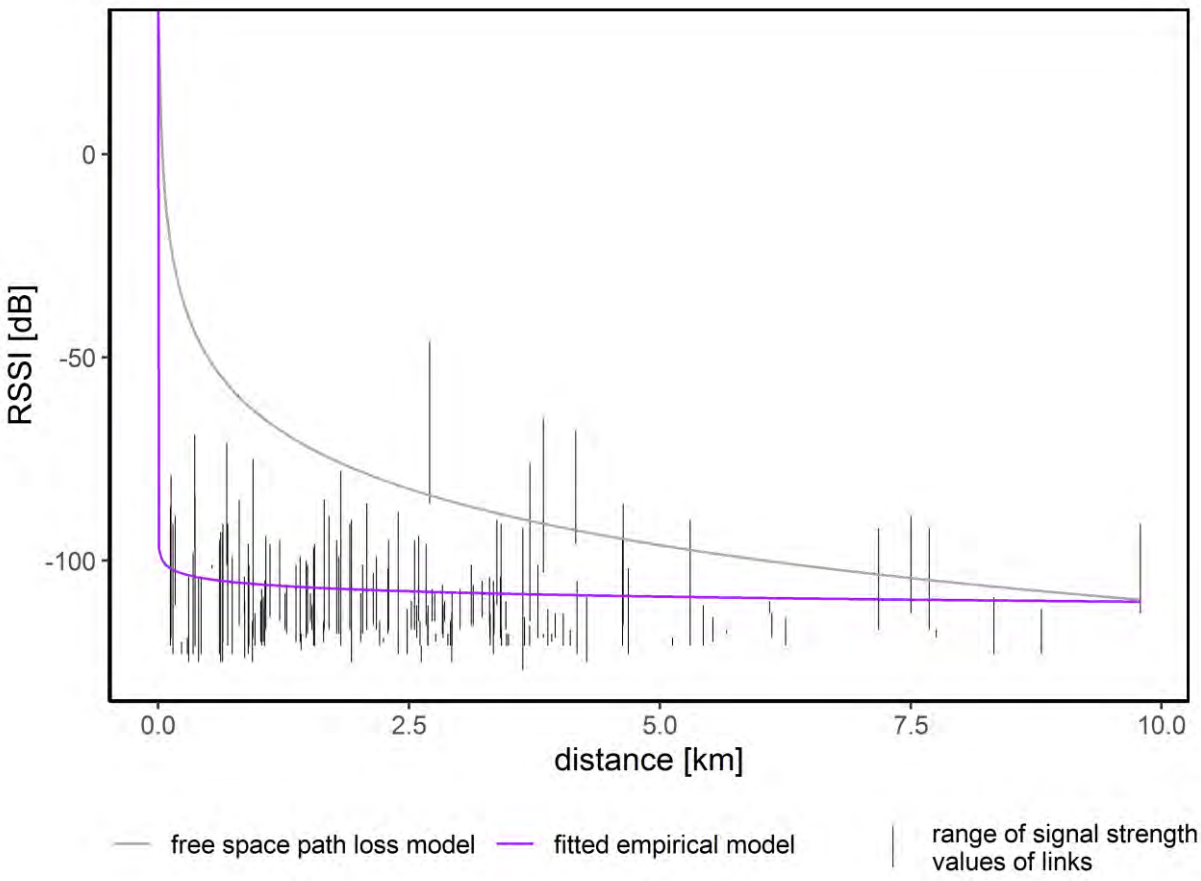

Figure 5.6: Experiment 2, Vauban: Dry weather signal strength ranges of links, fitted empirical path loss model and free space path loss model.

5.2.3 Attenuation along a Path

The comparison of the free space path loss model with the empirical fitted model is extended in Figure 5.7 by incorporating different weather scenarios for one specific example transmission path.

In this example, the signal travels from the node towards the first gateway. The weather condition for this first leg is characterized by the weather station on the way. Then, the signal continues to a second gateway with a weather station on the way or nearby the gateway.

In this case, the signal strength at the second gateway is lower than the first gateway, demonstrating the relation between signal strength and distance. In general, the difference between free space path loss model and recorded signal strength at dry weather

is much bigger than the differences between the different weather conditions. This indicates that the exterior path loss contributors like multi-path fading and attenuation by buildings and random effects (moving obstacles like cars or people) are more influential than the weather conditions.

Since the figure does not contain any information about rainfall intensity, we cannot evaluate the conditions per gateway, but rather compare the ratio of signal strengths between the weather conditions of one gateway with the ratio of the same of the other gateway. In this example, at the first gateway, the medians of signal strength during precipitation at both nodes are lower than no precipitation or precipitation only at the second gateway. Intuitively, this makes sense: precipitation at the second weather station does not influence the first gateway, so if there is precipitation, the signal strength is lower, if not, it stays high.

However, this ratio does not hold for the second gateway: the median is nearly equal regardless of weather conditions and the range of values even reaches better signal strengths during precipitation events.

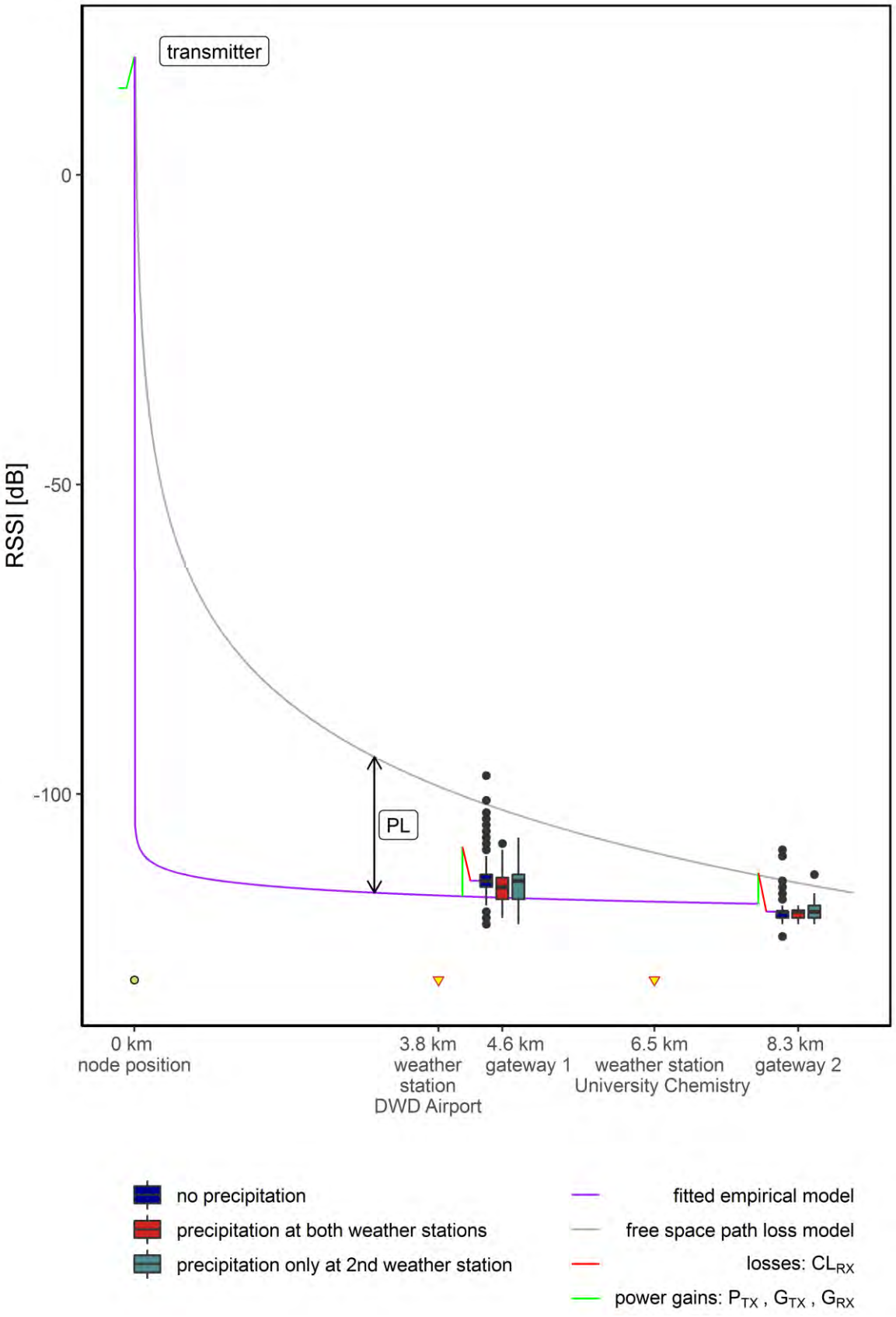

Figure 5.7: Experiment 2, Vauban: Attenuation along a path. The path loss due to environment and obstruction is the difference between free space path loss and actual measured signal strength. This difference is much bigger than the difference between different weather conditions.

5.2.4 Effect of Covariates

A linear regression has been calculated for each link and for each variable. The results are given in Figure 5.8. The R^2-values were sorted into bins equivalent to the effect sizes stated by Sullivan and Feinn (2012) and given in Table 5.5.

Table 5.5: Effect sizes as stated by Sullivan and Feinn (2012)

Effect Size	Small	Medium	Large
R^2	0.04 – 0.25	0.25 – 0.64	> 0.64

CPU-temperature has the lowest effect, as 100 % of the regression had an R^2 of 0.04 or less. There are fewer links for CPU-temperature because this parameter was measured only at the study-gateway. The two strongest covariates are environmental temperature and absolute humidity. However, even here around 90 % of the links experienced weak or no effects. The difference between atmospheric pressure and relative humidity is minimal, though relative humidity has slightly fewer no-effect links. Because relative humidity is considered skewed due to the relation to environmental temperature, atmospheric pressure has been chosen instead (Wennerstrom *et al.*, 2013). The three parameters chosen for the decoupling are therefore environmental temperature, absolute humidity and atmospheric pressure.

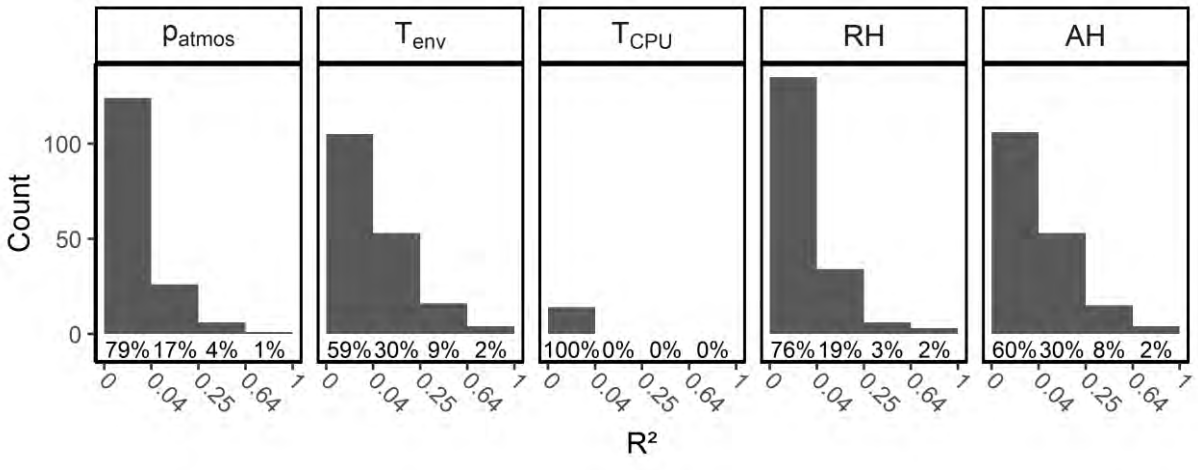

Figure 5.8: Experiment 2, Vauban: R^2-values of linear regressions between the covariates and signal strength for all links. R^2 were sorted into bins according to effect sizes. The number below the bars is the percentage of all links falling into the respective bin.

5.2.5 Precipitation

Before the analysis of the path loss due to precipitation, a path-averaged precipitation value had to be computed for each transmission. The high-resolution (1 km^2) precipitation raster data was available only in 1-h intervals, hence the data from the four weather stations had to be interpolated. This approach was validated by comparing the precipitation computed from precipitation-radar-rasters to the interpolated station data. Figure 5.9 shows the cumulative precipitation measured by the weather stations and the precipitation extracted from the Radolan-radar at the cells at the respective locations of the weather stations. The volume error by Radolan for the 6-month timespan was 72.95 mm for *DWD Airport* (17.4 % overestimation), 36 mm for *University Chemistry* (6.7 % underestimation), 124.3 mm for *University Vauban* (43.6 % overestimation) and 25.4 mm for *WBI* (6.6 % overestimation).

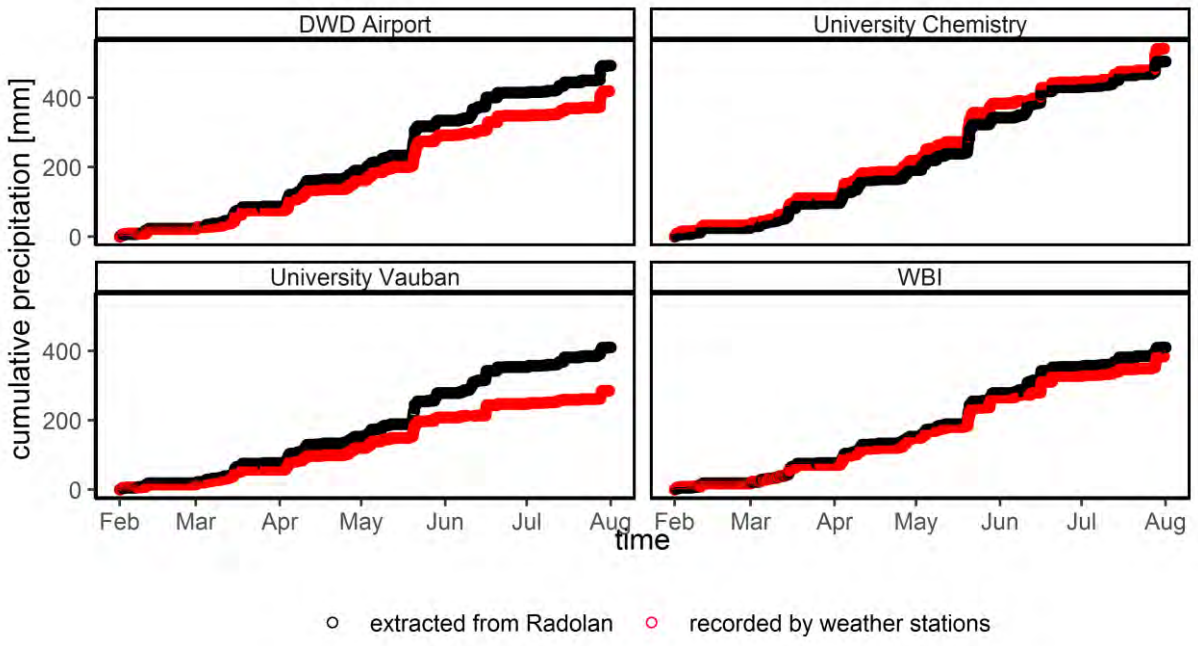

Figure 5.9: Experiment 2, Vauban: Comparison of Radolan-data with weather station measurements.

The differences of the 1-hour-precipitation sums of the weather stations to the Radolan precipitation values are depicted in Figure 5.10. Here it can be seen, that the measurements from the two formats are inconsistent when looked at from the perspective of temporal resolution. There are significant differences on nearly every hour of precipitation with the largest gap being 16 mm. These differences swing in both directions, so that they balance each other out and result in the satisfying alignment of the total precipitation volumes.

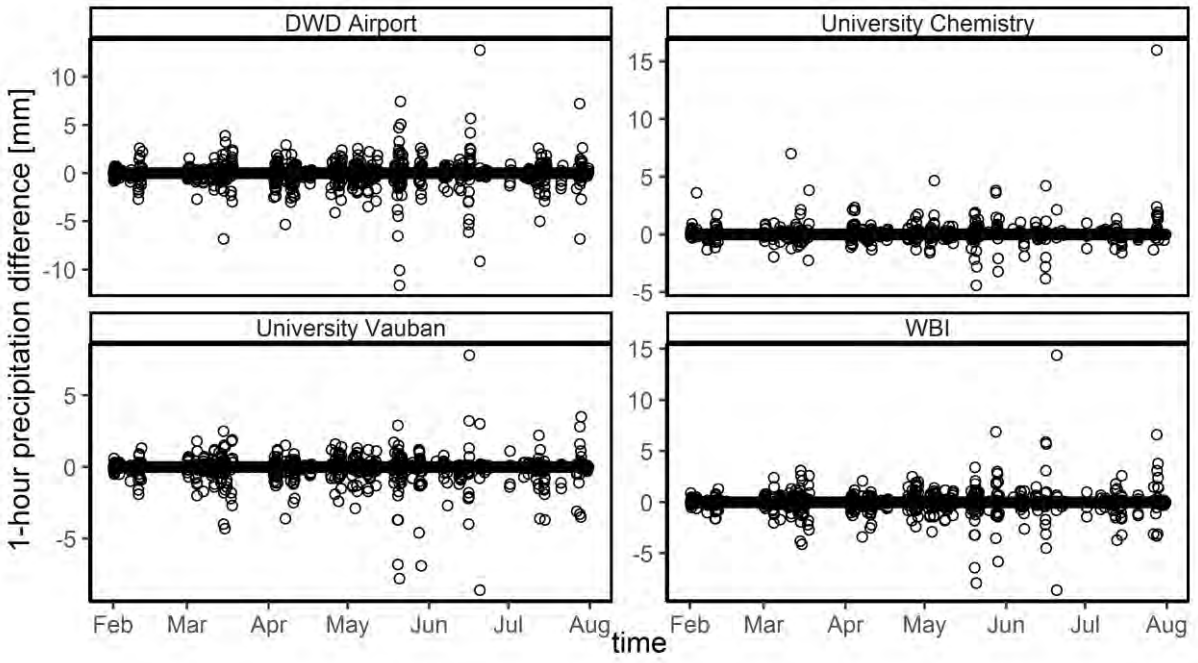

Figure 5.10: Experiment 2, Vauban: Comparison of 1-hour-precipitation sums from weather stations to Radolan data.

In regard of the high hourly precipitation sum differences, the weather stations are assumed to represent precipitation better than Radolan on a temporal scale while the total volume of precipitation within a timespan reported by both media should be more or less in agreement. Thus, the weather station data was interpolated using IDW with a power of 1 and a spatial resolution of 10 m; then the mean of the cells lying on its connecting line was extracted for each link. The result was adopted as the path-averaged precipitation. Figure 5.11 displays four examples of the extraction and a comparison to the data indicated by Radolan. While link 03 and link 04 show good agreement,

the interpolated data outdoes the Radolan data in link 01 and undercuts it in link 02. Figure 5.12 shows the histogram of the deviations of the Radolan-data from the interpolated weather station data for all links. Most Radolan-precipitation-values underestimate the weather station data (indicated by volume deviations lower than 100 %). Consequently, the path-averaged precipitation values used in the regressions in section 5.2.6 are in general overestimations.

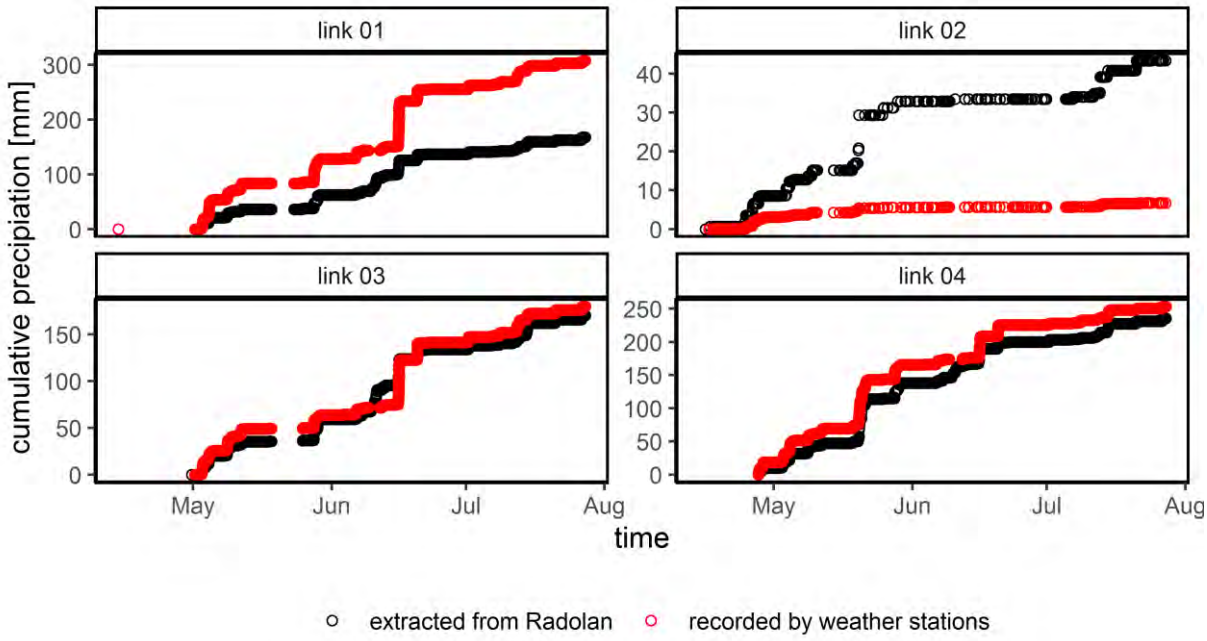

Figure 5.11: Experiment 2, Vauban: Comparison of Radolan-raster-data with interpolated weather station data for example links.

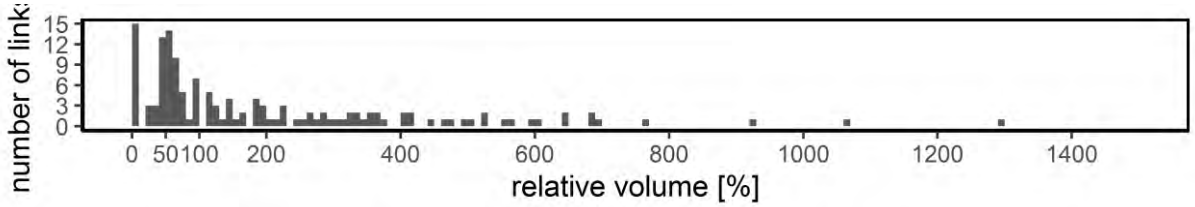

Figure 5.12: Experiment 2, Vauban: Histogram of volume deviations of all links. Volume error as deviation of precipitation given by Radolan from the precipitation extracted from the interpolated weather stations.

5.2.6 Decoupling Covariates and Effect Sizes of Precipitation

After the determination of the three parameters with the greatest effect sizes regarding the signal strength in chapter 5.2.5, two at a time where decoupled (following Wennerstrom *et al.* (2013)). The signal strength data was sorted into bins (5 °C bin width for environmental temperature, 5 hPa bin width for atmospheric pressure and 3 g/m³ bin width for absolute humidity); then, within each bin, equation (3) was fitted to the data with precipitation as the predictor. These fits are Figure A.2, Figure A.3 and Figure A.4 in appendix A, with insets of the histograms of the R^2-values of all regressions of the respective graphs. The R^2-values are also collected in Figure 5.13. The bins of the histograms have been chosen according to the effect sizes as listed in Table 5.5.

The regressions do not show a uniform trend. While many of them have almost no slope - i.e. change of signal strength regardless of precipitation intensity - some of them point downwards (negative impact of precipitation intensity) or even upwards (positive impact of precipitation intensity).

Most of the regressions have a broad base of highly varying signal strength even while there is no precipitation.

The vast majority of R^2-values are classified as no effects in all three decoupling variants. The best effect sizes are yielded by the decoupling variant absolute humidity and atmospheric pressure, the worst by absolute humidity and environmental temperature but the difference is minimal. There are occasional high effect values which can be attributed to a low number of scatter points: here, the linear model can easily achieve good fits.

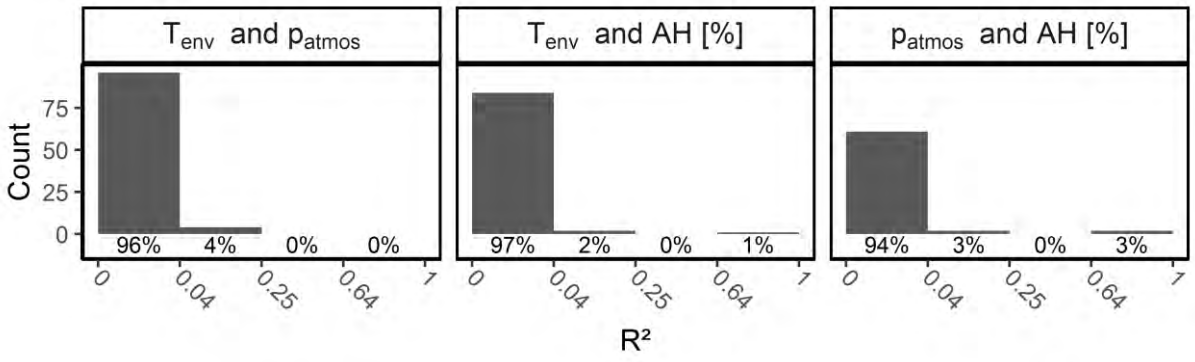

Figure 5.13: Experiment 2, Vauban: R^2-values from the regressions of precipitation and signal strength after decoupling the covariates in the header of the respective graphs. The R^2-values are sorted into categories according to Sullivan and Feinn (2012). The counts are different because the number of bin combinations depends on the bin width and range of the decoupling covariates.

5.2.7 Decoupling Covariates and Effect Sizes of High Resolution Precipitation

Since the temporal resolution of the precipitation data is quite high, the same steps have been repeated for the node located at the weather station *University Chemistry*, were 1-minute-increment precipitation data was available. Instead of averaging the precipitation along the link path, the weather station data was simply adopted as representative input. This was the only node of the experiment with these conditions. Also in this case – as depicted in Figure 5.14 –, atmospheric pressure, absolute humidity and environmental temperature yielded the strongest correlations and were chosen for the decoupling.

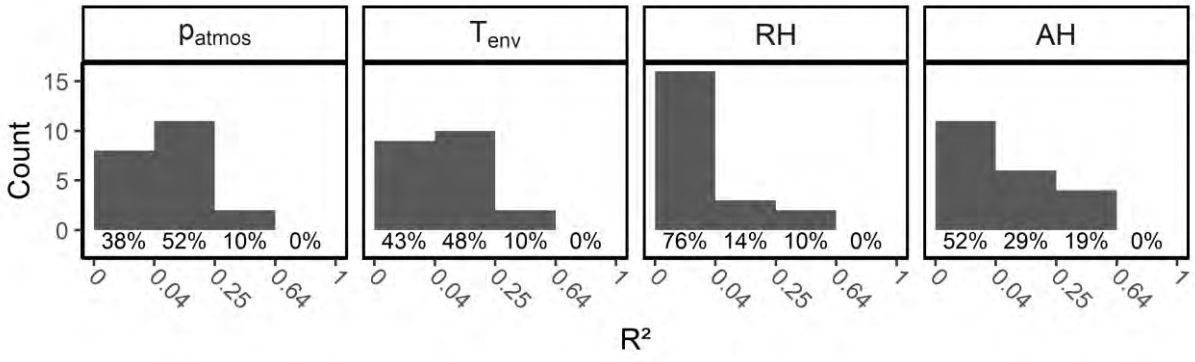

Figure 5.14: Experiment 2, Vauban: R^2-values of linear regressions between the covariates and signal strength for all links of the node at weather station *University Chemistry*. The R^2-values are sorted into categories according to Sullivan and Feinn (2012). The number below the bars is the percentage of all links falling into the respective bin.

The regressions within their respective decoupling-pairs are illustrated Figure A.5, Figure A.6 and Figure A.7 in appendix A. In the figures of the decoupling pairs environmental temperature - absolute humidity and atmospheric pressure - absolute humidity, there are a few scatter plots where higher precipitation values mostly rank in at lower signal strengths, but this seems to be valid only for absolute humidity values lower than 12 g/m³.

Also here, the R²-values are mostly close to zero with a few crossing the threshold to small effect sizes (see Figure 5.15) which is even worse than for the interpolated precipitation values.

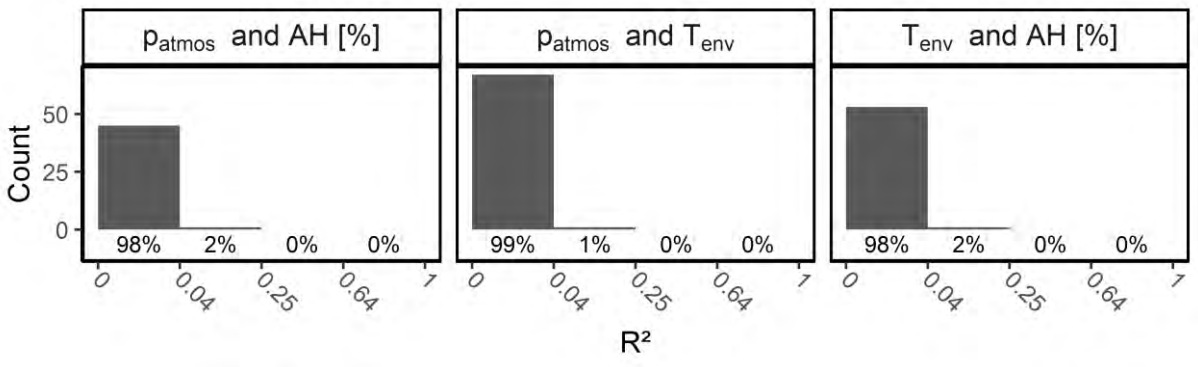

Figure 5.15: Experiment 2, Vauban: R²-values from the regressions of high resolution precipitation and signal strength after decoupling the covariates in the header of the respective graphs. The R²-values are sorted into categories according to Sullivan and Feinn (2012). The counts are different because the number of bin combinations depends on the bin width and range of the decoupling covariates.

5.3 Experiment 3: Rektorat

5.3.1 Overview

Experiment 3, like experiment 1, was conducted over two days; overviews are given in Figure 5.16 and Figure 5.17. The sensor of reference 01 did not work during setup E, hence data for the covariates is missing there.

While the basic arrangement remained the same for most of the time, the distance between transmitter and receivers, the transmission frequency and the sprinkling intensity were varied. On the first day, only one sprinkler was used, delivering 32 to 42 mm/h. On the second day, the sprinkler count was increased to three, delivering 330 to 400 mm/h. Just like in experiment 1, the highest value recorded by the totalizators placed along the line of sight between transmitter and receiver was adopted as representative.

Only two out of the 8 setups made use of the 2.4 GHz frequency. This was decided upon the fact that the preliminary investigation during the experiment did not show any obvious attenuation effect for 5 GHz, thus a degradation of the signal strength of 2.4 GHz seemed unlikely. The lower frequency seems to have a much higher variability than the higher frequency, clearly visible in sudden increase of signal strength range in Figure 5.16. The operating ranges were were 50.5 to 73.1 °C receiver temperature, 10.5 to 51.1 % relative humidity and 979 to 986 hPA atmospheric pressure.

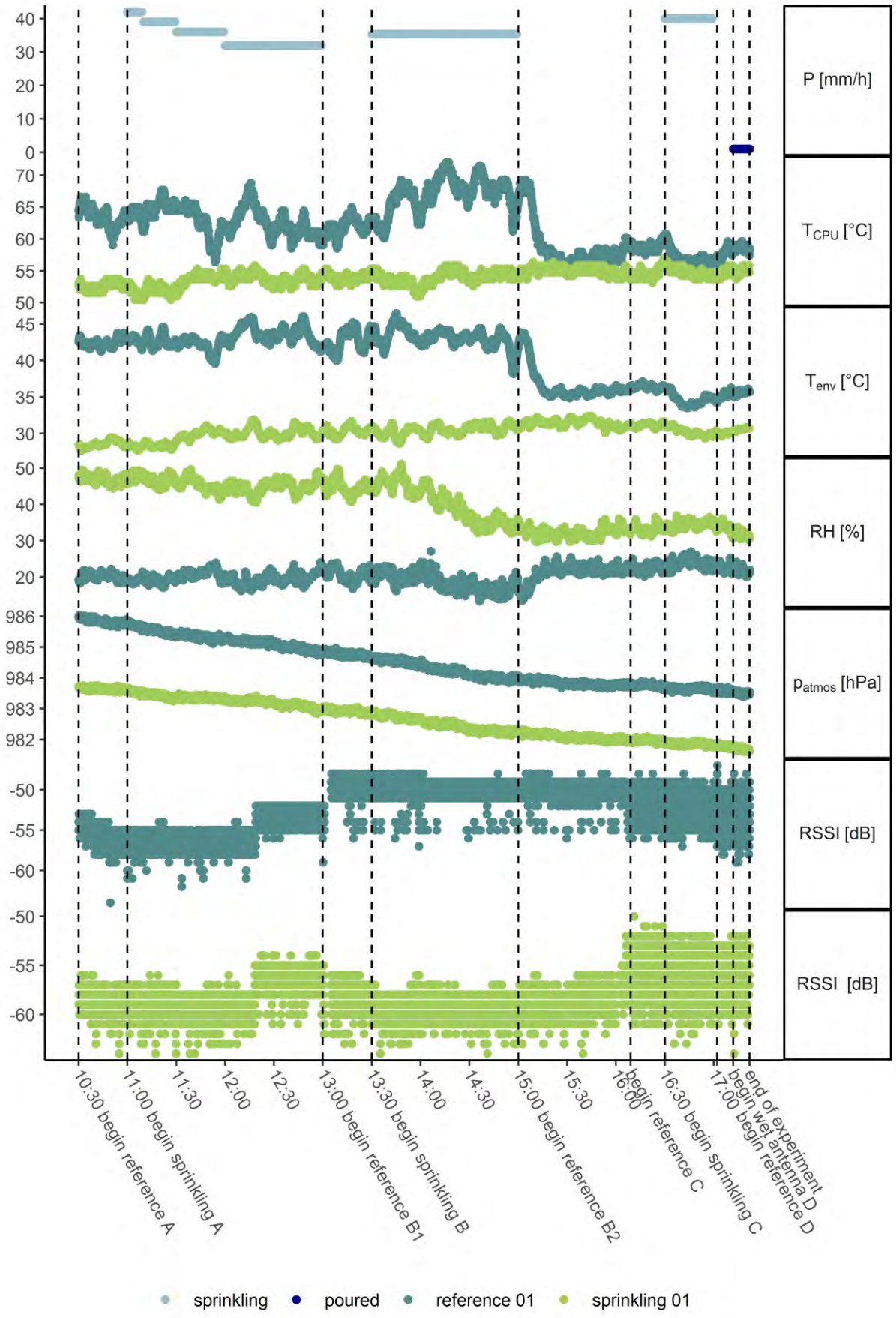

Figure 5.16: Experiment 3, Rektorat, Overview and timeseries of recorded parameters, day 1.

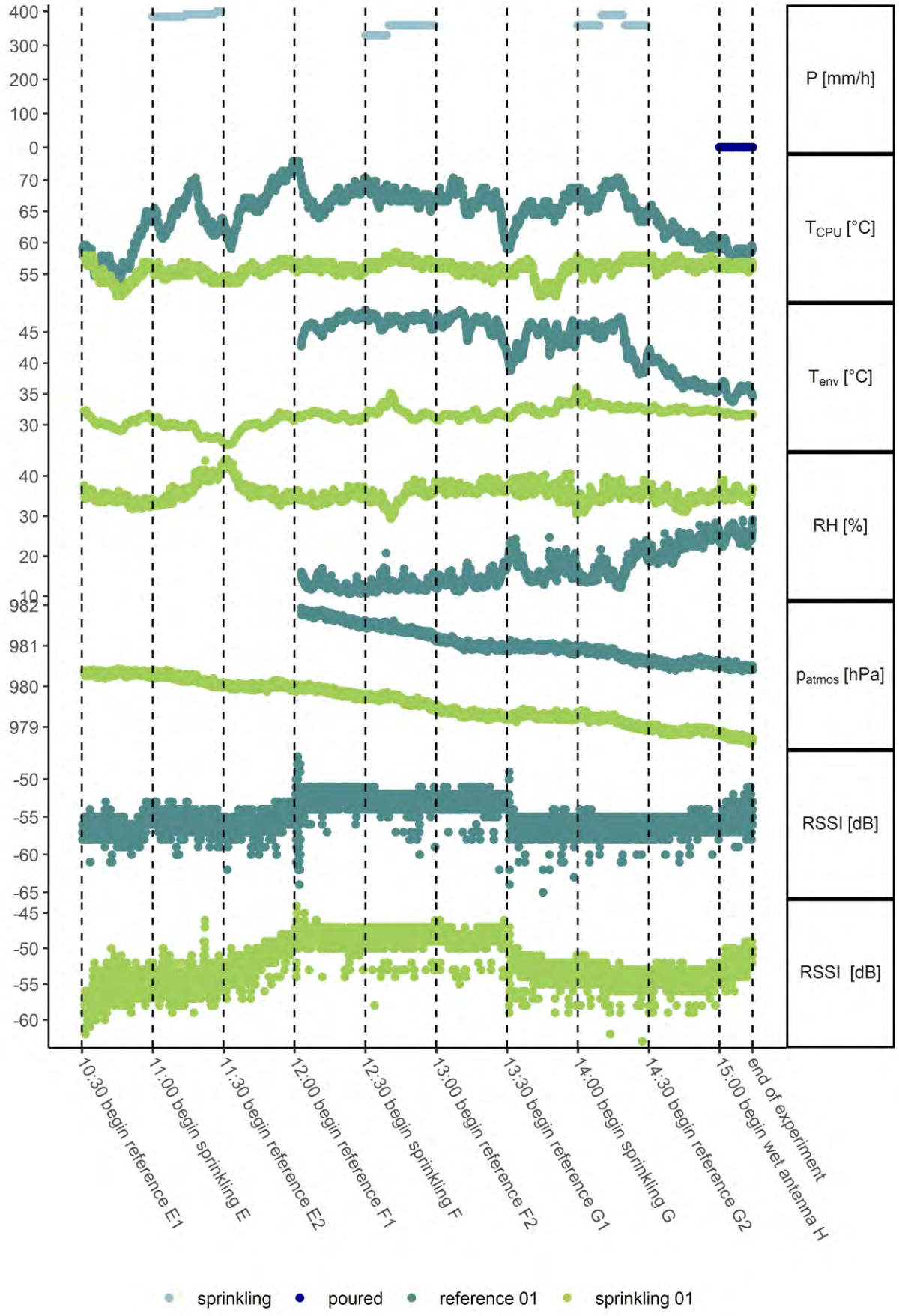

Figure 5.17: Experiment 3, Rektorat, Overview and timeseries of recorded parameters, day 2.

The setups are listed in Table 5.6. Each setup consisted of a sprinkling and one or more reference periods. In setup D and H, the sprinkling system was turned off. Instead, water was manually poured on the transmitter's plastic cover in order to simulate the wet antenna attenuation effect.

Table 5.6: Experiment 3, Rektorat: Overview of periods

setup	periods	time [h]	frequency [GHz]	distance to transmitter [m]
A	reference A	10:30 – 11:00	5	15
	sprinkling A	11:00 – 13:00		
B	reference B1	13:00 – 13:30		
	sprinkling B	13:30 – 15:00	5	13
	reference B2	15:00 – 16:05		
C	reference C	16:06 – 16:30	2.4	13
	sprinkling C	16:30 – 17:02		
D	reference D	17:02 – 17:12	2.4	13
	wet antenna D	17:12 – 17:22		
E	reference E1	10:30 – 11:00		
	sprinkling E	11:00 – 11:30	5	6
	reference E2	11:30 – 12:00		
F	reference F1	12:00 – 12:30		
	sprinkling F	12:30 – 13:00	5	8
	reference F2	13:00 – 13:30		
G	reference G1	13:30 – 14:00		
	sprinkling G	14:00 – 14:30	5	13
	reference G2	14:30 – 15:00		
H	wet antenna H	15:00 – 15:14	5	13

The covariates temperature, relative humidity, atmospheric pressure and CPU-temperature were measured at both nodes. For most of the time on both days, node reference 01 was under direct sunlight, until shadows from the nearby building brought some

shade in the afternoon. Node sprinkling 01 was covered by tree canopy. This difference manifests in the sudden drop of temperature and CPU-temperature and rise of relative humidity of reference 01 on both days. Day 2 was slightly cloudier.

The significant Spearman-correlations of RSSI to the covariates for each period and node are given in Figure 5.18. The correlations have been connected by lines to increase the visibility of patterns. Some of the correlations vary extremely such as CPU-temperature which changes from 0.66 to -0.49 within two periods for the reference node. During other periods, the change is subliminal. The same behavior can be found for all other covariates in all setups and for both nodes. Thus, there is no distinct pattern of correlation change related to the periods omnipresent in all setups.

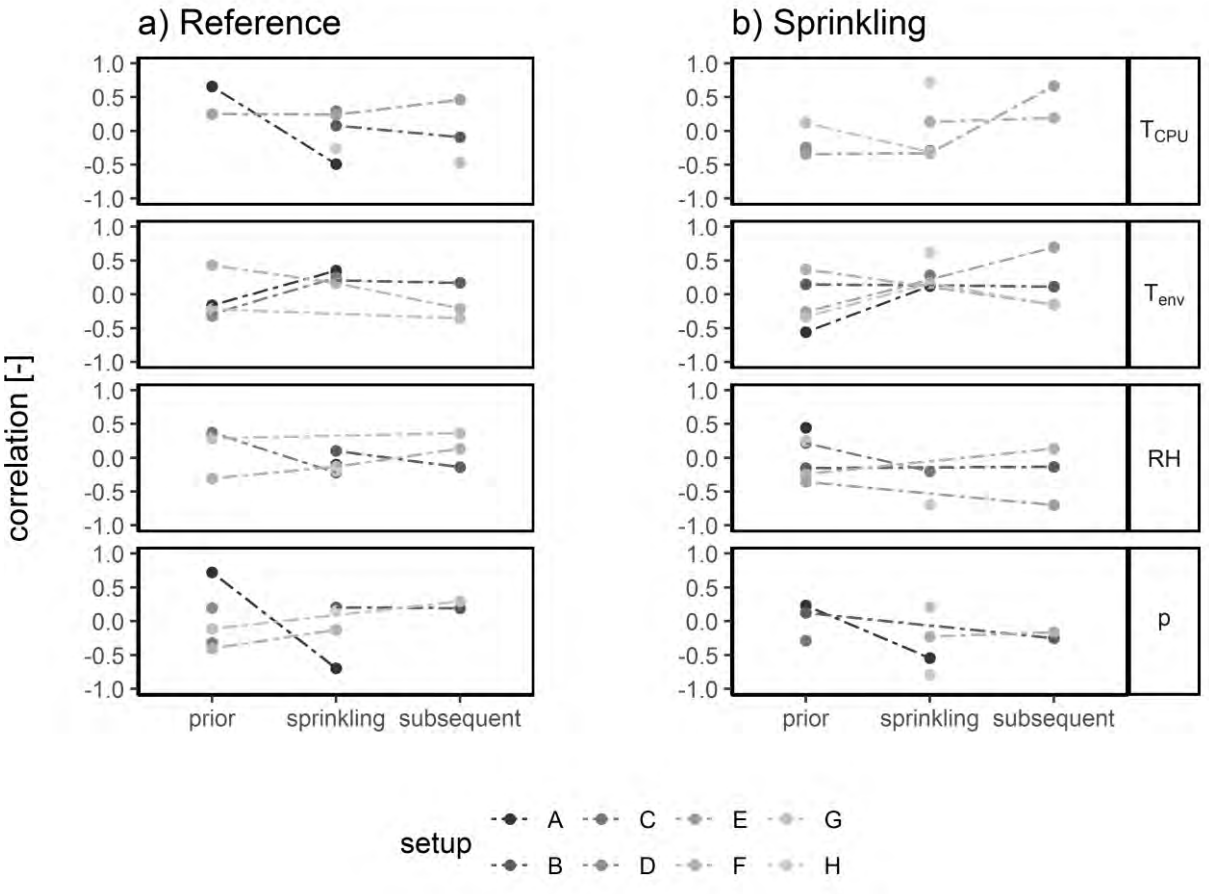

Figure 5.18: Experiment 3, Rektorat: Spearman-correlations between RSSI and covariates.

5.3.2 Distributions

The distributions of the reference and sprinkling node are more or less uniform for most of the setups (Figure 5.19). For example, in setup A and C, both nodes show the same shape, including a characteristic dip (indicating a mixture distribution). Hence, the distribution defining factors might originate rather on the transmitter's side than from the receivers. The only setup where the distributions of the two nodes map distinct shapes is setup H.

The 2.4 GHz-setups appear (setups C and D) to be more stable than the 5 GHz-setups. Their distributions are broader and display a little bend during the sprinkling period, but they stay more or less around the same mean. The 5 GHz-setups (at least B, E and G) are more versatile and move their center along with the periods.

Interestingly, neither distance nor frequency seems to be significant when it comes to general signal strength. Setup E, the smallest distance, had one of the worst connectivities of reference 01, and only third best for sprinkling 01. On the other hand, setup A with the highest distance was one of the worst performing setups for both nodes. The lower frequency, which should have a higher range according to the general scientific consensus, did not have a definite signal strength advantage over the lower frequency.

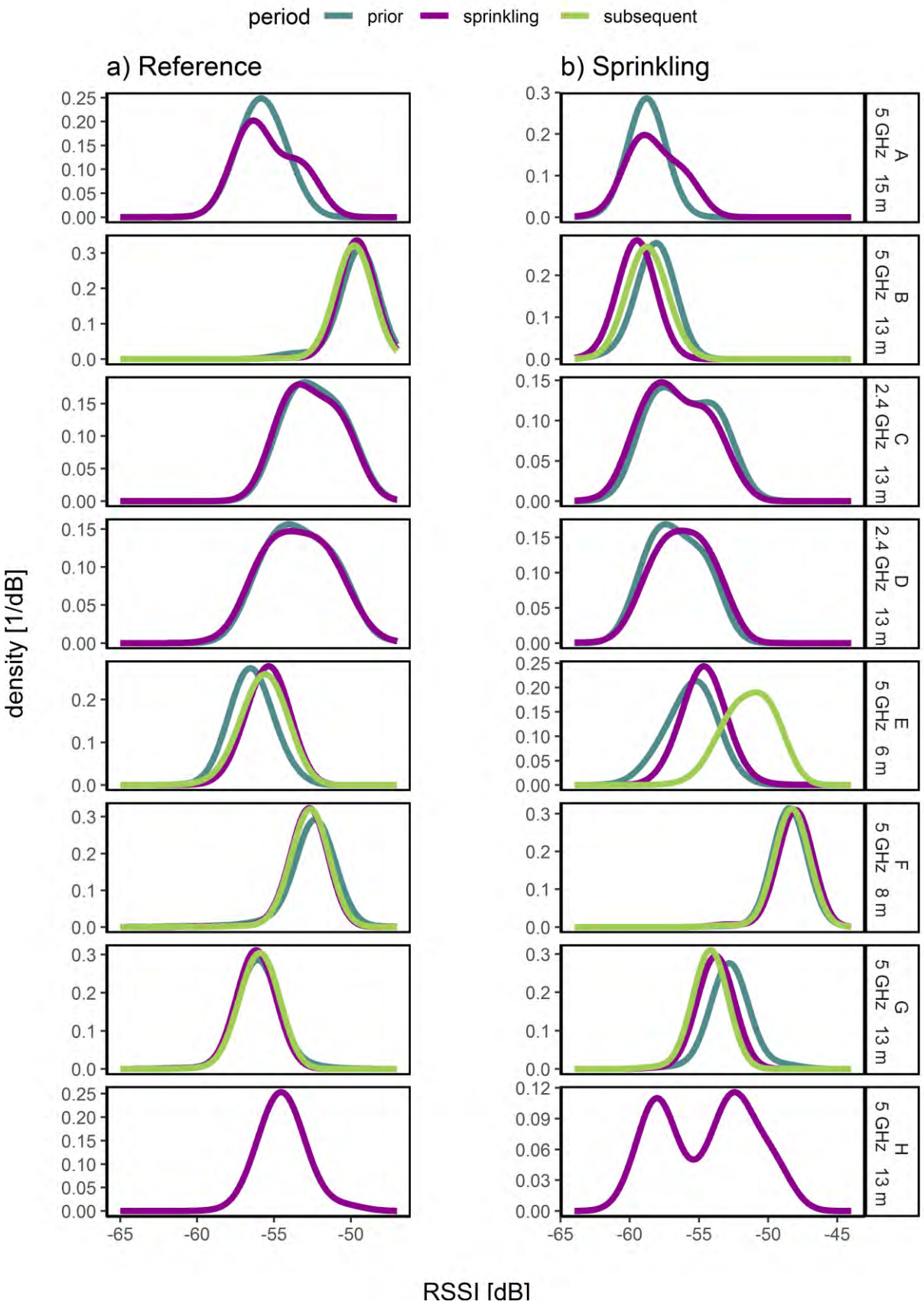

Figure 5.19: Experiment 3, Rektorat: Density estimates of the distributions of signal strength for reference and sprinkling nodes and different setups / periods. The frequency and distance are given in the boxes on the right.

5.3.3 Homoskedasticity

The mean-centered Levene's test somewhat reflects the observations from the distributions' plot. Most of the times, when the distributions did not overlap, the test also states heterogeneous variances.

Setup A, E and H are not fit for ANOVA at all. The 2.4-GHz-setups C and D can be analyzed without concern; from remaining setups are only partly qualified.

In total 5 out of 11 groupings have sufficient homogeneity of variance for an ANOVA for both reference 01 and sprinkling 01.

Table 5.7: Experiment 3, Rektorat: Results of the Levene's test. *: p <= 0.05, **: p <= 0.01, ***: p <= 0.001, -: p > 0.05

setup	period	reference 01	sprinkling 01
A	prior - sprinkling	***	***
B	prior - sprinkling	-	***
	sprinkling - subsequent	***	-
C	prior - sprinkling	-	-
D	prior - sprinkling	-	-
E	prior - sprinkling	***	*
	sprinkling - subsequent	***	***
F	prior - sprinkling	-	***
	sprinkling - subsequent	-	-
G	prior - sprinkling	***	***
	sprinkling - subsequent	**	-
H	prior (subsequent from G) - sprinkling	***	***

5.3.4 ANOVA and Effect Size

The ANOVA revealed an omnipresent difference between the groups for the sprinkling node with high significance within each group-pair as can be seen in Table 5.8. For the reference node, out of the five pairs which were qualified for the ANOVA by the

Levene's test, only one pair yielded a high significant inter-group-difference (setup F prior-sprinkling). Of the others, one had medium, one low and two no statistical significance at all.

Table 5.8: Experiment 3, Rektorat: Results of the ANOVA. *: p <= 0.05, **: p <= 0.01, ***: p <= 0.001, -: p > 0.05

setup	period	reference 01	sprinkling 01
A	prior - sprinkling		
B	prior - sprinkling	-	
	sprinkling - subsequent		***
C	prior - sprinkling	*	***
D	prior - sprinkling	-	***
E	prior - sprinkling		
	sprinkling - subsequent		
F	prior - sprinkling	***	
	sprinkling - subsequent	**	***
G	prior - sprinkling		
	sprinkling - subsequent		***
H	prior (subsequent from G) - sprinkling		

The effect sizes (Table 5.9) showed a similar one-sided picture: six pairs asserted a small effect, two a medium effect, two a large effect and one very large effect for the sprinkling node. On the other hand, five small effects and only one large effect where observed for the reference node.

Setup D and H should not be taken into consideration, because the influence taken on the transmitter was supposed to be equivalent for both nodes. The 2.4 GHz-setups have smaller effect sizes than the 5 GHz which is in agreement with the theoretical higher attenuation along with higher frequencies.

Except for E prior-sprinkling and H, the observed effect was always larger for the sprinkling node, however, the direction of the effect is not always uniform. When comparing the effect sizes to the distributions in Figure 5.19, there is only one setup (namely setup B) out of eight, where the signal strength during the sprinkling period is clearly lower than during the prior and subsequent period.

Table 5.9: Experiment 3, Rektorat: Cohen's d. d >= 0.2: small, d >= 0.5: medium, d >= 0.8: large, d > 1.3: very large (Sullivan and Feinn, 2012)

setup	period	reference 01	sprinkling 01
A	prior - sprinkling	0.24	0.37
B	prior - sprinkling	0.02	1.28
	sprinkling - subsequent	0.2	0.74
C	prior - sprinkling	0.09	0.23
D	prior - sprinkling	0.06	0.22
E	prior - sprinkling	0.93	0.63
	sprinkling - subsequent	0.23	2.12
F	prior - sprinkling	0.22	0.33
	sprinkling - subsequent	0.1	0.21
G	prior - sprinkling	0.15	0.92
	sprinkling - subsequent	0.23	0.41
H	prior (subsequent from G) - sprinkling	1.3	0.09

6 Discussion

The findings presented in the previous chapter will be discussed in the following. Before the results can be related to the hypotheses formulated in section 3, the methodology and error sources have to be explored.

6.1 Experiment 1: Experimental Uncertainties and Error Analysis

Regarding the results of experiment 1, the initial considerations have to be directed at the actual ambient conditions of the experiment. The experiment was originally modelled to be under controlled conditions. However, it might not have been as undisturbed as hoped for. First of all, there has been a second parallel experiment going on during the run-time of the experiment. Occasionally, people were passing through the plots and the transmission-line of the transmitters which naturally added attenuation to some of the transmissions. Due to the magnitude of the dataset, it was not possible to remove those observations from the data analysis - however, they probably comprise only a small portion of the data. Furthermore, a tarp was spanned between receiver and reference node and nodes were moved which all in all made it necessary to dismiss an entire day of experimental time because the conditions changed significantly. Although in remote location, the receiver captured a few outside 868 MHz-transmissions. While there was no interferences which the gateway which was able to keep apart packet collisions, the SDR did not observe the packet structures and captures raw antenna excitations only. Still, the probability that these foreign transmissions have altered the SDR-data is low because of the packet detection algorithm. Interference from the 2.4 GHz network used for remote controlling the gateway and from cell phones used by the experimenters was present but should be negligible (Madariaga, Panza and Bustos-Jimenez, 2018).

Even without taking those disturbances in account, it cannot be said if the temporal variability of the environmental conditions was small enough throughout the experiment to be considered stable. Wennerstrom *et al.* (2013) state the presence of diurnal

cycles of signal strength of WSN, which might be related to temperature. Nonetheless, this temperature effect is ignored in this experiment because temperatures were quite low. A severe temperature effect has therefore not to be expected. Due to the rainy weather conditions, the formation of droplets on the gateways antenna and the plastic sheet covering the SDR was unavoidable and not constant. Wet antenna attenuation does not depend on frequency (Overeem, Leijnse and Uijlenhoet, 2011) and is therefore probably present in the dataset but it is unknown if it is constant or variable throughout the experiment. This effect might have even obliterated any difference between the sprinkling and non-sprinkling periods: if the wet antenna attenuation is much higher than the rainfall attenuation, there would be significant differences between the groups because the antenna was wet before, during or after the sprinkling period due to natural precipitation, an issue also pointed out by Overeem, Leijnse and Uijlenhoet (2011). Even if there was no wet antenna attenuation, the resolution of the signal strength of the gateway and the SDR was far too low at 1 dB. In theory (equation (3)), 1 GHz-waves have a specific attenuation of 0.00113 dB/km while the longest distance of the setup was only 29 m. The highest resolution encountered during the research of this thesis was presented by Christofilakis *et al.* (2018) who used a setup with a resolution of 10^{-4} dB.

The precipitation measurements can be rated reliable because the records from the seven gauges were compared and validated between each other. Furthermore, the approach of using precipitation as categorical variable negates the requirement of accuracy.

6.2 Experiment 1: Discussion and Assessment of Results

The correlation coefficients did not reveal a distinct pattern which might point to a strong influence of the covariates on the signal strength. If there was an actual effect of atmospheric pressure, its correlation coefficients are too low and uncertain to be

exploited in order to make reliable statements about the impact of this parameter. It is therefore concluded that none of the covariates play a significant role for the signal strength, at least not at present conditions (rainy day in a forest, 7 to 14 °C) and at such low distances.

Due to the condition of homoscedasticity, only four out of nine possible period-pairs could be assessed with the ANOVA. The results show that there were significant differences between the measurements before, during and after the sprinkling period, but only for those nodes located on the sprinkling plot. This result might be misleading, because in fact only one assessment could be made on the reference site (as asserted by the Levene's test) and three on the sprinkling site, plus the ANOVA might have yielded significant results purely because of the large sample size. Given that requisite, even small differences of about 1 dB can appear significant, but the question remains if such differences are meaningful compared to the typical range of variation of the signal strength.

The effect size yielded large effect sizes for both sides, so there's no conclusive result. The origin of the extremely large effect size for node reference 02, periods prior to sprinkling is unknown but it is doubtful if the measurements of the two periods actually originate from the same population. One explanation for the large difference might be the antenna malfunction, where the antenna had to be carefully re-erected at the same place and in the same orientation which might have led to slight changes in the reception characteristics for that specific node and a decrease of variance. Nonetheless, the effect sizes are not unequivocally located at the sprinkling side and do not indicate a significant effect of precipitation on signal strength.

The results of the SDR also do not show a clear difference between reference and sprinkling plot: the mean signal strength for the sprinkling period form the lowest group on both sides. This implicates that the difference is not caused by the sprinkling system turned off and turned on again, but rather because of external (non-linear) influences which might have changed during the experiment. There is definitely no frequency-

shift or sub-frequency attenuation, because the shape of the boxplots is widely constant throughout periods and nodes.

The fact that the ratio or sequence of the means of the periods of the SDR differs from the ones in the records of the gateway confirms the irrelevance of precipitation in this experiment. This implicates that the properties of the measurement devices might play a bigger role for the reception than the periods and whatever external influences they bear.

To sum it up, the SDR and the effect size results do not imply an effect of precipitation, while the ANOVA brought out an impact of precipitation but was dismissed due to limitations of the method and low number of ratable results. Hypothesis H1 for 868 MHz must therefore be considered falsified, at least for such small distances of 29 m maximum. The same conclusion must be drawn for H2, because the correlations did not show a uniform pattern and the difference between periods is likely to be due to the reception characteristics of the devices.

6.3 Experiment 2: Experimental Uncertainties and Error Analysis

In experiment 2, a LoRaWAN-network operating at 868 MHz was investigated at the urban scale. The most compromising factor of this experiment was the complexity of the surroundings: the uncertainty regarding what causes which attenuation is very high. Static external effects such as buildings, nodes and receiver design were excluded from the analysis through linkwise standardization of the signal strength. However, even those parameters could have changed in theory, since it is unknown, if and how any of those conditions have changed over the course of the experiment. Have new buildings been erected in the transmission path of a link? Did one of the third-party-gateways receive a new antenna with higher gain or was it moved 15 m to a different corner of a roof? How exactly did vegetation growth impair the transmission? The experiment took place during the growth season of many plants and some of the nodes

were positioned behind hedges or trees which developed a noticeable canopy until the end of experiment. Iova *et al.* (2017) and Ahmad *et al.* (2018) both observed a heavy decrease of connectivity range for LoRa-devices attributed to vegetation canopy.

Additionally, random obstructions by vehicles or interactions by humans and animals with the nodes might also have caused temporary changes in signal strength. Several insects had adopted the nodes housings as shelter and one even managed to push out the batteries from the battery holder by setting up a web-like structure underneath them. Finally, those external effects will remain obscure, but they attribute to a rather large volume of uncertainty.

The amalgamation of all path loss contributors has been presented in Figure 5.6. A large portion of the high variability between links can probably explained by the different reception characteristics of the gateways. Since difference between free space path loss model and the recorded signal strength is quite high compared to the ranges of some of the links, the effect of precipitation, if there was any at all, must have been marginal.

Another source of error is the formation of dew on the antennas of transmitters and receivers, as emphasized by Overeem, Leijnse and Uijlenhoet (2011) and Overeem, Leijnse and Uijlenhoet (2016). Temperatures close to the dew point can basically induce the wet antenna attenuation effect and therefore distort the signal strength unrealistically, weighing in especially severe on short distance links. For 5.98 % of the transmissions by the nodes and 8.1 % of the deployment time of the study-gateway relative humidity was reported to be 95 %. Taking into account small fluctuations in temperature or humidity as well as the accuracy of the sensors, dew formation on the receivers or transmitter-antennas or housing has likely taken place. Furthermore, information about the antennas wetness or dryness were generally sparse. Truth values can only be obtained for those nodes and gateways which situated right next to a weather station but not for the other third-party gateways. Even for the study-gateway, which was

located at weather station *University Vauban*, it is unknown how long the effect endured after a rainfall event because there was no information about the drying process of the antenna.

Due to the apparent differences in the transmission characteristics of the nodes and reception characteristics of the gateways, it is also difficult to assess the effect of temperature on the electronical components of transmitter and receiver. Cattani, Boano and Römer (2017) had found an evident correlation between temperature and PRR and Boano, Cattani and Römer (2018) named a reduction of 3-4 dB for an increase of temperature from 0 to 50 °C for the exact same transmission chip used in this thesis. Some of the nodes were periodically exposed to sunlight, others were not. The study-gateway was intentionally placed in the shade, but the other gateways might or might not have been exposed to the sun and might have been subject to a diurnal cycle as mentioned by Wennerstrom *et al.* (2013). For 30% of the links a small, for 9 % a medium and for 2 % a large effect of environmental temperature has been observed. 59 % did not experience any effect of environmental temperature. Also, no effect of CPU-temperature has been found.

Of course, there was also some inaccuracy induced by the sensor measurements. The sensors used had an accuracy of ±3 % for relative humidity, ±1 °C for temperature and ±1.7 hPa for the operating ranges of this thesis (Bosch Sensortec, 2018). These errors are assumed to be negligible for the data analysis. Angain, the most problematic is the low resolution of the signal strength data with of only 1 dB and the low resolution of precipitation measurements of only 10 minutes. Precipitation events, however, might show a higher variability, where minute or sub-minute resolution would have been more accurate (Crane, 2003). Even though it was attempted to investigate the rain attenuation with high accuracy precipitation data, there was only one node available throughout the network were such conditions were present. For reliable statements, more of such configurations would have been necessary.

6.4 Experiment 2: Discussion and Assessment of Results

Overall, the experiment provided a stable network with a satisfying coverage of a large portion of the city. The network remained functional until the end of the experiment and would have probably continued to do so. The results show that LoRaWAN is less dependent on the environment than the theory and research of others had implicated; at least at urban scale, because the variability of variance between the links is quite high and the correlations of signal strength to the covariates are very low. Static obstructions seem to play the major role here. One explanation might be the typically high elevation of the receiving gateways which means that every transmission must cross about the same amount of building mass. Distance plays another important role, as much fewer connections could have been established at distances higher than approx. 4.5 km. Compared to obstruction and distance the influence of the environment is faded out almost entirely. The correlations clearly showed that assuming any relation here would be a mistake.

Even after decoupling some of the environmental effects, no distinct pattern was visible. The regressions with precipitation as the predictor and signal strength as the response yielded extremely low R^2-values, therefore precipitation cannot be considered a predictor for signal strength. Any pattern which might be present should rather be considered random or an artifact. Since the rain attenuation for 868 MHz has been determined to be virtually non-existent further steps like the identification of wet periods and derivation of the rain rate from the path loss were obsolete.

Conclusively, as already found in experiment 1, the outcome of experiment 2 also supports the dismissal of H1 for 868 MHz, even at the larger distances of the urban scale. Since there was no correlation of the covariates to the signal strength and since the link variability is quite high and must mainly be attributed to obstruction and distance, H2 is also considered falsified.

6.5 Experiment 3: Experimental Uncertainties and Error Analysis

The third experiment examined a small Wi-Fi-network operating at 2.4 and 5 GHz. Although the experiment was conducted on an open and even lawn, there were still some exterior influences which might have disturbed the transmissions. Occasionally, passersby were walking through the signal path of the reference node and through the signal path of the sprinkling node during the readouts of the totalizators. These periods of disturbance were filtered by removing them from the data set. Additionally, the signal path of the reference node might have been blocked by sprinklers and totalizators but these obstructions can be considered static. The passersby's cell phones and the Wi-Fi-network in the adjacent building probably emitted Wi-Fi-radiation. This might have caused interference with the transmissions of the setup. However, it is unlikely that those were strong enough to induce a severe signal degradation.

Since the experiment was conducted over the course of two full days, diurnal cycles have to be considered as well. Changing conditions of sunlight were observed during the day as the shadows cast by buildings and trees changed and exposed the nodes to the sun periodically. The setup durations were kept short in order to minimalize the variation of external conditions within one setup.

Occasionally, splattering of the sprinkling system led to droplet formation on the housings of the receivers and the plastic bag covering the transmitter but the amount of water was much lower than the amount poured in setup D and H. Since no significant effect has been observed in these setups it is assumed that the accidental splattering did not impact the signal strength.

As with the previous experiments, the resolution of the recorded signal strength of 1 dB was again very low. Attenuation effects were probably too low to be detectable: Using equation (3) for 2.5 and 5 GHz for a rain rate of 400 mm/h, the expected specific attenuation is 0.0001 dB/m and 0.006 dB/m respectively.

6.6 Experiment 3: Discussion and Assessment of Results

The correlations did not yield any obvious pattern. For both nodes, the effects of environmental temperature, CPU-temperature and humidity do not follow a distinct direction. Therefore, none of the influences summarized in the theoretical chapters can either be confirmed or dismissed. Higher correlations to atmospheric pressure are particularly surprising. While pressure plays a role in changing the refractive index between atmospheric layers which can cause ducting effects - a phenomenon important for precipitation radars - this is not expected at such small distances (Crane, 2003). Since there is no uniform pattern of correlations, there is probably also no significant connection between any of the covariates and the signal strength.

Compared to the 868 MHz frequency, the ANOVA yielded much higher differences between the periods for the sprinkling node than for the reference node. The calculation of the effect sizes supports this outcome. Furthermore, the effect sizes for 5 GHz are higher than for 2.4 GHz, which supports the theory of increasing attenuation with higher frequency. However, the direction of the effect does not confirm this assumption: five out of ten times the signal strength during the sprinkling period was higher than during the reference period.

Since there was no definite deterioration of signal strength during the sprinkling periods, hypothesis H1 for both 2.4 and 5 GHz at 15 m and less has to be rejected. While the correlations of the covariates did not result in any distinct pattern, H2 for 2.4 and 5 GHz should not be completely dismissed because there was a definite difference between the nodes and between the periods as the ANOVA and the effect sizes show. What exactly caused this difference is cannot be extracted from the recorded data but it might be related to the formation of water surfaces on the lawn due to the heavy sprinkling. At times, the lawn resembled a giant puddle of 5 m diameter. The formation of reflective planes, as reported by Michalek *et al.* (2015) therefore seems to be a valid explanation.

7 Conclusion and Outlook

Three experiments have been conducted to investigate the applicability of the methods used in the estimation of precipitation rates from the attenuation of microwave radio waves for two types of widespread open radio networks: LoRaWAN networks operating at 868 MHz and Wi-Fi networks operating at 2.4 GHz and 5 GHz.

The results confirm – as the theory and literature review predicted – that the attenuation of radio waves at these frequencies is virtually nonexistent – at least at ranges typical for the networks under investigation.

In an alternate approach, the reaction of the networks to variations of the environmental conditions during precipitation events has been examined. While 868 MHz was not affected at all, 2.4 GHz showed a slight and 5 GHz a notable change in transmission quality during rainfall– but not necessarily a degradation of signal strength. This is attributed to the formation of wet surfaces acting as reflective planes thereby altering the transmission paths of the connection. The actual applicability of this finding, however, is probably low. The effect has been observed for precipitation rates of 400 mm/h which is unlikely to occur naturally for longer time spans. At this rate the ground was unable to infiltrate the precipitated water. Nevertheless, there is some potential such as a rain detection mechanism for 5 GHz networks operating over surfaces where infiltration is low and the formation of wet surfaces can be expected but probably not for the quantification of precipitation.

In general, open radio networks do not per se represent a good option for precipitation measurements because there is a conflict of interest: While network designers aim at maximum stability and connectivity, it is the weakness of links that meteorologists want to exploit. With increasingly sophisticated devices and network protocols, networks will become more and more reliable. One of the advantages of LoRaWAN is that it can dynamically adapt the transmission configurations (transmission power, channel, and retransmission) to overcome instable links (Augustin *et al.*, 2016). Even if there

was significant attenuation, this would complicate the tracing of signal strengths during precipitation events drastically.

For any network to be useful at all, the rain attenuation must be measurable. This can be achieved by fulfilling at least one of the following conditions: transmission over long distances or by high specific attenuation which comes along with high frequency. The high benefit of the exploitation of microwave link transmissions is an exception because the cellphone towers are not only widespread, but they also transmit over long distances and at high frequencies. Another technology which has proven to be useful is GPS: It has been successfully used to detect changes in the cloud formation prior to precipitation events (Sapucci *et al.*, 2019).

Most other common widespread networks fulfill only one condition or no condition at all. The upcoming 5G standard for cellphones for example includes also frequencies around 30 GHz, but the expected ranges of the new network are only a few tens of meters. WiGig, a technology aiming to replace cables through high data rate transmission operates at 60 GHz but is limited to a few meters at common transmission powers. These two technologies might have potential for local precipitation measurements as alternative to traditional totalizators. However, even these frequencies still have a theoretical specific attenuation of only 0.004 and 0.01 dB/m. To overcome this limitation, high accuracy measurements of the attenuation are required, for example as used by Christofilakis *et al.* (2018).

Bibliography

Ahmad, K.A. *et al.* (2018) 'Impact of foliage on LoRa 433MHz propagation in tropical environment', *INTERNATIONAL CONFERENCE ON ENGINEERING AND TECHNOLOGY (IntCET 2017)*, Putrajaya, Malaysia, 23–24 November 2017: Author(s), p. 20009. doi: 10.1063/1.5022903

Alonso, J. *et al.* (2017) 'Modelling the influence of climatic variables on the received power of a wireless link using an unlicensed U-NII band: A case study in Ecuador', *2017 IEEE 9th Latin-American Conference on Communications (LATINCOM), 2017 IEEE 9th Latin-American Conference on Communications (LATINCOM)*, Guatemala City, 8-10 November: IEEE, pp. 1–6. doi: 10.1109/LATINCOM.2017.8240195

Anastasi, G. *et al.* (2004) 'Performance measurements of motes sensor networks', *Proceedings of the 7th ACM international symposium on Modeling, analysis and simulation of wireless and mobile systems - MSWiM '04, the 7th ACM international symposium*, Venice, Italy, 4-6 October. New York, New York, USA: ACM Press, p. 174. doi: 10.1145/1023663.1023695

Aref, M. and Sikora, A. (2014) 'Free space range measurements with Semtech Lora™ technology', *2014 2nd International Symposium on Wireless Systems within the Conferences on Intelligent Data Acquisition and Advanced Computing Systems, IDAACS-SWS*, Odessa, Ukraine, 11-12 September: IEEE, pp. 19–23. doi: 10.1109/IDAACS-SWS.2014.6954616

Augustin, A. *et al.* (2016) 'A Study of LoRa: Long Range & Low Power Networks for the Internet of Things', *Sensors (Basel, Switzerland)*, 16(9) (18pp). doi: 10.3390/s16091466

Aurel S.p.A. (2019) *GP868 Datasheet*. Modigliana.

Bannister, K., Giorgetti,, G. and Gupta, S.K.S. (2008) 'Wireless Sensor Networking for "Hot" Applications: Effects of Temperature on Signal Strength, Data Collection and Localization', *Proc. of the 5th HotEmNets,* 2008.

Boano, C.A., Cattani, M. and Römer, K. (2018) 'Impact of Temperature Variations on the Reliability of LoRa - An Experimental Evaluation', *Proceedings of the 7th International Conference on Sensor Networks, 7th International Conference on Sensor Networks*, Funchal, Madeira, Portugal, 22-24 January: SCITEPRESS - Science and Technology Publications, pp. 39–50. doi: 10.5220/0006605600390050

Boano, C.A. *et al.* (2010) 'Low-Power Radio Communication in Industrial Outdoor Deployments: The Impact of Weather Conditions and ATEX-Compliance', in Komninos, N. (ed.) *Sensor Applications, Experimentation, and Logistics.* (Lecture Notes of the Institute for Computer Sciences, Social Informatics and Telecommunications Engineering). Berlin, Heidelberg: Springer Berlin Heidelberg, pp. 159–176.

Boano, C.A. *et al.* (2010) 'The Impact of Temperature on Outdoor Industrial Sensornet Applications', *IEEE Transactions on Industrial Informatics*, 6(3), pp. 451–459. doi: 10.1109/TII.2009.2035111

Boano, C.A. *et al.* (2013) 'Hot Packets: A Systematic Evaluation of the Effect of Temperature on Low Power Wireless Transceivers', *Extreme Conference on Communication*, pp. 7–12.

Bosch Sensortec (2018) *BME280 - Data sheet.* Available at: https://ae-bst.resource.bosch.com/media/_tech/media/datasheets/BST-BME280-DS002.pdf (Accessed: 29 September 2019).

Bri, D. *et al.* (2012) 'The influence of meteorological variables on the performance of outdoor wireless local area networks', *2012 IEEE International Conference on Com-*

munications (ICC), ICC 2012 - 2012 IEEE International Conference on Communications, Ottawa, ON, Canada, 10-15 June: IEEE, pp. 5418–5422. doi: 10.1109/ICC.2012.6364448

Bri, D. *et al.* (2015) 'Measuring the weather's impact on MAC layer over 2.4GHz outdoor radio links', *Measurement*, 61, pp. 221–233. doi: 10.1016/j.measurement.2014.10.047

Capsuto, B. and Frolik, J. (2006) 'A System to Monitor Signal Fade Due to Weather Phenomena for Outdoor Sensor Systems', *Fifth International Conference on Information Processing in Sensor Networks (IPSN 2006)*, Nashville, TN, USA, April 2006.

Cattani, M., Boano, C.A. and Römer, K. (2017) 'An Experimental Evaluation of the Reliability of LoRa Long-Range Low-Power Wireless Communication', *Journal of Sensor and Actuator Networks*, 6(2), p. 7. doi: 10.3390/jsan6020007

Cermak, D. *et al.* (2004) 'Study of electromagnetic scattering by rain drops', *10th International Conference on Mathematical Methods in Electromagnetic Theory, 2004, 10th International Conference on Mathematical Methods in Electromagnetic Theory, 2004*, Dniepropetrovsk, Ukraine, Sept. 14-17, 2004: IEEE, pp. 592–594. doi: 10.1109/MMET.2004.1397132

Cheffena, M. and Mohamed, M. (2017) 'Empirical Path Loss Models for Wireless Sensor Network Deployment in Snowy Environments', *IEEE Antennas and Wireless Propagation Letters*, p. 1. doi: 10.1109/LAWP.2017.2751079

Christofilakis, V. *et al.* (2018) 'Rainfall Measurements Due to Radio Frequency Signal Attenuation at 2 GHz', *Journal of Signal and Information Processing*, 09(03), pp. 192–201. doi: 10.4236/jsip.2018.93011

Chwala, C. *et al.* (2012) 'Precipitation observation using microwave backhaul links in the alpine and pre-alpine region of Southern Germany', *Hydrology and Earth System Sciences*, 16(8), pp. 2647–2661. doi: 10.5194/hess-16-2647-2012

Crane, R.K. (1996) *Electromagnetic wave propagation through rain*. (Wiley series in remote sensing). New York, N.Y.: J. Wiley and Sons.

Crane, R.K. (2003) *Propagation handbook for wireless communication system design*. (The electrical engineering and applied signal processing series, 13). Boca Raton, Fla: CRC Press.

Dormann, C.F. (2017) *Parametrische Statistik*. Berlin, Heidelberg: Springer Berlin Heidelberg.

Doumounia, A. *et al.* (2014) 'Rainfall monitoring based on microwave links from cellular telecommunication networks: First results from a West African test bed', *Geophysical Research Letters*, 41(16), pp. 6016–6022. doi: 10.1002/2014GL060724

DWD Abteilung Messnetze und Daten (2017) *Richtlinie: Automatische nebenamtliche Wetterstationen im DWD*. Offenbach am Main.

DWD Climate Data Center (DWD CDC) (2019a) *Recent 1-minute station observations of precipiation for Germany, version recent*. Available at: https://opendata.dwd.de/climate_environment/CDC/observations_germany/climate/1_minute/precipitation/recent/1minutenwerte_nieder_01443_akt.zip (Accessed: 29 September 2019).

DWD Climate Data Center (DWD CDC) (2019b) *Recent hourly RADOLAN-rasters of precipiation depth (GIS-readable), Version V001*. Available at: https://opendata.dwd.de/climate_environment/CDC/grids_germany/hourly/radolan/recent/asc/ (Accessed: 29 September 2019).

Fang, S.-H. and Yang, Y.-H.S. (2016) 'The Impact of Weather Condition on Radio-Based Distance Estimation: A Case Study in GSM Networks With Mobile Measurements', *IEEE Transactions on Vehicular Technology*, 65(8), pp. 6444–6453. doi: 10.1109/TVT.2015.2479591

Fencl, M. *et al.* (2017) 'Gauge-adjusted rainfall estimates from commercial microwave links', *Hydrology and Earth System Sciences*, 21(1), pp. 617–634. doi: 10.5194/hess-21-617-2017

Fohrer, N. *et al.* (eds.) (2016) *Hydrologie* (Utb Basics, 4513).

Heuberger, A. and Gamm, E. (2017) *Software Defined Radio-Systeme für die Telemetrie*. Berlin, Heidelberg: Springer Berlin Heidelberg.

IMST GmbH (2018) *WiMOD iC880A Datasheet*. Kamp-Lintfort: IMST GmbH.

Iova, O. *et al.* (2017) 'LoRa from the City to†the Mountains: Exploration of Hardware and Environmental Factors', *EWSN '17 Proceedings of the 2017 International Conference on Embedded Wireless Systems and Networks*, pp. 317–322.

Ismail, D., Rahman, M. and Saifullah, A. (2018) 'Low-power wide-area networks', *Proceedings of the Workshop Program of the 19th International Conference on Distributed Computing and Networking - Workshops ICDCN '18, the Workshop Program of the 19th International Conference*, Varanasi, India, 4-7 January. New York, New York, USA: ACM Press, pp. 1–6. doi: 10.1145/3170521.3170529

ITU (2005) *Specific attenuation model for rain for use in prediction methods: ITU-R P.838-3*.

ITU (2019) *Calculation of free-space attenuation: ITU-R P.525-4*.

J. C. Logan and J. W. Rockway (1997) *Dipole and Monopole Antenna Gain and Effective Area for Communication Formulas: Technical Report*.

Jorke, P. *et al.* (2017) 'Urban channel models for smart city IoT-networks based on empirical measurements of LoRa-links at 433 and 868 MHz', *2017 IEEE 28th Annual International Symposium on Personal, Indoor, and Mobile Radio Communications (PIMRC), 2017 IEEE 28th Annual International Symposium on Personal, Indoor, and*

Mobile Radio Communications (PIMRC), Montreal, QC, 8-13 October: IEEE, pp. 1–6. doi: 10.1109/PIMRC.2017.8292708

Kirby, A. (2019) *lora-packet: GitHub-Respository*. Available at: https://github.com/anthonykirby/lora-packet (Accessed: 29 September 2019).

Labuguen, R.T. *et al.* (2015) *Nationwide 5GHz-fixed wireless network for prototype rain alarm system. 2015 IEEE Tenth International Conference on Intelligent Sensors, Sensor Networks and Information Processing (ISSNIP)*. 2015 IEEE Tenth International Conference on Intelligent Sensors, Sensor Networks and Information Processing (ISSNIP).

Leijnse, H., Uijlenhoet, R. and Stricker, J.N.M. (2007) 'Hydrometeorological application of a microwave link: 2. Precipitation', *Water Resources Research*, 43(4), p. 1322. doi: 10.1029/2006WR004989

López-Vicario, J. *et al.* (2014) 'Generic empiric propagation model for low power wireless networks operating at the 868 MHz band in smart cities', *IET Microwaves, Antennas & Propagation*, 8(14), pp. 1143–1153. doi: 10.1049/iet-map.2013.0566

LoRa Alliance Technical Committee (2017) *LoRaWAN 1.1 Specification*. Beaverton, OR: LoRa Alliance, Inc.

Luomala, J. and Hakala, I. (2015) 'Effects of Temperature and Humidity on Radio Signal Strength in Outdoor Wireless Sensor Networks', *Proceedings of the 2015 Federated Conference on Computer Science and Information Systems, 2015 Federated Conference on Computer Science and Information Systems,* 13-16 September: IEEE, pp. 1247–1255. doi: 10.15439/2015F241

Madariaga, D., Panza, M. and Bustos-Jimenez, J. (2018) 'I'm Only Unhappy when it Rains: Forecasting Mobile QoS with Weather Conditions', *2018 Network Traffic Measurement and Analysis Conference (TMA), 2018 Network Traffic Measurement and*

Analysis Conference (TMA), Vienna, 26-29 June: IEEE, pp. 1–6. doi: 10.23919/TMA.2018.8506509

Marfievici, R. *et al.* (2013) 'How Environmental Factors Impact Outdoor Wireless Sensor Networks: A Case Study', *2013 IEEE 10th International Conference on Mobile Ad-Hoc and Sensor Systems, 2013 IEEE 10th International Conference on Mobile Ad-Hoc and Sensor Systems (MASS)*, Hangzhou, China, 14-16 October: IEEE, pp. 565–573. doi: 10.1109/MASS.2013.13

Markham, A., Trigoni, N. and Ellwood, S. (2010) *Effect of rainfall on link quality in an outdoor forest deployment. 2010 International Conference on Wireless Information Networks and Systems (WINSYS).* 2010 International Conference on Wireless Information Networks and Systems (WINSYS).

Matthijs Kooijman (2017) *Arduino-LMIC library: GitHub-Respository.* Available at: https://github.com/matthijskooijman/arduino-lmic (Accessed: 29 September 2019).

Medhurst, R. (1965) 'Rainfall attenuation of centimeter waves: Comparison of theory and measurement', *IEEE Transactions on Antennas and Propagation*, 13(4), pp. 550–564. doi: 10.1109/TAP.1965.1138472

Messer, H., Zinevich, A. and Alpert, P. (2006) 'Environmental monitoring by wireless communication networks', *Science (New York, N.Y.)*, 312(5774), p. 713. doi: 10.1126/science.1120034

Michalek, L. *et al.* (2015) 'Analysis of Signal Attenuation in UHF Band', *Advances in Electrical and Electronic Engineering*, 13(4) (6pp). doi: 10.15598/aeee.v13i4.1484

Oguchi, T. (1983) 'Electromagnetic wave propagation and scattering in rain and other hydrometeors', *Proceedings of the IEEE*, 71(9), pp. 1029–1078. doi: 10.1109/PROC.1983.12724

Okamura, S. and Oguchi, T. (2010) 'Electromagnetic wave propagation in rain and polarization effects', *Proceedings of the Japan Academy. Series B, Physical and Biological Sciences*, 86(6), pp. 539–562. doi: 10.2183/pjab.86.539

Olsen, R., Rogers, D. and Hodge, D. (1978) 'The aRbrelation in the calculation of rain attenuation', *IEEE Transactions on Antennas and Propagation*, 26(2), pp. 318–329. doi: 10.1109/TAP.1978.1141845

Overeem, A., Leijnse, H. and Uijlenhoet, R. (2011) 'Measuring urban rainfall using microwave links from commercial cellular communication networks', *Water Resources Research*, 47(12), p. 1322. doi: 10.1029/2010WR010350

Overeem, A., Leijnse, H. and Uijlenhoet, R. (2016) 'Two and a half years of country-wide rainfall maps using radio links from commercial cellular telecommunication networks', *Water Resources Research*, 52(10), pp. 8039–8065. doi: 10.1002/2016WR019412

Petajajarvi, J. *et al.* (2015 - 2015) *On the coverage of LPWANs: range evaluation and channel attenuation model for LoRa technology. 2015 14th International Conference on ITS Telecommunications (ITST).* Copenhagen, Denmark, 2-4 December: IEEE.

Rankine, C.J., Sanchez-Azofeifa, G.A. and MacGregor, M.H. (2014) 'Seasonal wireless sensor network link performance in boreal forest phenology monitoring', *2014 Eleventh Annual IEEE International Conference on Sensing, Communication, and Networking, SECON*, Singapore, Singapore, 30 June - 3 July: IEEE, pp. 302–310. doi: 10.1109/SAHCN.2014.6990366

Sapucci, L.F. *et al.* (2019) 'Global Positioning System precipitable water vapour (GPS-PWV) jumps before intense rain events: A potential application to nowcasting', *Meteorological Applications*, 26(1), pp. 49–63. doi: 10.1002/met.1735

Schleiss, M. and Berne, A. (2010) 'Identification of Dry and Rainy Periods Using Telecommunication Microwave Links', *IEEE Geoscience and Remote Sensing Letters*, 7(3), pp. 611–615. doi: 10.1109/LGRS.2010.2043052

Sullivan, G.M. and Feinn, R. (2012) 'Using Effect Size—or Why the P Value Is Not Enough', *Journal of Graduate Medical Education*, 4(3), pp. 279–282. doi: 10.4300/JGME-D-12-00156.1

Tatsis, G. *et al.* (2018) 'Rainfall events' correlation with S-band signal attenuation', *2018 7th International Conference on Modern Circuits and Systems Technologies (MOCAST), 2018 7th International Conference on Modern Circuits and Systems Technologies (MOCAST)*, Thessaloniki, 7-9 May: IEEE, pp. 1–4. doi: 10.1109/MOCAST.2018.8376582

The Things Network (2013) *LoRa Gateway project: GitHub-Respository.* Available at: https://github.com/TheThingsNetwork/lora_gateway (Accessed: 29 September 2019).

The Things Network (2019) *The Things Network Arduino Library: GitHub-Repository.* Available at: https://github.com/TheThingsNetwork/arduino-device-lib (Accessed: 29 September 2019).

Thelen, J., Goense, D. and Langendoen, K. (2005) 'Radio Wave Propagation in Potato Fields', *Proceedings from the 1st Workshop on Wireless Network Measurements.*

Thiagarajah, S.P. *et al.* (2013) 'The effect of rain attenuation on S-band terrestrial links', *2013 IEEE Symposium on Wireless Technology & Applications (ISWTA), 2013 IEEE Symposium on Wireless Technology & Applications (ISWTA)*, Kuching, Malaysia, 22-25 September: IEEE, pp. 192–197. doi: 10.1109/ISWTA.2013.6688768

TP-Link (2019) *AC750 Wi-Fi Range Extender Datasheet.* Available at: https://static.tp-link.com/2018/201810/20181022/RE200(US)%203.0%20Datasheet.pdf (Accessed: 8 August 2019).

TTN Zurich (2019) *The Things Network: iC880a-based gateway: GitHub-Respository.* Available at: https://github.com/ttn-zh/ic880a-gateway (Accessed: 29 September 2019).

Tyler Glenn (2017) *BME280: GitHub-Respository.* Available at: https://github.com/finitespace/BME280 (Accessed: 29 September 2019).

Uijlenhoet, R., Overeem, A. and Leijnse, H. (2018) 'Opportunistic remote sensing of rainfall using microwave links from cellular communication networks', *Wiley Interdisciplinary Reviews: Water*, 5(4), e1289. doi: 10.1002/wat2.1289

University of Freiburg, Chair of Environmental Meteorology (2019) *Data of the Rooftop Weather Station, Highrise of the Department of Chemistry, 2019-02-01 to 2019-07-31.* Available at: http://wetter.uni-freiburg.de/start_en.php (Accessed: 29 September 2019).

University of Freiburg, Chair of Hydrology (2019) *Data from the Meterological Station in Vauban, 2019-02-01 to 2019-07-31.* Available at: https://hydrologie.shinyapps.io/MeteoVauban/ (Accessed: 29 September 2019).

Wark, T. *et al.* (2008) 'Springbrook: Challenges in developing a long-term, rainforest wireless sensor network', *2008 International Conference on Intelligent Sensors, Sensor Networks and Information Processing, ISSNIP*, Sydney, Australia, 15-18 December: IEEE, pp. 599–604. doi: 10.1109/ISSNIP.2008.4762055

Weinbauinstitut Freiburg (2019) *Data from the Meterological Station at the WBI, Freiburg, 2019-02-01 to 2019-07-31.*

Wennerstrom, H. *et al.* (2013) 'A long-term study of correlations between meteorological conditions and 802.15.4 link performance', *2013 IEEE International Conference on Sensing, Communications and Networking (SECON), 2013 10th Annual IEEE Communications Society Conference on Sensing and Communication in Wireless Networks*

(SECON), New Orleans, LA, USA, 24-27 June: IEEE, pp. 221–229. doi: 10.1109/SAHCN.2013.6644981

Yim, D. *et al.* (2018) 'An experimental LoRa performance evaluation in tree farm', *2018 IEEE Sensors Applications Symposium (SAS), 2018 IEEE Sensors Applications Symposium (SAS)*, Seoul, Korea (South), 12-14 March: IEEE, pp. 1–6. doi: 10.1109/SAS.2018.8336764

Zinevich, A., Messer, H. and Alpert, P. (2009) 'Frontal Rainfall Observation by a Commercial Microwave Communication Network', *Journal of Applied Meteorology and Climatology*, 48(7), pp. 1317–1334. doi: 10.1175/2008JAMC2014.1

Appendix A

A.1 Experiment 1: Möhringen, Software Defined Radio (SDR

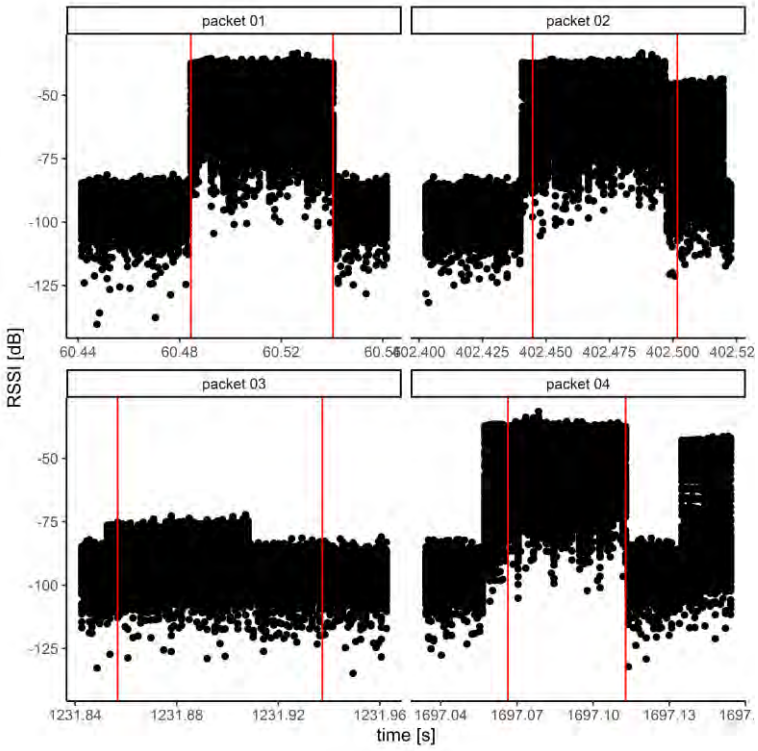

Figure A.1: Experiment 1, Möhringen: Examples of the result of the packet-matching process.

A.2 Experiment 2: Vauban, Regressions of Precipitation and Signal Strength After Decoupling

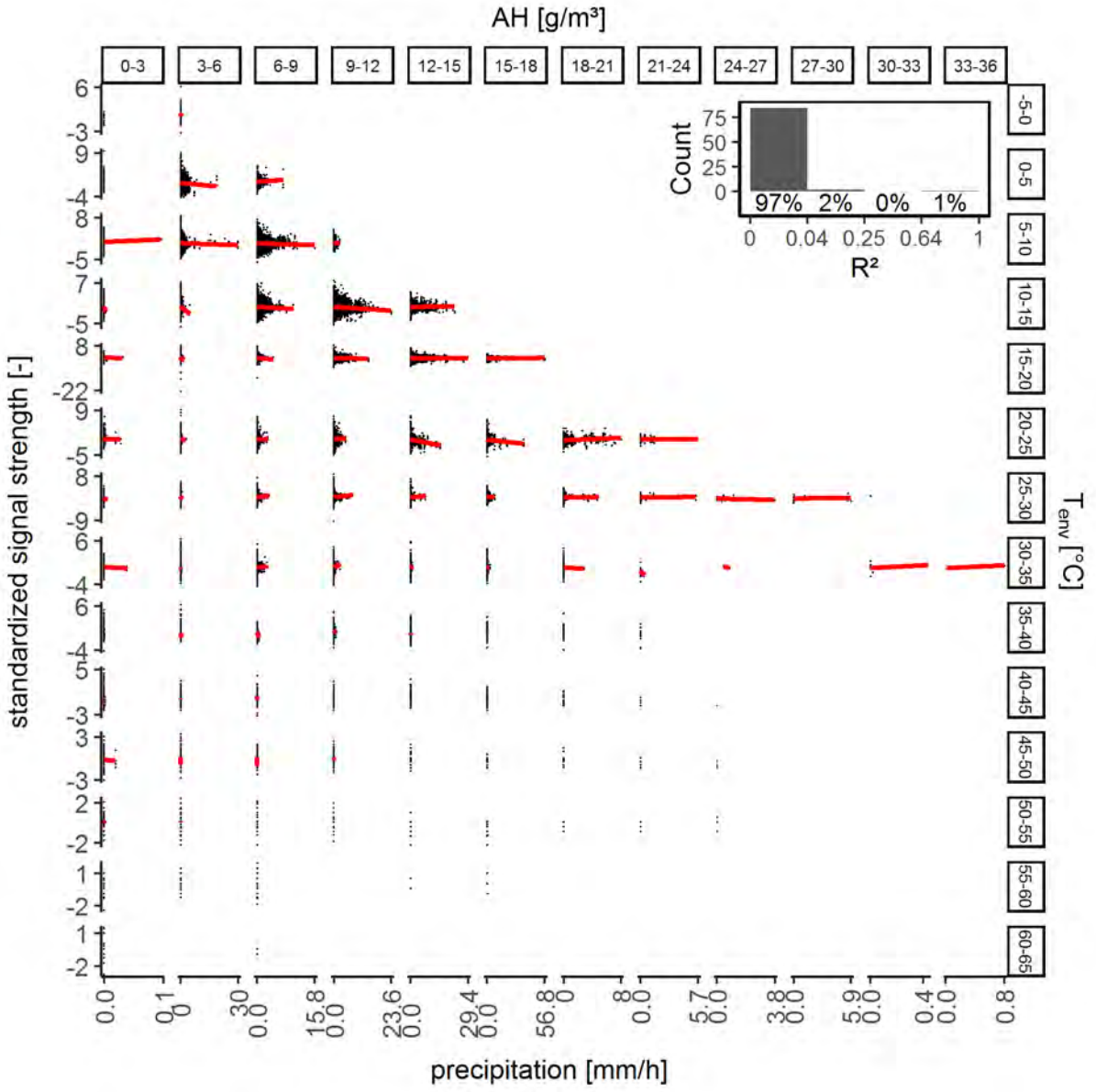

Figure A.2: Experiment 2, Vauban: Regression of precipitation and standardized signal strength after decoupling absolute humidity and environmental temperature. Inset shows the R^2-values of all regressions sorted into bins according to effect sizes: 0 - 0.04: no effect, 0.04 - 0.25: small effect, 0.25 - 0.64: medium effect, > 0.64: large effect. The number below the bars is the percentage of all links falling into the respective bin.

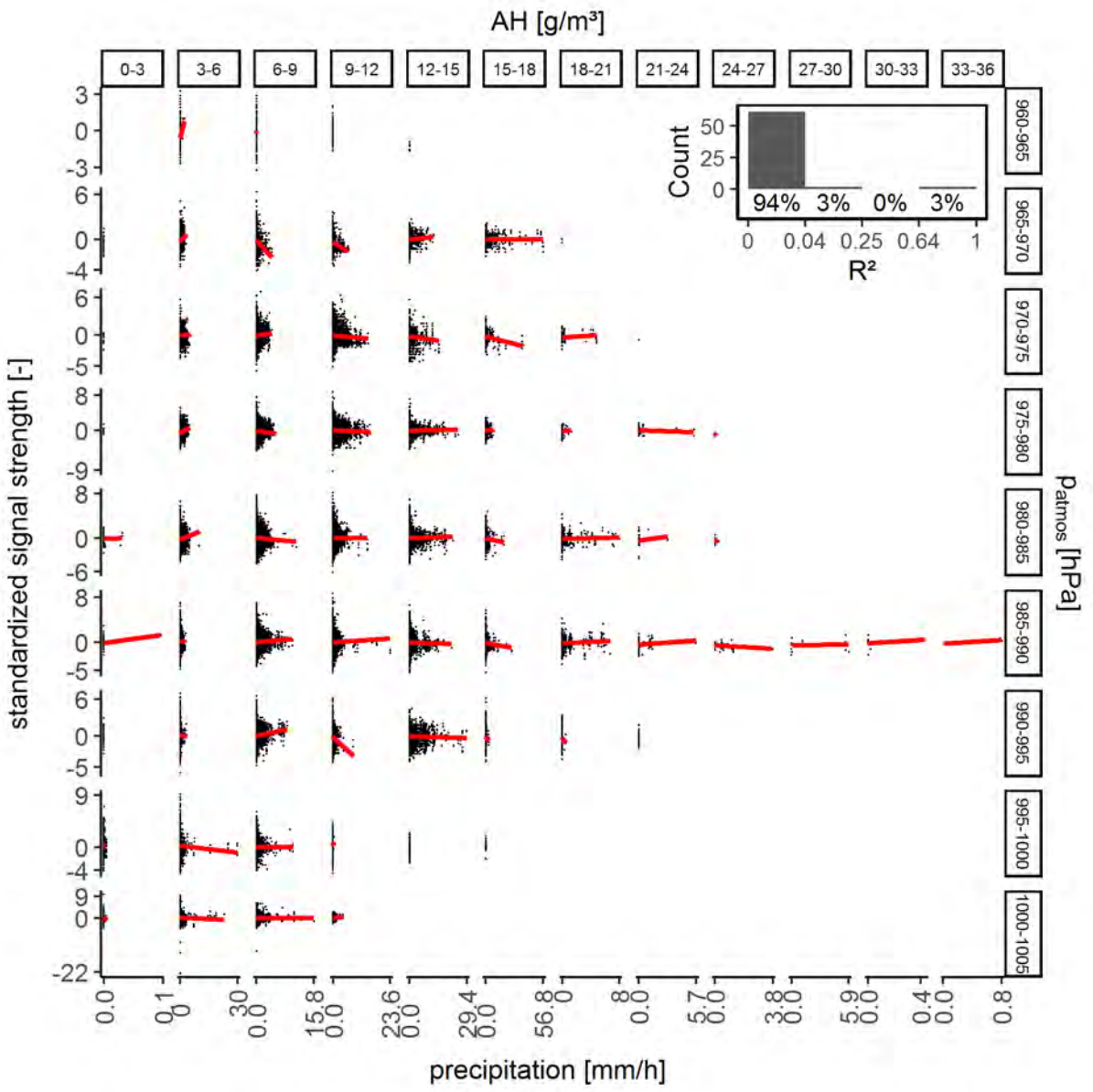

Figure A.3: Experiment 2, Vauban: Regression of precipitation and standardized signal strength after decoupling absolute humidity and atmospheric pressure. Inset shows the R^2-values of all regressions sorted into bins according to effect sizes: 0 - 0.04: no effect, 0.04 - 0.25: small effect, 0.25 - 0.64: medium effect, > 0.64: large effect. The number below the bars is the percentage of all links falling into the respective bin.

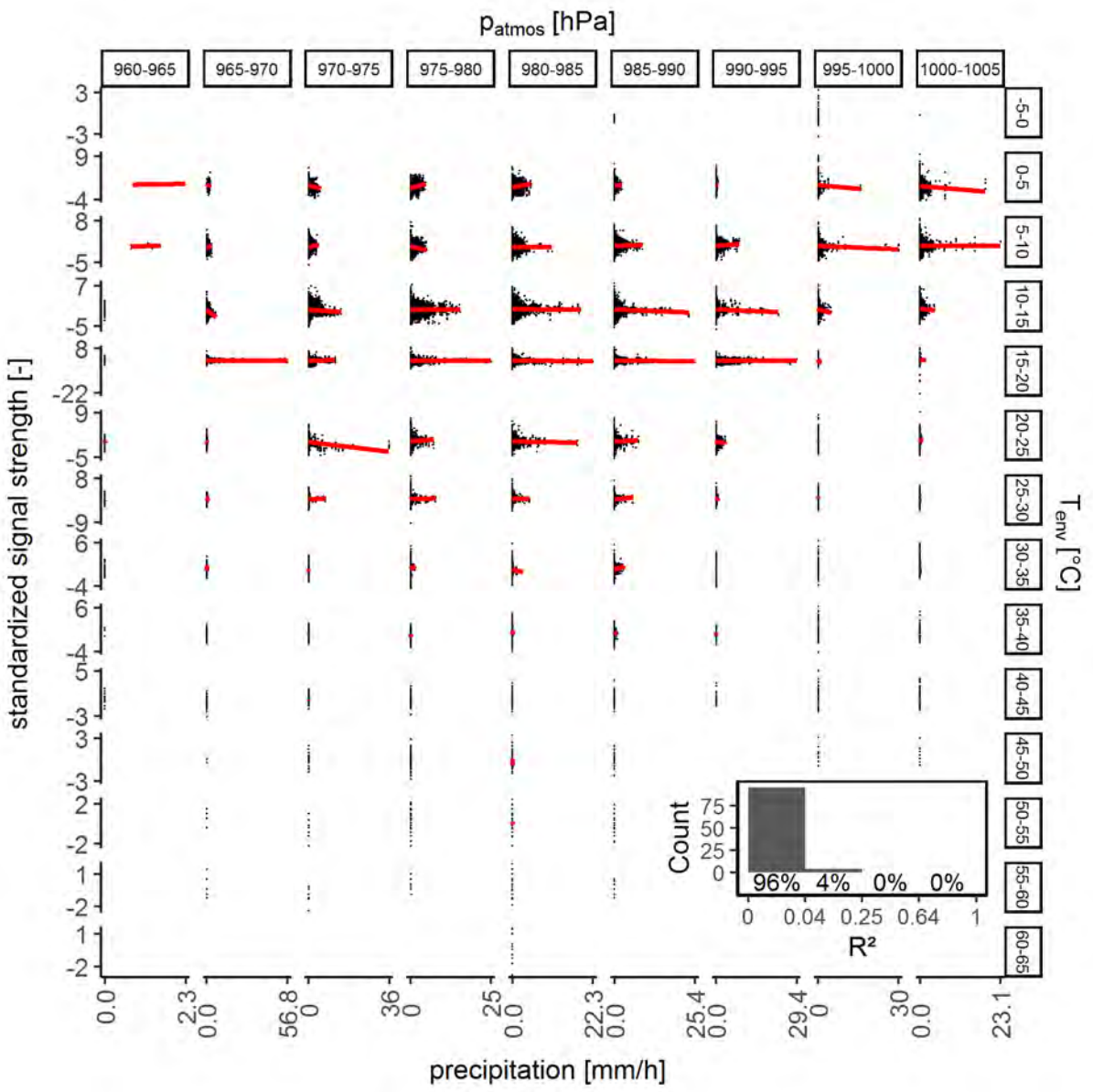

Figure A.4: Experiment 2, Vauban: Regression of precipitation and standardized signal strength after decoupling atmospheric pressure and environmental temperature. Inset shows the R^2-values of all regressions sorted into bins according to effect sizes: 0 - 0.04: no effect, 0.04 - 0.25: small effect, 0.25 - 0.64: medium effect, > 0.64: large effect. The number below the bars is the percentage of all links falling into the respective bin.

A.3 Experiment 2: Vauban, Regressions of Precipitation and Signal Strength After Decoupling: High Resolution Precipitation

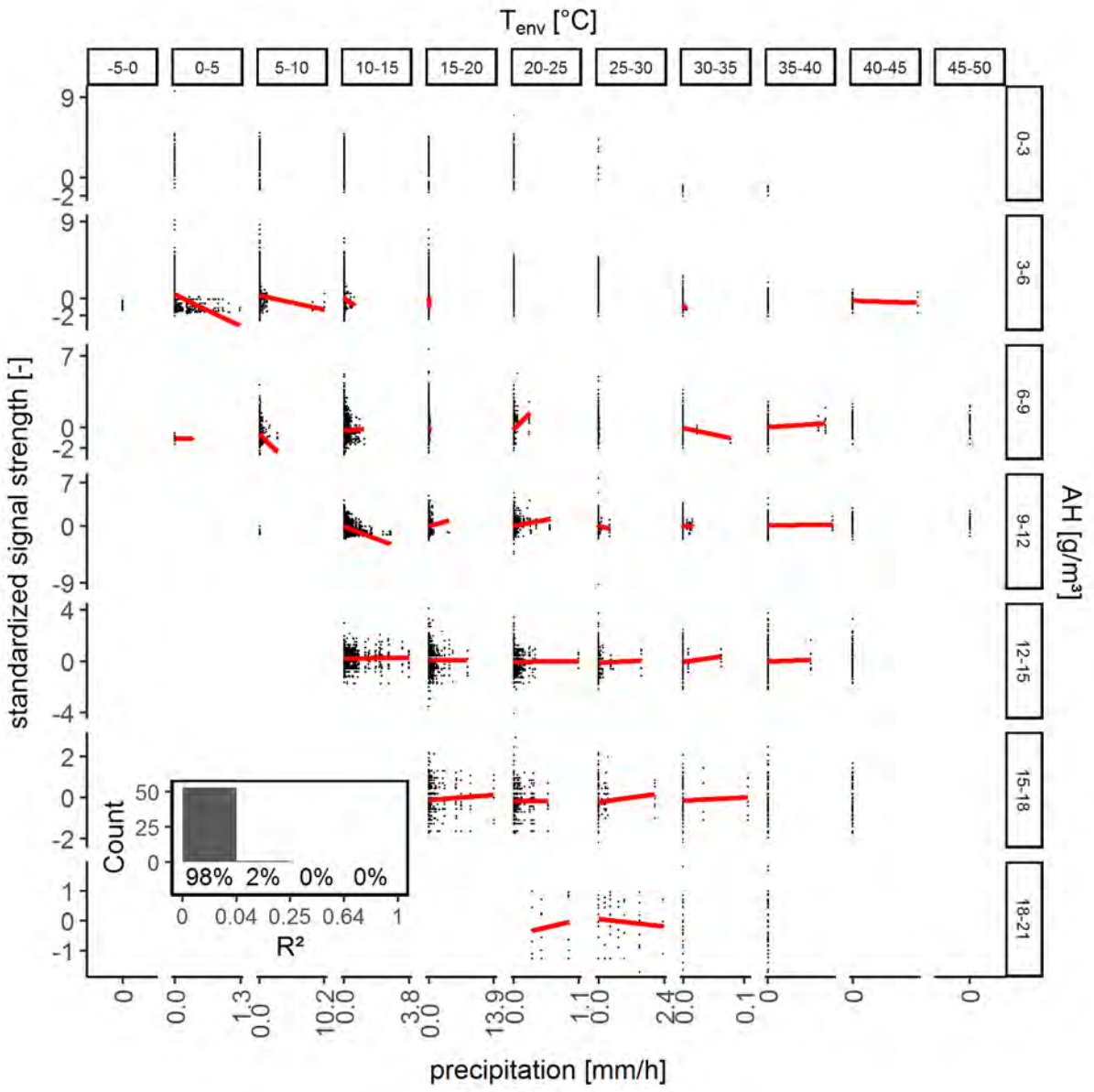

Figure A.5: Experiment 2, Vauban: Regression of high resolution precipitation and standardized signal strength after decoupling environmental temperature and absolute humidity. Inset shows the R^2-values of all regressions sorted into bins according to effect sizes: 0 - 0.04: no effect, 0.04 - 0.25: small effect, 0.25 - 0.64: medium effect, > 0.64: large effect. The number below the bars is the percentage of all links falling into the respective bin.

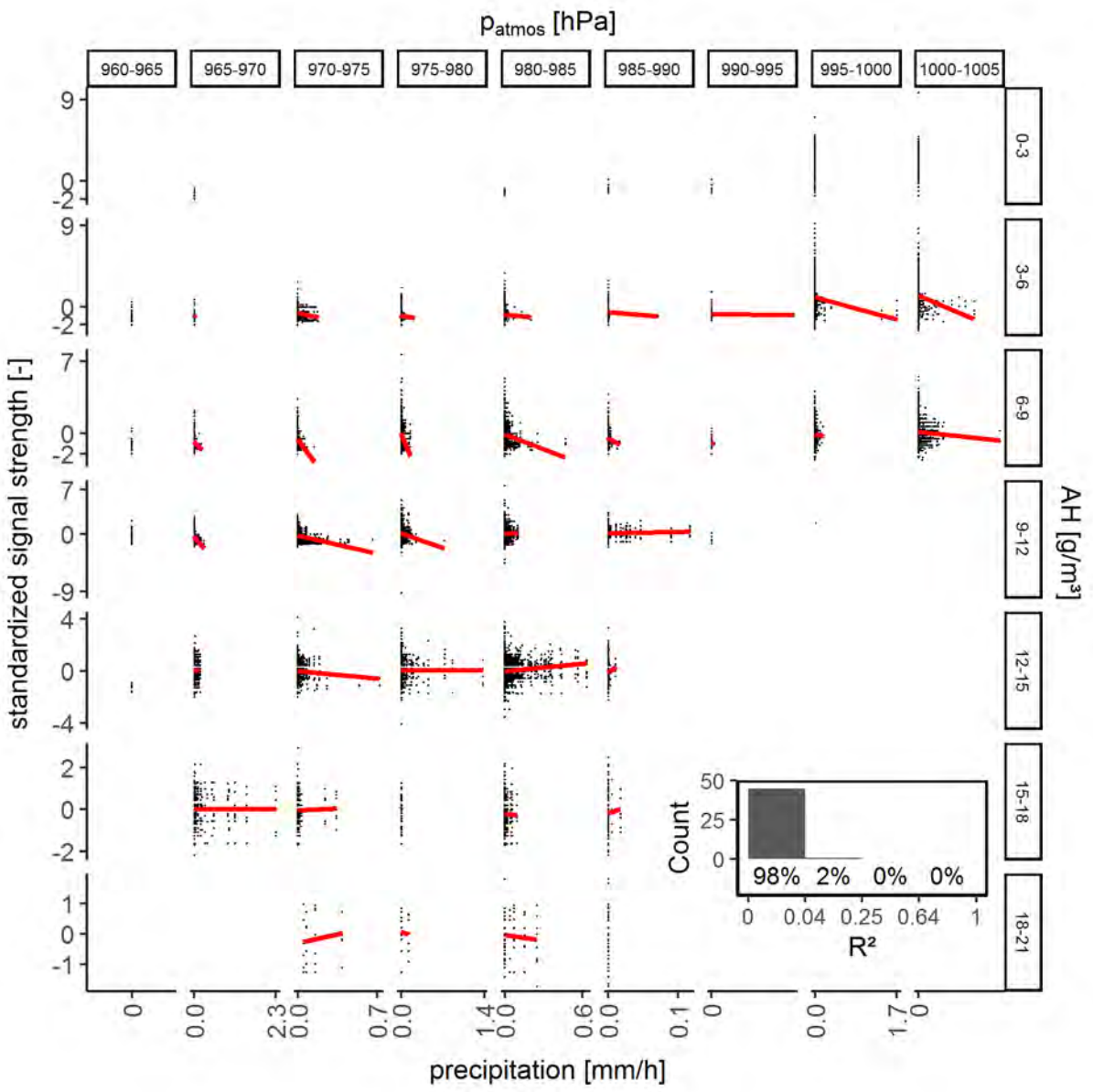

Figure A.6: Experiment 2, Vauban: Regression of high resolution precipitation and standardized signal strength after decoupling atmospheric pressure and absolute humidity. Inset shows the R^2-values of all regressions sorted into bins according to effect sizes: 0 - 0.04: no effect, 0.04 - 0.25: small effect, 0.25 - 0.64: medium effect, > 0.64: large effect. The number below the bars is the percentage of all links falling into the respective bin.

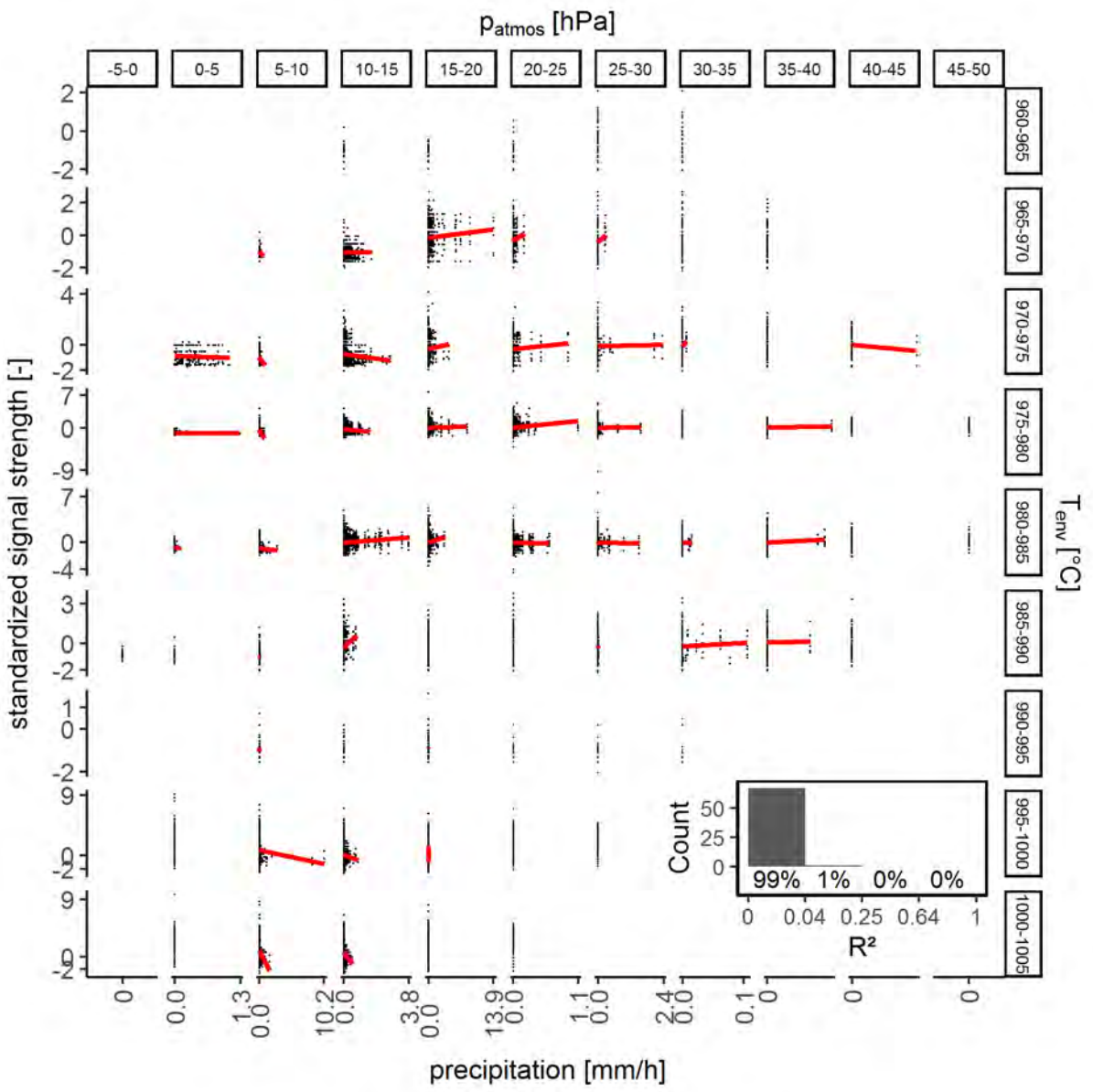

Figure A.7: Experiment 2, Vauban: Regression of high resolution precipitation and standardized signal strength after decoupling atmospheric pressure and absolute humidity. Inset shows the R^2-values of all regressions sorted into bins according to effect sizes: 0 - 0.04: no effect, 0.04 - 0.25: small effect, 0.25 - 0.64: medium effect, > 0.64: large effect. The number below the bars is the percentage of all links falling into the respective bin.

Appendix B

B.1 Devices and Software

B.1.1 Nodes

Two different types of nodes where used: the self-made Arduino Pro Mini and the The Things Uno manufactured by The Things Network.

B.1.1.1 Arduino Pro Mini

B.1.1.1.1 Hardware

These nodes were self-made devices consisting of 6 main parts:

- microcontroller, acting as its “brain”
- sensor
- transmission unit
- antenna
- battery
- case

The microcontrollers were Arduino Pro Mini 8 MHz-clones - inexpensive and user-friendly devices. They can programmed with the Arduino IDE which has a large user community and a very good documentation. To save power the Arduino Pro Minis were stripped from one of their LEDs and their voltage regulator.
The sensor was a BME280 which is used in a lot of mobile devices. They measure temperature, relative humidity and atmospheric pressure. None of the sensors used in this thesis were calibrated. The atmospheric pressure measurements displayed in this thesis refer to the local pressure and are not standardized to sea level as it is common in weather forecasts etc. The pressure in Möhringen (645 masl) and Freiburg (278 masl) might therefore be lower than expected.
The transmitting unit was a RF95W chip.
The antenna was not much more than a piece of wire cut at the length of a quarter of

the wavelength of the 868 MHz waves: 8.2 cm. The antennas where not uniformly bent in the same direction but randomly curved into the free space of the housing.

The battery where three 1.5 V AA batteries. As they each deliver 1.5 V, they greatly surpassed the recommended operating voltage of the microcontroller and the transmitting unit. However, as the results did not show any corruption this was neglected trading battery lifetime for machine fatigue.

The case were wide neck plastic bottles. The node itself was fixed to the underside of the lid. Holes were drilled near the foot of the bottom in order to provide enough air exchange for the sensor to make accurate measurements.

Figure B.8: Nodes in their white plastic housing at weather station University Chemistry.

B.1.1.1.2 Software

The software for the nodes (called “sketch”) is based mostly on the LMIC-library for the transmission (Matthijs Kooijman, 2017) of the data and the BME280-library for

the measurements of the sensor (Tyler Glenn, 2017). It is a very simple sketch where temperature, relative humidity, atmospheric pressure and additionally battery voltage are measured and transmitted every 3 minutes with a total packet size of 20 bytes and spreading factor 7. This interval is the minimum time which has to pass before the next transmission in order to stay within the The Things Network fair of use policy. For those nodes which were at larger distances the spreading factor was changed to 9, therefore the transmission interval grew to 9 minutes. During experiment 2, assuming that nobody would be disturbed in this remote area the transmission interval was reduced to 45 seconds at spreading factor 7.

B.1.1.2 The Things Uno

B.1.1.2.1 Hardware

The second node model was a different Arduino model called The Things Uno. This model is designed by The Things Network therefore it is perfectly configured and ready to deploy upon delivery. The device is powered via USB and has an inbuilt transmission unit. Only the sensor had to be connected to the board. The disadvantage of this device is the low range: a stable link could only be established within about 1 km. Additionally, it depended on wall power which made the search for suitable locations difficult. Consequently, the Arduino Pro Mini nodes made up the largest part of the experiment and were complemented by a few The Things Unos.

B.1.1.2.2 Software

The software for the The Things Uno was adopted from the examples from The Things Network (The Things Network, 2019). Since there was no battery in these nodes and no battery voltage to be reported, the size of the packet was smaller and could be transmitted at a 2 minutes interval.

B.1.1.3 Raspberry Pi 3B+

B.1.1.3.1 Hardware

The third node type were Raspberry Pi 3B+. These microcontrollers possess Wi-Fi-cards capable of 2.4 GHz and 5 GHz, therefore they were only used during experiment 3. They also had BME280 sensors and were placed in cut plastic bottles as protection from liquid water.

B.1.1.3.2 Software

They ran the operating system Raspbian and three small Python scripts to record the sensor measurements, CPU-temperature and the Wi-Fi-connections signal strength (ping the router, then save the updated signal strength).

B.1.2 Receiver

B.1.2.1 Gateway

The gateway or the receiver was the main component of experiment 1 and 2. Here, the packets sent by the nodes where demodulated and saved along with the signal strength. For the The Things Network, it serves as the backhaul from LoRaWAN to the servers and databases. Packets transmitted with the LoRaWAN-frequency reach the gateway, are then demodulated into human readable content and forwarded to the servers. Hence, a gateway should normally be connected to the internet.

B.1.2.1.1 Hardware

The gateway consists of four main parts:

- microntroller
- concentrator board
- antenna
- case

A Raspberry Pi 3B microcontroller acted as the server for the software and the user interface for the gateway. The concentrator board is the reception unit of the gateway and processes the antenna excitations. It was a WiMOD iC880A-SPI LoRaWAN Concentrator Board for 868 MHz. It goes hand in hand with the Raspberry Pi and does not require any configuration. The manufacturer states that is able to demodulate eight packets simultaneously thereby easily overcoming the issue of packet collisions. The reception range is indicated as 15 km within line of sight and several km in an urban environment. The operating temperature is between -5 and +55 °C but can be "extended" to -40 and +85 °C according to the manual. It is optimized for an impedance of 50 Ω (IMST GmbH, 2018), which corresponds to the stated impedance of the antenna, an Aurel GP868 Ground Plane Omnidirectional Antenna with an operating temperature between -20 and +80 °C (Aurel S.p.A., 2019).
The microcontroller and the concentrator board were connected through a backplane and placed in a generic waterproof case ready to be mounted on a wall or a pole.

B.1.2.1.2 Software

The microcontroller was running the Linux-base operating system Raspbian. The software for the gateway, i.e. the packet forwarder which saves the received packets and forwards them to the server of The Things Network as well as the complete tutorial on how to assemble this gateway was taken from the GitHub-repository of the The Things Network community of Zurich (TTN Zurich, 2019) This is an adapted version of the original software provided by The Things Network which has been designed by Semtech (The Things Network, 2013). This forwarder software comes with several utility programs, one of them called "util_pkt_logger" which allows to store the received packets in a file instead of forwarding them to the server environment. On the upside, more information about the packets (such as CRC state) is stored, on the downside, the payload which contains the encrypted measurements is not decrypted and has to be processed later on. Furthermore, the utility allowed to use the gateway in areas where

there was no connection to the internet.

Additionally the gateway ran a small script querying the CPU-temperature of the microcontroller in a 30 seconds interval and storing it in a file.

B.1.2.2 Router

An ordinary Wi-Fi-router provided the Wi-Fi-network in experiment 3. It was a TP-Link AC750 Wi-Fi Range Extender which can operate on 2.4 GHz and 5 GHz (TP-Link, 2019).

B.1.2.3 SDR

An SDR allows the user to record radio waves not only in one frequency but in any frequency within a certain range because the antenna excitations are not evaluated by hardware but by software. With this device one could for example search a range for a desired signal or, like in this case, record the raw excitations in a whole range and not just save the demodulated data packets like the gateway did.

B.1.2.4 Hardware

The SDR (software defined radio) was a cheap USB-dongle, a copy of the popular RTL-SDR. The reception frequency range is between 25 and 1760 MHz. It was used with 21 cm antenna.

B.1.2.5 Software

The software used with the SDR was the open source GNU Radio. It was run on an Ubuntu-based laptop for periods of maximum of 20 minutes length, since the amount of required hard disk space grew quite quickly.

Appendix C

C.1 Abbreviations

total attenuation	[dB]	A
absolute humidity	[g/m³]	AH
functions of frequency and rain properties	[-]	c *and* d, a *and* b
receiver cable loss	[dB]	CL_{RX}
transmitter cable loss	[dB]	CL_{TX}
distance	[km]	d
frequency	[MHz]	f
receiver antenna gain	[dB]	G_{RX}
transmitter antenna gain	[dB]	G_{TX}
specific attenuation	[dB/km]	k
path-averaged specific attenuation	[dB/km]	$\bar{k}$
link length	[km]	L
atmospheric pressure	[hPA]	p_{atmos}
path loss	[dB]	PL
free space path loss	[dB]	PL_{FS}
packet reception ratio		PRR
received power	[dB]	P_{RX}
transmittion power	[dB]	P_{TX}
rainfall intensity	[mm/h]	R
path-averaged rainfall intensity	[mm/h]	$\bar{R}$
relative humidity	[%]	RH
received signal strength indicator	[dB]	$RSSI$
software defined radio		SDR
spreading factor	[-]	SF
CPU-temperature	[°C]	T_{CPU}
environmental temperature	[°C]	T_{env}
wireless sensor network		WSN
space variable	[km]	x

Ehrenwörtliche Erklärung

Hiermit erkläre ich, dass diese Arbeit selbständig und nur unter Verwendung der angegebenen Hilfsmittel angefertigt wurde.

Ort, Datum Unterschrift